DESIGN, CONSTRUCTION AND INVESTIGATION OF AN AMMONIA BEAM MASER OPERATED UNDER CONDITIONS OF STRONG OSCILLATION

A thesis presented for the Degree of Doctor of Philosophy
at the University of Keele

by

A.K.H. MAROOF B.Sc., M.Sc., M.Inst.P.

Department of Physics
University of Keele

February 1975

IMAGING SERVICES NORTH
Boston Spa, Wetherby
West Yorkshire, LS23 7BQ
www.bl.uk

Appendix 1 and Appendix 2 (pages 141-144) have not been digitised at the request of the university

TO: SHAWKI,

NAZIK,

& NADA

ACKNOWLEDGEMENTS

I am indebted to Dr. D.C.Lainé, to whom I would like to express my grateful thanks and appreciation for acting as a constant source of stimulus and encouragement, active concern, constructive guidance and excellent supervision.

The author would also like to thank:

his colleagues Dr. P.R.Lefrère, Mr. A.I.Corb, Mr. M.J.Truman for many useful discussions.

Professor W.Fuller, Professor D.J.E.Ingram for the provision of research laboratory facilities.

Mr. G.Dudley and the Technical Staff of the Physics Department Mr.G.Marsh, Mr. M.Wallace, Mr. E.J.T.Greasley, and Mr. H.Wardell and his Staff of the University workshop.

Mr. M.G.Davies, Mr. B.J.Minshull, Mr. A.C.Smallman, and the Electronics Staff of the Physics Department.

Mr. F.Rowerth, Mr. C.B.Harrison for their invaluable assistance.

Mr. M.Daniels for the preparation of the photographs reproduced in this thesis.

Friends and other members of the Physics Department for their occasional assistance.

Mrs. L.Markham for typing this thesis.

The University of Baghdad and College of Science for provision of the study leave from 1971-1974.

Especial thanks are due to my wife for her forbearance, continuous and sustained assistance over three years.

ABSTRACT

In this thesis, the principle, construction and operation of an ammonia beam maser oscillator of advanced design are described.

The maser discussed is characterized by the production of an intense molecular beam with a nozzle-skimmer gas source combination. This system has permitted a particularly strong oscillation to be obtained which has led to the observation of several novel phenomena associated with non-linearities of the maser. These include strong oscillation pulsations on the four quadrupole satellite lines of the J=K=3 inversion transition of $^{14}NH_3$. In addition, oscillation settling transients and various complex oscillation amplitude pulsation phenomena in both single and two-cavity maser systems are reported and discussed.

Other characteristics are also described, including two-cavity maser operation with the second cavity either as a molecular beam polarization detector or as a spectrometer cavity. In the former case, cavity detuning phenomena are examined and in the latter, multiple population inversion is investigated.

Furthermore, continuous oscillation with several inversion lines of $^{14}NH_3$ including J=K=3; J=3, K=2 and J=K=2 are obtained without cryogenic pumping or time limit.

Some of these results have already been published and reprints of the papers may be found at the end of the thesis.

CONTENTS

CHAPTER 1

FINE AND HYPERFINE STRUCTURE

1.1 Introduction

Since 1934, the inversion spectrum of the $^{14}NH_3$ molecule has been the subject of a great deal of study by many workers. Great attention has been given to this gas because of the intensity of its microwave spectral lines, chemical stability, cheapness, low toxicity and high temperature of its freezing point relative to other gases.

The first experiments were carried out in 1934 by Cleeton and Williams. A spectrometer was used in recording the absorption spectrum of ammonia gas in the region of 1 to 4 cm wavelength. The maximum absorption region was found to be at 1.25 cm wavelength, and theoretical predictions had shown that the inversion absorption frequency for ammonia should be in this region. This experiment employed ammonia gas at atmospheric pressure and as a result, pressure broadening obscured all the fine structure of the spectrum and only a broad hump of absorption centered on a wavelength of 1.25 cm (24,000 MHz) was obtained.

In 1946 Bleaney and Penrose were the first to construct a $^{14}NH_3$ microwave spectroscope employing the radiation produced by a klystron. Microwave power passed into a cavity resonator which acted as the absorption cell in transmission. The output power and frequency of the klystron were monitored by means of a directional coupler and wavemeter respectively. A silicon crystal was employed as a detector at the output of the cavity, this being connected to a sensitive galvanometer to measure the output power transmitted through the cavity resonator. The output was noted for each different

frequency setting of the klystron, the cavity resonator always being kept tuned to the klystron frequency. With far more sensitive detecting systems and by reducing the pressure of the ammonia gas to 1 torr and below, they were able to resolve all the fine structure of the spectrum (30 lines) corresponding to the different rotational energy states.

Since a cavity resonator was used as an absorption cell, saturation broadening became greater than pressure broadening at a pressure of the order of 0.4 torr. Thus they were unable to reduce the line width any further and could not resolve the hyperfine structure of these lines. However, soon after this pilot experiment W.E.Good (1946) at the Westinghouse Research Laboratories in the United States, used a new technique of a waveguide type absorption cell. Being able to reduce the pressure below 10^{-2} torr before any saturation broadening became noticeable, he announced the discovery of hyperfine structure in the wings of the absorption lines. His technique was based on the basic principle of "crystal-video" detection and allowed direct display of the spectrum on an oscilloscope as well as reducing saturation broadening. The klystron frequency was swept across the absorption line by means of a saw-tooth sweep at an audiofrequency which was applied to the klystron reflector. Then the power detected was amplitude modulated by the line shape as the klystron frequency was scanned across the absorption spectrum. The output signal was then fed into a video amplifier and the different components of the spectrum were displayed on an oscilloscope screen.

With more improved techniques of radiofrequency absorption measurements, and with the aid of quantum mechanical theory, J.M.Jauch in 1947, was able to get valuable information of the

hyperfine structure and their relative intensities in the ammonia inversion spectrum (J=K=3) line. Furthermore, he considered the displacement of the absorption lines in a weak and strong electric field (Stark effect).

In 1954, Gordon, Zeiger and Townes created the first molecular maser, thus a new powerful tool was added as a fundamentally new method to the techniques of microwave spectroscopy. The new device appeared to have great potentialities as a high resolution spectrometer, very low-noise quantum mechanical amplifier and a practical microwave frequency standard of very high frequency stability. By using molecular beams, they observed the inversion spectra of ammonia with high resolution, and obtained a linewidth of only 7kHz. This was due to the reduction in the Doppler broadening as a result of high directivity and small velocity spread of the molecules. The first clear spectrum of the (J=K=3) inversion line of $^{14}NH_3$ was obtained by their molecular beam techniques. The magnetic satellite lines were resolved in the main quadrupole hyperfine transitions. Each of these lines was expected to split into four components due to mutual interaction between hydrogen magnetic moments and the molecular magnetic field.

Since the introduction of molecular beam masers increasingly detailed theoretical explanations of the observed hyperfine structure of $^{14}NH_3$ lines have been published by many workers (Gunther-Mohr 1954, Gordon 1955, Shimoda 1955, Kukolich 1967 and others).

Since some of the results of operation of a molecular beam maser under strong oscillation conditions are determined by the detailed hyperfine structure of ammonia, a more detailed

discussion of the spectroscopy of the molecule is given in the following sections.

1.2 Symmetric-Top Molecules

Symmetric-Top molecules have three principal axes about which the moments of inertia about two of these axes are equal, i.e. $I_X = I_Y = A$ and $I_Z = B$ (Vuylsteke 1960). The motion of this molecule is such that, while the whole molecule rotates about its axis of symmetry, this axis itself precesses about the direction of the total angular momentum vector. The different vectors representing the angular relation of ammonia molecule and the quantum components are illustrated diagrammatically in Figure (1.1) and (1.2).

The quantized rotational energies of the molecule may be given by:

$$E_{J,K} = hBJ(J+1) + h(A-B)K^2 \qquad (1)$$

where, $A = h/8\pi^2 I_A$ and $B = h/8\pi^2 I_B$

J is the total angular momentum which is actually equal to $\sqrt{J(J+1)}$. K is the quantum number defining the component of J along the molecular figure axis. I_A is the moment of inertia with respect to the axis passing through the centre of mass of the molecule perpendicular to the axis of symmetry. A and B are the rotational constants of the molecule.

The molecule spins about its figure axis with an energy prescribed by the quantum number K which takes the values $J_Z = K\hbar$ ($K\hbar$ is the component of the total angular momentum J resolved along the figure axis), where $K = 0, \pm 1, \pm 2, \ldots \pm J$. In addition to the spin motion described above, J is space quantized and orientates relative to an arbitrary space-axis such that its component along the axis is given by $\hbar M$, M is the magnetic quantum number and may have the values $0, \pm 1, \pm 2, \ldots, \pm J$.

In the absence of an external field, each M level has (2J+1) different equivalent positions all having the same energy, i.e. the energy level is (2J+1) fold degenerate. Likewise, each K level is also (2J+1) degenerate, thus it follows that the total degeneracy for levels with $K \neq 0$ is 2(2J+1). Moreover, according to equation (1), states whose only difference is in the sign of K have the same energy. They correspond to the two opposite directions of rotation about the figure axis, i.e. all states with $K \neq 0$ are doubly degenerate. The selection rules for dipole transitions between the rotation states of a molecule of the symmetric-top type are: $\Delta J = 0, \pm 1; \Delta K = 0$. (Since, in the pure rotational spectrum, $\Delta J = J_2 - J_1 = -1$ does not apply if J_2 and J_1 are the J values of the upper and lower state respectively). Thus, the only important rule is $\Delta J = +1$, that is only neighbouring levels with the same K may combine with one another.

The corresponding frequencies of these transitions are expressed by:

$$f_{J,K} = \frac{E_{J+1,K} - E_{J,K}}{h} = 2B(J+1) \qquad (2)$$

which is only applied to a rigid symmetric-top molecule as well as for linear molecules. Since the ammonia molecule is a non-rigid oblate symmetric top, a correction has to be applied for the centrifugal distortion which increases with rotational energy:

$$\frac{E}{h} = BJ(J+1)+(A-B)K^2-C_J J^2(J+1)^2-C_{JK}J(J+1)K^2-C_K K^4 \qquad (3)$$

where C_J is a measure of the centrifugal distortion due to rotation of the moleule, C_K is due to rotation about the symmetry axis, C_{JK} is the interaction distortion between the

two rotations. The order of these constants C_J, C_K and C_{JK} are 19, -28 and 298,000 MHz respectively.

The selection rule for a transition in the rotational energy $\Delta J = \pm 1$, $\Delta K = 0$; thus the frequency of the absorption line corresponding to a change from J to J+1 is given by:

$$f = 2B(J+1) - 4C_J(J+1)^2 - 2C_{JK}(J+1)K^2 \qquad (4)$$

The last two terms are very small compared with the first and only this term contains the parameter B, therefore, the frequencies of the rotational lines depend mainly on the moment of inertia of the molecule about an axis perpendicular to the axis of symmetry.

The main effect of the centrifugal distortion is to remove the degeneracy of the different K states and as a result, each of the main transitions is split into (J+1) components with a separation between each component of the order of 0.5 MHz. In the absence of the distortion, only one line would appear for each different transition of J because of the $\Delta K = 0$ selection rule. However, if the electric dipole moment does not lie along the molecular figure axis, then in addition to $\Delta K = 0$, $\Delta K = \pm 1$ is also possible which gives rise to rather complicated spectra.

1.3 The ammonia molecule inversion spectrum

The ammonia molecule has four type of energy spectra;

(a) Electron spectra with levels of energy transitions at optical frequencies.

(b) Vibrational spectra for which its transition frequencies are in the infrared region.

(c) Rotational spectra which lie in the sub-millimeter wave region

(d) Hyperfine spectra with energy transitions which lie in the microwave region.

The ammonia molecule is a molecule of the symmetrical top type. Three atoms of hydrogen and one atom of nitrogen are located at the apexes of a right pyramid. The distance between hydrogen atoms is 1.014°A and the angle is 67°58′, (Figure 1.3 and 1.4).

A number of different oscillatory and rotational motions are possible, in particular oscillations of the nitrogen at right angles to the plane of the hydrogen atoms. The potential energy of the molecule as a function of the distance between the nitrogen and the plane of the hydrogen atoms has the form of a symmetrical curve with two minima. If we neglect the tunnel effect, then each of the lower oscillation levels is doubly degenerate since there are two equivalent possibilities for positioning the nitrogen on one side or other of the potential barrier. These oscillations are identical because of the function of potential energy is symmetrical with respect to the plane of hydrogen atoms. The presence of the tunnel effect eliminates the degeneracy. Since the potential barrier dividing the positions of equilibrium is not very high, owing to the tunnel effect the nitrogen nucleus can penetrate the potential hill from one side of the plane of hydrogen atoms to the other. The height of this potential barrier determines the frequency region in which the inversion spectrum will be found and two energy levels are obtained. The amount of the splitting of the vibrational levels, and the frequency of the inversion line is very sensitive to changes of the height and width of the potential barrier and in turn its shape will be a function of the molecular rotational state. The rotation of the molecule about the axis of symmetry will cause the hydrogen atoms to move outwards, and thus reduce the height of the

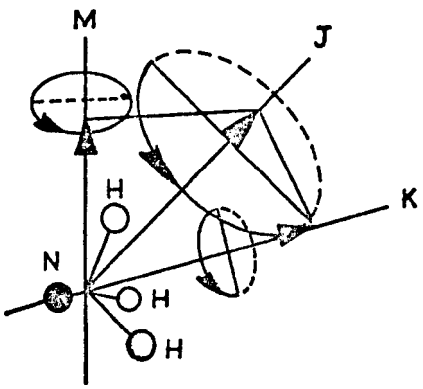

Fig (1.1) COMPONENTS OF ROTATIONAL MOTION OF NH_3 MOLECULE.

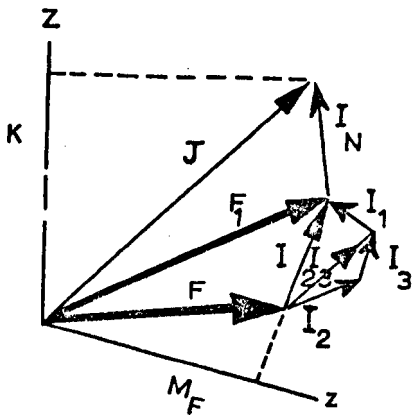

Fig (1.2) $^{14}NH_3$ MOLECULAR COUPLING SCHEME.

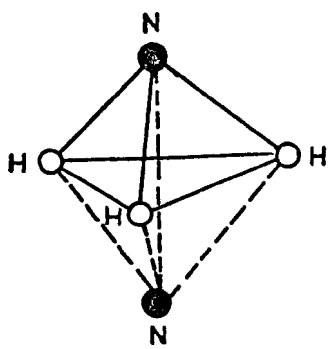

Fig (1.3) THE TETRAHEDRAL STRUCTURE OF AMMONIA MOLECULE.

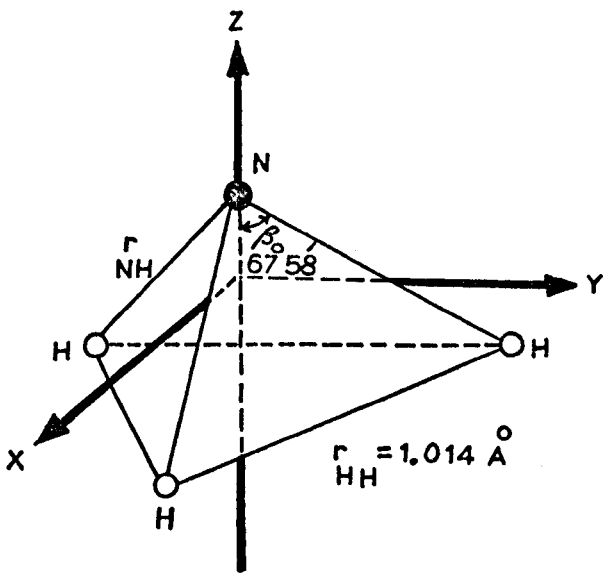

Fig(1.4) GEOMETRICAL STRUCTURE OF AMMONIA MOLECULE.

potential barrier and increase the inversion frequency. On the other hand, the increase in the height of the potential barrier, which is due to end-over-end rotation of the molecule causes a decrease in the inversion frequency. The transition that gives rise to the inversion is the one between the two levels of the split vibrational ground state. Thus with each rotational state, there is associated a finite splitting which lies, in the case of ammonia, in the microwave region of the spectrum.

Sheng, Baker and Dennison (1941) explained the inversion fine structure of the ammonia molecule on the basis of a different degree of centrifugal distortion caused by the different molecular rotational states. With each rotational state, there is an associated splitting, thus a particular spectral line. They derived an expression for the wave numbers of the lines in the inversion fine structure of the ammonia molecule. This formula is:

$$\frac{1}{\lambda}\,(cm^{-1}) = 0.79347 - 0.0011(J^2+J) + 0.0016K^2 \qquad (5)$$

while the expression obtained based on the measured frequencies for the ammonia inversion fine structure has the formula (Good 1946):

$$\frac{1}{\lambda}\,(cm^{-1}) = 0.79347-0.005048(J^2+J)+0.007040K^2+0.0000154(J^2+J)^2 -0.0000426(J^2+J)K^2+0.0000292K^2 \qquad (6)$$

Good obtained thirty lines of the ammonia fine structure which were predicted by Sheng and et al(1941) as in the figures (1.5) and (1.6). The intensities and frequencies of the lines have been measured for two different temperatures according to the equation (6). It was found that the average deviation of the measured lines from equation (5) is about 0.01%.

The low temperature data Figure (1.6) shows the effect of the thermal distribution. It can be seen that the inten-

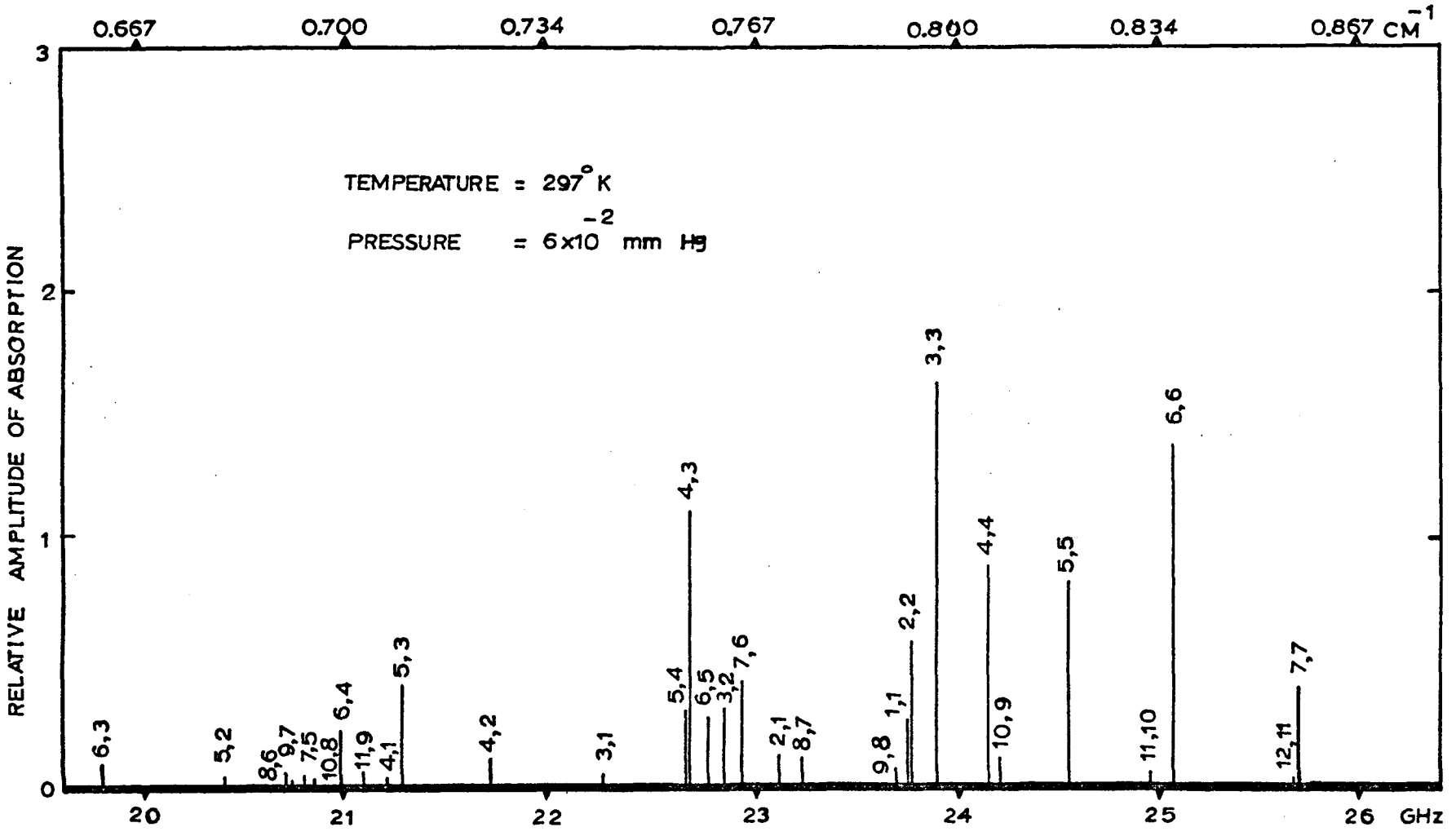

Fig(1.5) AMMONIA INVERSION SPECTRUM.

sities of lines having lower values of J and K would increase and those lines having higher values of J and K would decrease. (The numbers above each line indicate the value of J and K respectively). The intensities of the lines are dependent on the number of molecules in each rotational state and their transition probabilities. On the other hand, the number of molecules in a given level depends on the distribution of thermal energies and the statistical weights. Careful examination of Figure (1.6) reveals that the levels with K = 3,6,9, etc have twice the statistical weight of those with K = 1,2,4,5,7, etc. Furthermore, for the lines K = 3,6, and 9 a uniform distribution can be obtained if these intensities are reduced by a factor of two.

A comparison between the two experimental results shows a differential dependence of the intensities of each individual line upon the temperature. This was attributed to the increase in the number of molecules in lower rotational states, reduction in their average velocity and fewer collisions, thus narrower lines are obtained with an enhanced intensity of particular lines relative to others.

The oscillatory condition of the nitrogen atom is similar to two coupled oscillators in which the oscillations split into two, even when the partial frequencies of both oscillators are identical. Therefore, every energy level splits into two sublevels. The selection rules for the rotational inversion are: $\Delta J=0, \pm 1, \Delta K=0$, and for a pure inversion spectrum is: $\Delta J=\Delta K=0$.

The best fitting empirical formula for the transition frequencies is found to be:

$$f = f_0 \exp\left[aJ(J+1)+bK^2+cJ^2(J+1)^2+dJ(J+1)K^2+eK^4\right]+\Delta f' \qquad (7)$$

where a,b,c,d and e are constants determined from

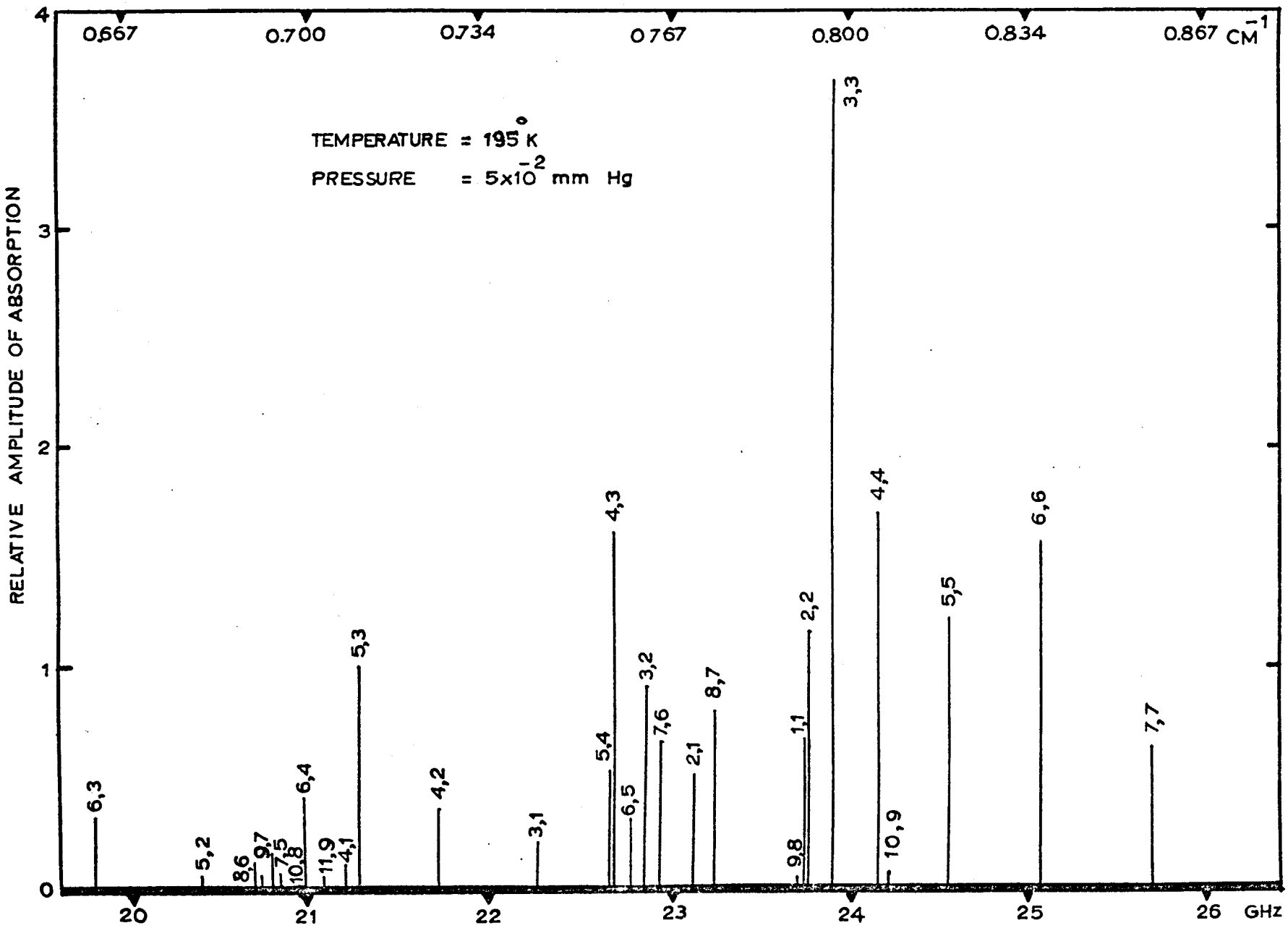

Fig (1.6) AMMONIA INVERSION SPECTRUM .

experimental microwave frequencies: f_o = 23785 MHz, $a = -6.36996 \times 10^{-3}$, $b = 8.88986 \times 10^{-3}$, $c = 8.6922 \times 10^{-7}$, $d = -1.7845 \times 10^{-6}$, $e = 5.3075 \times 10^{-7}$. For $K \neq 3; \Delta f' = 0$, and for $K = 3$;

$$\Delta f' = 3.5 \times 10^{-4} J(J+1) \left[J(J+1)-2\right] \left[J(J+1)-6\right] \qquad (8)$$

1.4 Hyperfine structure of $^{14}NH_3$

When the hyperfine interactions are taken into account, the energy levels of various transitions of the molecule should be characterized by the quantum numbers J, I_N, I_H, F_1 and F where J is the vector of total rotational angular momentum of the molecule, I_N is the spin vector of the nitrogen nucleus, I_H is the vector of total spin of the three hydrogen nuclei. Figure (1.2) shows the coupling scheme referred to the laboratory axis. The z axis coincides with the molecular symmetry axis, Z is the fixed direction in the laboratory and K is the projection of J on the symmetry axis. Thus we have;

$$F_1 = J + I_N , \quad I = I_1 + I_2 + I_3 , \quad F = F_1 + I$$

The energy spectrum of the $^{14}NH_3$ (J=K=3) line possesses a rich hyperfine structure caused by different molecular interactions. The strongest interaction is the electric quadrupole moment of the nitrogen nucleus with the molecular electrical field. The quadrupole interaction is responsible for the removal of the degeneracy of the energy levels of the ammonia molecule as a result of mutual spin orientation of the nitrogen nucleus (I_N) and the molecular field with the total angular momentum (J). The orientation of the nitrogen nucleus and the ammonia molecule can be characterized by independent quantum numbers, M_{I_N} the projection of the nitrogen spin onto the Z axis and M_I the projection of moment of

rotation of the molecule on the Z axis. But a calculation of the interaction showed that these two quantum numbers are not preserved. This necessitates the introduction of two other quantum numbers; $F_1 = I_N + J$ and M_{F_1} which is the projection of F_1 onto the Z axis. The quantum number F_1 can take values from $I_N + J$ to $|I_N - J|$. Since every value of F_1 corresponds to an energy level, it turns out that the degeneracy of energy levels due to spin orientation of the nitrogen nucleus and the molecule is removed by a factor equal to $(2I_N+1)(2J+1)$.

Owing to selection rules, every component of quadrupole hyperfine structure corresponding to a given value of F_1 is split into three times the number of different values taken by F where it can take values from $F_1 + I_H$ to $|F_1 - I_H|$ through one. The least of the numbers, $(2I_H+1)$ or $(2F_1+1)$ are the number of different values of F.

In the case of the inversion transition of ammonia (J=K=3) line; $I_H = 3 \times \frac{1}{2}$ and $I_N = 1$, therefore F_1 can take three values; 4, 3 and 2. From the relationship between F_1 and F and due to the different couplings possible and orientation of the hydrogen nucleus, F can take 12 values which are determined from; $F = F_1 + 3/2,\ F_1 + \frac{1}{2},\ F_1 - \frac{1}{2},\ F_1 - 3/2$.

In order to describe completely the ammonia spectrum, including the main line, magnetic and quadrupole structure, it is necessary to apply the selection rules as follows;

$\Delta F_1 = \Delta F = 0$ (components of the main line)

$\Delta F_1 = 0, \pm 1$ (components of the magnetic and quadrupole satellites)

As it is clear from Figure (6.9) the main line of $^{14}NH_3$ (J=K=3) is composed of 12 individual hyperfine transitions

which have frequencies very close to the frequency of transitions in the absence of hyperfine structure. The satellite on the high frequency side of the main line is composed of 9 transitions for which $\Delta F = +1, \Delta F_1 = 0$, while the one on the low frequency side has $\Delta F = -1$, $\Delta F_1 = 0$ and also has 9 components, 65 kHz on each side of the main line transition. On either side of the main line lie the quadrupole satellites each of which has 7 components. For the inner quadrupole satellites ($\Delta F_1 = \pm 1$, $F_1 = 4 \leftrightarrow 3$) are 1.690 MHz from the centre line ($\Delta F_1 = 0$) and the outer quadrupole satellites ($\Delta F_1 = \pm 1, \Delta F_1 = 2 \leftrightarrow 3$) are 2.350 MHz from the centre line. The outer quadrupole satellites are split over the range of $\pm$ 50 kHz and the inner satellites by $\pm$10 kHz

1.5 Theory of the hyperfine structure of ammonia

It is possible for any individual nucleus in the molecule to possess its own spin, magnetic moment and electric quadrupole moment. Interactions of these with the rotational energy of the molecule, cause changes in the quantum states of the molecular rotation as a whole. Mainly, these are magnetic and electric interactions which arise from the nuclear magnetic moment coupling with the magnetic field due to molecular rotation, and the nuclear electric quadrupole moment interacting with the gradient of the electric field produced by the rest of the molecule. Since the electric interaction strength is quite large compared with that of the magnetic interactions caused by the molecular rotation, the splitting of the energy levels caused by quadrupole moment transitions produce a well resolved hyperfine structure, while the splitting of the energy levels by the magnetic field is comparatively small.

In the case of symmetric top molecules, the energy of the electric quadrupole interactions (Coles and Good 1946, Jauch 1947 and Van Vleck 1947), can be expressed by:

$$E = \left(\frac{\partial^2 V}{\partial Z^2}\right) eQ \left[\frac{3K^2}{J(J+1)} - 1\right] \left[\frac{\frac{3}{4}G(G+1) - I(I+1)J(J+1)}{2(2J+3)(2J-1)(2I+1)I}\right] \qquad (9)$$

where $G = F(F+1) - I(I+1) - J(J+1)$

$$Q = \frac{1}{e}\int \left[3Z^2 - (X^2+Y^2+Z^2)\right] dq$$

$$V = \frac{ne}{r} - \frac{eQ}{4r^5}(X^2+Y^2-2Z^2)$$

$$r^2 = X^2+Y^2+Z^2$$

F is the total angular momentum including the nuclear spin

$\left(\frac{\partial^2 V}{\partial Z^2}\right)$ is the gradient of the electric field and equal to $\int \frac{3Z^2 - r^2}{r^5} dq$

Q is the electric quadrupole moment

dq is an element of charge within the nucleus with the co-ordinates X,Y, and Z.

The selection rules for transition between these levels are:

$$\Delta J = \pm 1, \quad \Delta K = 0, \quad \Delta F = \pm 1.$$

Experimental measurements on the hyperfine structure produced by quadrupole interactions to fit equation (9) showed some deviations of the order of a megacycle. Gunther-Mohr and et al (1954) and Gordon (1955) and others extended the theory to account for these deviations and accurate determinations of hyperfine structure. In their attempt, the discrepancies between the theory and experimental data became much smaller. They introduced a correction term $\vec{I}_N \cdot \vec{J}$ to the molecular Hamiltonian.

It was found that with a high resolution spectrometer, the quadrupole coupling constant (eqQ), under the effect of

centrifugal distortion was larger for the lower inversion state by 0.01% than for the upper inversion state and the sign of this constant was directly measured to be negative.

Hunderson and Van Vleck (1948) first derived an expression with special reference to the case of an ammonia molecule for different interaction energies by relating the molecular magnetic field to the different rotational quantum numbers;

$$\Delta E = \left\{aK^2 \left[J(J+1)^{-1}\right] + b\right\}\left[F(F+1)-J(J+1)-I(I+1)\right] \qquad (10)$$

Simmons and Gordy (1948) noticed a shift in the position of the nitrogen quadrupole hyperfine structure relative to the previous result, which was attributed to the interaction of the nitrogen magnetic moment with the molecular magnetic field. An additional splitting of the line was observed by Good et al (1951).

In 1954 Gunther-Mohr and et al, carefully re-examined the structure of the hyperfine spectrum of the ammonia molecule in the microwave region. They found that the quadrupole line spacing for $K \neq 1$ can be fitted within experimental error to previous theory taking into account the change in the quadrupole coupling constant (eqQ) due to centrifugal distortion of the molecule.

In 1955 Gordon used a high-resolution microwave spectrometer with a total width at half maximum of 7 kHz. With this narrow line width, the magnetic hyperfine structure caused by the orientation of the spins of hydrogen nuclei was resolved and fitted to the theoretical data within an error of about 1 kHz. A theoretical treatment of the magnetic interactions has been made which is different from that which has previously been used and the theoretical analysis of Gunther-Mohr et al (1954) has been extended to include evaluation of the mutual spin-spin interaction of the hydrogen nuclei. The final form for the complete hyperfine energy was expressed by:

$$W_{JKF_1} = -\langle eqQ \rangle \left(1 - \frac{3K^2}{J(J+1)} \right) \Omega_1 (J, I_N)$$
$$+ \left[a + \frac{(b-a)K^2}{J(J+1)} \right] (\vec{I}_N \cdot \vec{J})$$
$$+ \left[A + \frac{CK^2}{J(J+1)} \right] \frac{(\vec{I} \cdot \vec{F}_1)(\vec{F}_1 \cdot \vec{J})}{F_1(F_1+1)}$$
$$+ 2 g_H g_N \mu_o^2 \left\langle \frac{1 - 1.5 \sin^2\beta}{r_{NH}^3} \right\rangle \frac{(\vec{F}_1 \cdot \vec{I}) \Omega_2(J, I_N)}{F_1(F_1+1)} \left(1 - \frac{3K^2}{J(J+1)} \right)$$
$$- 0.25 (g_H \mu_o^2) \left\langle \frac{1}{r_{HH}^3} \right\rangle \frac{\phi(F_1, I)\, \phi(J, F_1)}{F_1(F_1+1)}$$
$$\times \left(1 - \frac{3K^2}{J(J+1)} \right) - \delta_{K_1} (-1)^{J+\nu} 2f \qquad (11)$$

where $2f = \left\langle \frac{1.5 \sin^2\beta}{r_{NH}^3} \right\rangle 2 g_H g_N \; 2 \frac{(\vec{F}_1 \cdot \vec{I})\; {}_2(J, I_N)}{F_1(F_1+1)} + \frac{(\vec{I} \cdot \vec{F}_1)(\vec{F}_1 \cdot \vec{J})}{F_1(F_1+1)}$

$$, \Omega_1(J, I_N) = \frac{3(\vec{I}_N \cdot \vec{J})^2 + 1.5(\vec{I}_N \cdot \vec{J}) - I_N(I_N+1)\, J\,(J+1)}{(2J-1)(2J+3)\, 2I_N(2I_N-1)}$$

$$\Omega_2(J, I_N) = \frac{3(I_N \cdot J)^2 + 2J(J+1)\,(I_N \cdot J) - I_N(I_N+1)\, J\,(J+1)}{(2J-1)\,(2J+3)}$$

From the above equation the energy term due to hyperfine interactions between the nitrogen atom and the remainder of the ammonia molecule is given by:

$$W_{JKF_1} = -\langle eqQ \rangle \left(1 - \frac{3K^2}{J(J+1)} \right) \frac{3(\vec{I}_N \cdot \vec{J})^2 + 1.5(\vec{I}_N \cdot \vec{J}) - I_N(I_N+1) J(J+1)}{(2J-1)\,(2J+3)\, 2I_N\,(2I_N-1)}$$
$$+ \left[a + \frac{(b-a)\,K^2}{J(J+1)} \right] \vec{I}_N \cdot \vec{J} \qquad (12)$$

Equation (11) can be used to express the energy levels of a given rotational state (J,K) in terms of five adjustable parameters. Each of these parameters determines the type and strength of the interaction as follows:

(1) $-\langle eqQ\rangle\left(1-\frac{3K^2}{J(J+1)}\right)$ quadrupole coupling $\Omega_1(I,I_N)$; Nitrogen quadrupole interaction.

(2) $\left[a+\frac{(b-a)K^2}{J(J+1)}\right]$ magnetic coupling ($I_N.J$) Nitrogen magnetic interaction with molecular rotation.

(3) $\left[A+\frac{CK^2}{J(J+1)}+K_1(-1)^{J+\nu}B\right]$ magnetic coupling (I.J); hydrogen magnetic interaction with molecular rotation.

(4) $g_H g_N/\mu_o^2\left\langle\frac{1-1.5\sin^2\beta}{r_{NH}^3}\right\rangle\left[1-\frac{3K^2}{J(J+1)}\right]-g_H g_N\mu_o^2\left\langle\frac{1.5\sin^2\beta}{r_{NH}^3}\right\rangle\delta_{K_1}(-1)^{J+\nu}$ hydrogen-nitrogen spin-spin interaction.

(5) $-0.25\,(g_H/\mu_o)^2\left\langle\frac{1}{r_{HH}^3}\right\rangle\left[1-\frac{3K^2}{J(J+1)}\right]$ hydrogen-hydrogenspin-spin interaction.

The values of the magnetic constants in kHz are: A=-17.3±0.5, B= -14.1±0.3, C= -2.0±1.0, a = 6.66±0.2 and b = 6.66±0.2 .

For high values of J and K:

$$\langle eqQ\rangle = 4089\left[1+7.7\times10^{-5}\,J(J+1)+K^2\right]\pm 1.5\ \text{kHz} \qquad (13)$$

For low values of J and K:

$$\langle eqQ\rangle = -4092.4\left[1+5\times10^{-5}\,J(J+1)\right]\pm 1.5\ \text{kHz}$$

The magnetic hyperfine splitting in terms of quantum numbers can be given by:

$$E_m = W_{JKF_1}+eqQ\left[1-\frac{3K^2}{J(J+1)}\right]\frac{3I_N.J+1.5I_N.J-I_N(I_N+1)J(J+1)}{2I_N(2I_N-1)(2J-1)(2J+3)} \qquad (14)$$

The energy term of the spin-spin interaction among the three hydrogen nuclei is given by:

$$G^{HH} = (g_H/\mu_o)^2\, r_{HH}^{-3}\sum_{i<j}\left[\vec{I}_i.\vec{I}_j-3\,r_{HH}^{-2}(\vec{I}_i.\vec{r}_{ij})(\vec{I}_i.\vec{r}_{ij})\right] \qquad (15)$$

where $\vec{r}_{ij}$ is the distance between hydrogen nuclei i and j, and r_{HH} is the distance between hydrogen nuclei, Figure (1.4).

Since the only matrix elements of this interaction which affect

the spectrum are those that are diagonal in K, then the above formula can be written in the equivalent form (Gordon, 1955):

$$G^{HH} = -0.25\,(g_H \mu_o)^2 \left\langle \frac{1}{r^3_{HH}} \right\rangle \frac{\phi(F_1, I)\,\phi(J, F_1)}{F_1(F_1+1)} \left(1 - \frac{3K^2}{J(J+1)}\right) \qquad (16)$$

Equation (16) is valid so long as the quadrupole energy term is large compared with the magnetic terms. However, in the case of ammonia for the (J=3, K=2) inversion line the quadrupole coupling energy disappears because of the factor $\left(1 - \frac{3K^2}{J(J+1)}\right)$ is equal to zero, hence this equation is no longer valid.

As a result of previous work (Gordon 1955 , Kukolich 1967 and others), and the existing analysis of the hyperfine structure theory, some conclusions can be drawn about the state of the theory of hyperfine structure of this particular molecule.

On the basis of the hyperfine structure theory developed and with the precision of molecular beam maser techniques, an accuracy of the order of 10 Hz can now be obtained. In order to increase the accuracy of calculation of molecular interactions, it is necessary to take into account the excitation of the spin moment of the electrons as a result of their interactions with the angular momentum of the molecule. Therefore, it is necessary to include an additional term for the electron spin excitation in the initial Hamiltonian for the hyperfine structure. Furthermore, owing to the dependence of the hyperfine structure constant on the vibrational-rotational perturbations which cause centrifugal distortion of the molecules, a modified treatment should be undertaken. However, the solution of this

complex problem requires the use of advanced methods using electronic computers to calculate the magnitude of the intermolecular fields created by the distribution of electronic charges.

1.6 Quantum analysis of wave functions of the inversion motion of nitrogen atom in the $^{14}NH_3$ molecule.

The penetration of a potential barrier has no analogue in classical mechanics because it corresponds to a situation in which a particle has a negative energy or imaginary momentum. If we consider the problem according to quantum mechanics when $E < E_0$ and $E > E_0$, the solution of Schrödinger's equation for regions 1,2 and 3 (Figure 1.7), for the first case ($E<E_0$) has the following components:

$$\psi_1 = A \exp(iKx) + B \exp(-iKx) \tag{17}$$

$$\psi_2 = C \exp(Lx) + D \exp(-Lx) \tag{18}$$

$$\psi_3 = \acute{A} \exp(iKx) \tag{19}$$

where $K^2 = 2mE/\hbar^2$, $L^2 = 2m(E_0-E)/\hbar^2$, E_0 is the height of the potential barrier and E is the energy of the particle. The wave function ψ_1 contains the incident and the reflected wave. ψ_2 decays exponentially within the potential barrier but it does not go to zero at x = a. Therefore it continues into region 3 with the oscillatory form ψ_3. This oscillatory condition represents the transmitted particles which have the same energy as the incident particle but with amplitude $\acute{A}$ different from A. Hence, quantum mechanically it is possible for a particle to penterate the potential barrier even if its kinetic energy is less than the height of the potential barrier. In the second case where $E > E_0$, some of

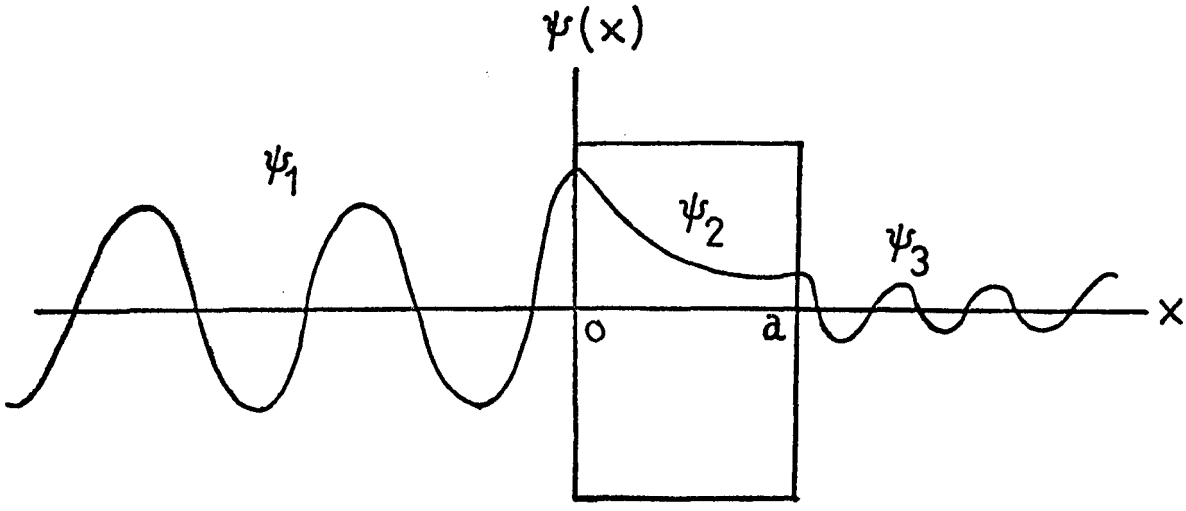

Fig(1.7) WAVE FUNCTION CORRESPONDING TO THE POTENTIAL BARRIER WHEN $E < E_0$.

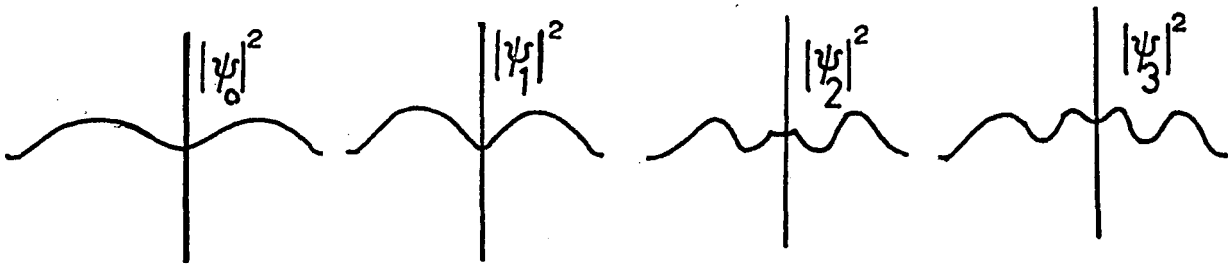

Fig(1.8) PROBABILITY DENSITIES OF THE WAVE FUNCTIONS ψ_0, ψ_1, ψ_2 AND ψ_3.

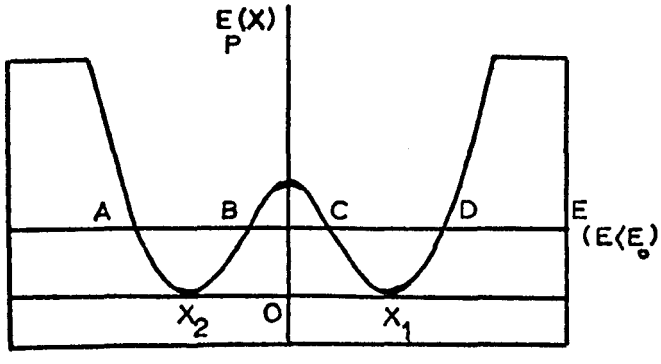

Fig(1.9) POTENTIAL ENERGY FOR THE INVERSION OF THE NITROGEN ATOM IN NH_3.

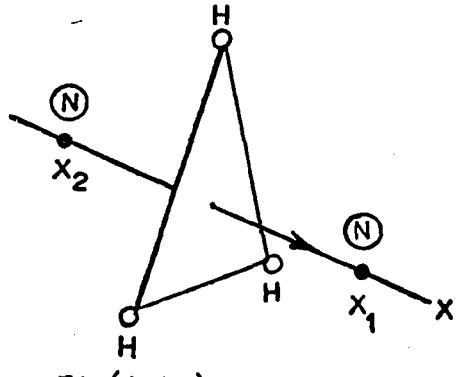

Fig(1.10) INVERSION MOTION OF THE NITROGEN ATOM IN NH_3.

the particles are reflected at x = 0 and x = a. Therefore the wave functions in the three regions are now:

$$\psi_1 = A \exp(iKx) + B \exp(-iKx) \qquad (20)$$

$$\psi_2 = C \exp(i\acute{K}x) + D \exp(-\acute{K}x) \qquad (21)$$

$$\psi_3 = \acute{A} \exp(iKx)$$

where $\acute{K}^2 = 2m(E-E_0)/\hbar^2$, $\hbar\acute{K}$ is the momentum of the particles while crossing the potential barrier.

Figure (1.8) indicates the probability densities corresponding to the wave functions. Quantum analysis of these probability densities show that $|\psi_0|^2$ and $|\psi_1|^2$ are almost identical except $|\psi_0|^2$ represents a slightly greater probability of finding the nitrogen atom closer to the potential barrier than $|\psi_1|^2$. Therefore, the energies E_0 and E_1 of the corresponding stationary states must be almost equal. Although the similarity of ψ_2 and ψ_3 is not so close as for ψ_0 and ψ_1 whereas $|\psi_2|^2$ and $|\psi_3|^2$ are almost the same, the energy levels E_2 and E_3 must be very close.

Figure (1.9) illustrates the potential barrier of the ammonia inversion motion. The wave function between A and B will be oscillatory, while to the right of B it must vary exponentially. However, at C the wave function still has a finite value. Between C and D, the wave function becomes oscillatory again and to the right of D the waveform decreases exponentially once more.

From the above argument we can conclude that, if the particle is initially between A and B, at a later time it may be between C and D or vice versa. Thus, there is always a finite probability that the particle will be found between A and B which means that the particle must penetrate the potential barrier between B and C.

In the case of the ammonia molecule in which the nitrogen atom is at the vertex of the pyramid and the three hydrogen atoms are at the triangular base, the nitrogen atom may be located at one of the two symmetric equilibrium positions X_1 and X_2, Figure (1.10) , on either side of the base of the pyramid. If the nitrogen atom is initially at X_1 it is possible to penetrate the potential barrier and appear at X_2. If the energy of this motion is less than the height of the potential barrier ($E < E_o$), the motion of the nitrogen atom is composed of an oscillatory motion between A and B or between C and D depending on which side of the plane it happens to be, plus a much slower oscillatory motion between the two classical regions passing through the potential barrier. The frequency of this second motion is 23.786×10^9 Hz for the ground state of $^{14}NH_3$.

The potential energy of the inversion motion in $^{14}NH_3$ is similar to the potential energy of a simple harmonic oscillator with a barrier at the centre. The effect of this barrier is that of a perturbation which affects the motion of the particle as it passes through the centre. For nitrogen atoms, $E < E_o$ causes a decrease in the probability of finding the nitrogen atoms in the central region. In other words the barrier distorts the wave functions of the harmonic oscillator potential in the central region, i.e. decreasing their amplitude in that region.

The potential energy for the inversion motion of the nitrogen atom in the NH_3 molecule has a centre of symmetry and the corresponding wave functions are even or odd. The even or symmetric wave functions are designated by (s) and odd or antisymmetric ones by (a). Successive even and odd wave functions are designated Os, Oa, 1s, 1a. Figure (1.11) shows the

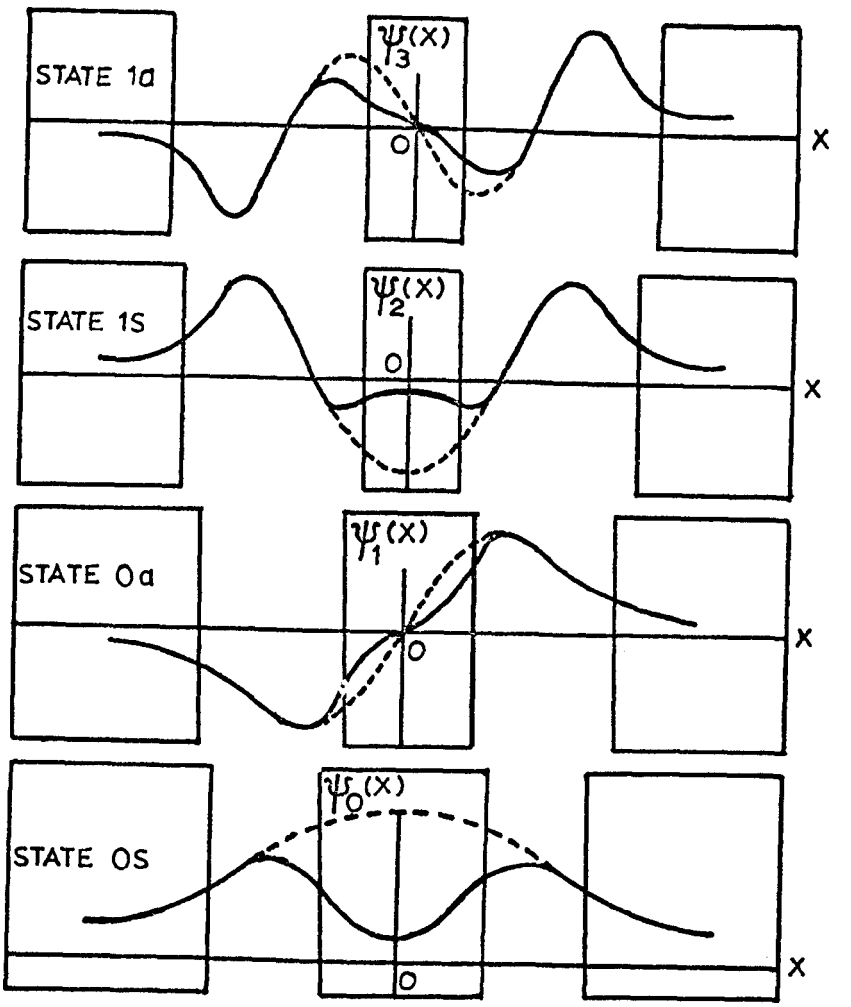

Fig (1.11) WAVE FUNCTIONS CORRESPONDING TO THE FOUR LOWEST ENERGY LEVELS OF THE INVERSION MOTION IN $^{14}NH_3$.

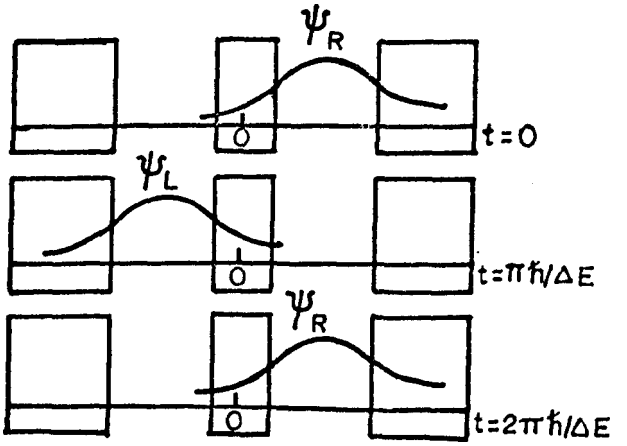

Fig (1.12) DESCRIPTION OF THE INVERSION MOTION IN $^{14}NH_3$ BY MEANS OF TIME-DEPENDENT WAVE FUNCTIONS.

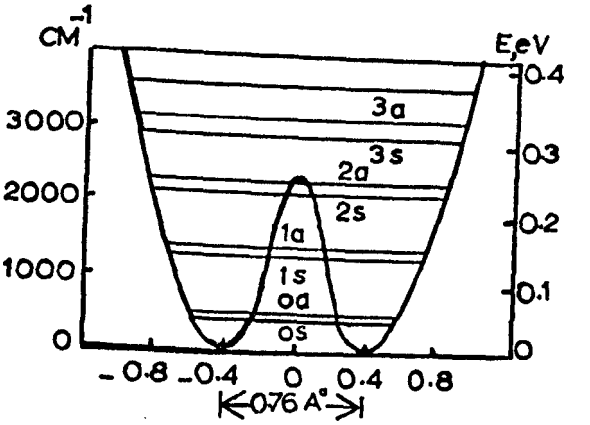

Fig (1.13) ENERGY LEVELS FOR THE INVERSION MOTION IN $^{14}NH_3$.

actual four wave functions corresponding to the four lowest energy levels Os, Oa, ls and la of the inversion motion in NH_3. The effect of the central barrier is taken into account (solid lines), whereas the dashed lines are the wave functions for the harmonic oscillator potential without the effect of the central barrier.

Figure (1.13) represents the energy levels for inversion motion in NH_3. The height of the potential barrier is about 0.254 eV. The separation between the pair of energy levels (inversion doublet) Os and Oa corresponding to wave functions ψ_0 and ψ_1 or between the pair of levels ls and la corresponding to ψ_2 and ψ_3 is very small compared with the separation between the two pairs of energy levels.

To describe the inversion motion in the ammonia molecule by means of a time-dependent Schrödinger equation, we suppose that the nitrogen atom is initially in the right hand potential well ground state which implies that the wave function at the right is larger than at the left, Figure (1.12). Therefore, the initial wave function can be written as:

$$\psi(x,0) = \psi_R$$

Since ψ_0 and ψ_1 are almost identical to each other then:

$$\psi(x,0) = \psi_R \simeq \psi_0 + \psi_1 \qquad (22)$$

After a certain time, the wave function takes the following form: $\psi(x,t) = \psi_0 \exp(-iE_0 t/\hbar) + \psi_1 \exp(-iE_1 t/\hbar)$ (23)

letting $E_1 - E_0 = \Delta E$ we get:

$$\psi(x,t) = \left[\psi_0 + \psi_1 \exp(-i\ Et/\hbar)\right] \exp(-E_0 t/\hbar) \qquad (24)$$

At a time $t = \pi\hbar/\Delta E$, the exponent in the parentheses is (-1), Hence:

$$\psi(x,t) = (\psi_0 - \psi_1) \exp(-iE_0 t/\hbar) = \psi_L \exp(-iE_0 t/\hbar) \qquad (25)$$

where, from the shape of ψ_0 and ψ_1 as shown in Figure (1.12)

it is clear that

$$\psi_L \simeq \psi_0 - \psi_1 \qquad \text{and is concentrated on the left} \qquad (26)$$

Therefore, the nitrogen atom has the maximum probability of being found in the left potential well, thus the ammonia molecule has been inverted. Moreover, at $t = 2\pi\hbar/\Delta E$ the nitrogen atom is again back on the right, and so on.

To calculate the frequency of inversion of NH_3 we use the formula:

$$\nu = \frac{\Delta E}{2\pi\hbar} = \frac{E_1 - E_0}{h} \qquad (27)$$

in which $\nu = 2.39 \times 10^{10}$ Hz where $E_1 - E_0 = 9.8 \times 10^{-5}$ eV. See Table 1.

Level	cm^{-1}	Energy (eV)
3a	2861	0.3547
3s	2380	0.2950
2a	1910	0.2367
2s	1597.4	0.1980
1a	986.00	0.1222
1s	950.16	0.1178
0a	0.79	9.84×10^{-5}
0s	0.00	0

$1 \text{ eV} = 8067.5 \text{ cm}^{-1}$

Table 1: Vibrational energy levels for axial motion of nitrogen atom in NH_3 relative to the ground state.

CHAPTER 2

THE STARK EFFECT

2.1 Introduction

Symmetric top molecules have a component of the electric dipole moment along the direction of the total angular momentum vector equal to $\mu K/\sqrt{J(J+1)}$. The first-order Stark splitting of the energy levels will occur for all values of K except when K = 0. Hence, the component of the dipole moment along the direction of the external electric field has the value of $\frac{\mu K}{\sqrt{J(J+1)}} \cdot \frac{M}{\sqrt{J(J+1)}}$. This splitting is large even for small external electric fields and independent of the moment of inertia of the molecule. The general expression of the interaction for a symmetric top type molecule without inversion is given by (Oraevskii 1967):

$$W_{JKM} = -\frac{KM}{J(J+1)}\mu_0 E + \left\{\frac{[3K^2-J(J+1)][3M^2-J(J+1)]}{J^2(J+1)^2(2J-1)(2J+3)} - \frac{M^2K^2}{J^3(J+1)^3}\right\}\frac{(\frac{1}{2}E)^2}{2hB} + \ldots \quad (1)$$

where E is the electric field, μ_0 is the dipole moment of the molecule, B is the rotation constant of the molecule.

In the case of a weak applied electric field, only the linear term of equation (2.1) should be taken. Hence, the first-order Stark splitting in a symmetric-top type molecule has an energy given by:

$$\Delta W = -\mu_E \cdot E = -\mu_0 \frac{KM}{J(J+1)} E \quad (2)$$

and the radial force on the molecule is:

$$F = -\text{grad } W = \mu_0 \frac{KM}{J(J+1)} \frac{dE}{dr} \quad (3)$$

which corresponds to frequency splitting of:

$$h.\Delta\nu = \frac{2\mu_0 K M}{J(J+1)(J+2)} E \quad (4)$$

2.2 The Stark effect in ammonia.

In ammonia beam masers, the Stark effect in the vibrational levels is used to produce more molecules in the upper of the two levels of an inversion doublet by employing inhomogeneous electric fields. The mechanism of sorting molecules into upper or lower states depends on the existence of various energy levels of the molecules which interact differently with an applied electric field. Although the ammonia molecule is a symmetric top, its Stark splitting is a special case due to its non-permanent dipole moment which changes the inversion frequency. Therefore, a second-order Stark splitting rather than first-order should be applied (Coles and Good 1946).

Neglecting the hyperfine effects, the energies of the inversion states of the ammonia molecule for all field strengths are given by:

$$W = W_o \pm \sqrt{\left(\frac{h\nu_o}{2}\right)^2 + \left(\frac{\mu_o EMK}{J(J+1)}\right)^2} \qquad (5)$$

where W_o is the average energy of the upper and lower inversion levels, ν_o is the inversion frequency in zero field. μ_o is the permanent dipole moment, E is the electric field, M is the projection of J on the direction of the field.

The electric interaction energy ΔW_E of molecules in the upper energy state is given by:

$$\Delta W_E = \left\{\left(\frac{h\nu_o}{2}\right)^2 + \left(\frac{\mu_o EMK}{J(J+1)}\right)^2\right\}^{\frac{1}{2}} - \frac{h\nu_o}{2} \qquad (6)$$

The force on the molecule along the direction of the field gradient is:

$$F = -\text{grad } W = \pm \frac{\left[\mu_o MK/J(J+1)\right]^2 E \frac{dE}{dr}}{\sqrt{(h\nu_o/2)^2 + \left[\mu_o EMK/J(J+1)\right]^2}} \qquad (7)$$

and the frequency splitting can be given by:

$$\Delta\nu\,(cm^{-1}) = 1.5 \times 10^{-4} \left[\mu_o EMK/J(J+1)\right]^2 \qquad (8)$$

The Stark energy as a function of transverse distance x from the molecular beam axis leads to a potential well of the form shown in Figure (2.1). This potential well confines the upper state molecules which satisfy the condition for focusing such that:

$$\tfrac{1}{2} m v_r^2 < W_{E_m} = \tfrac{1}{2} m v_c^2 \qquad (9)$$

where m is the mass of the molecule, v_r is the molecular transverse velocity and v_c the critical transverse velocity.

Figure (2.2) shows the Stark energy levels for J=3, K=3 inversion of NH_3. Molecules in an electric field with (M=0) levels are not deflected and molecules in the upper states with ($M \neq 0$) increase in energy, while molecules in the lower states decrease in energy.

The electric field of the state separator exerts forces on the molecules due to their induced dipole moments. A precession of total angular momentum vector J takes place around the direction of the electric field. Due to different orientations of the total angular momentum with respect to a direction fixed in space, the energy levels of the ammonia molecules have a $(2F_1+1)$ degeneracy. Each of the $(2F_1+1)$ levels corresponds to a different M value with different energy. On the other hand, in the absence of the electric field such quantization is not possible and $(2F_1+1)$ states will have identical energy levels. With an increasing field strength, the inversion starts to be quenched and an average dipole moment is obtained, while in zero field there will be no average dipole moment. The induced electric dipole transition perturbs the energy of the states so that the energy of the upper states increase in a high field

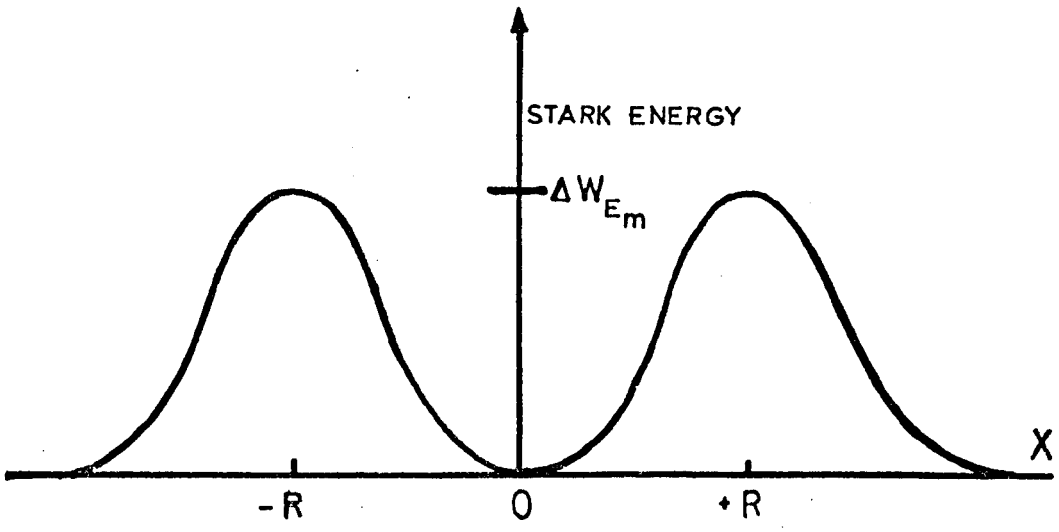

Fig (2.1) STARK ENERGY ΔW_E AS A FUNCTION OF DISTANCE X FROM THE MOLECULAR AXIS.

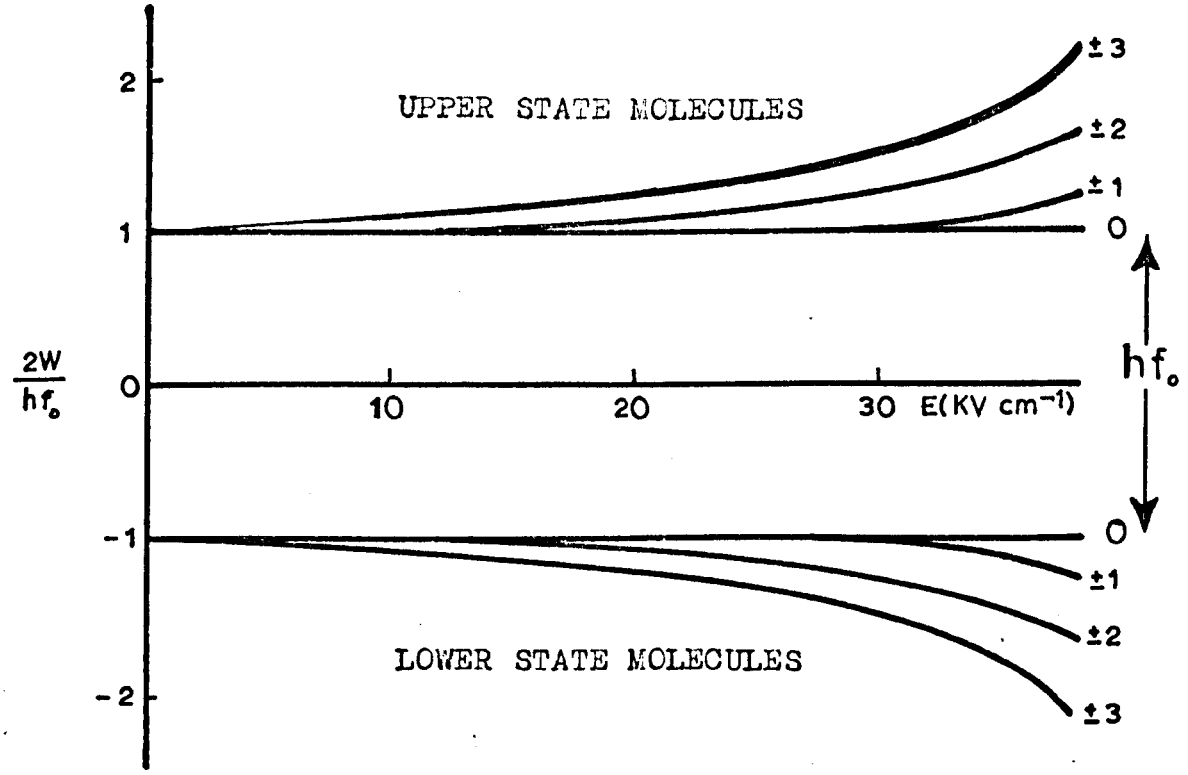

Fig (2.2) STARK EFFECT FOR J=3, K=3 INVERSION TRANSITION OF $^{14}NH_3$.

region whereas the energy of the lower states decrease in a high field region.

2.3 Energy states under the action of weak and strong electric fields.

A detailed theoretical treatment of the Stark splitting produced in ammonia, including the quadrupole interaction has been given by Jauch (1947). In his treatment the displacement of the absorption lines of ammonia molecules is considered under the conditions of weak electric field ($E < E_c$) and strong electric field ($E > E_c$).

It was observed that the hyperfine structure for intermediate values of $E_c \sim 30 - 100$ kV/m is quite complicated, and general solution for the secular equation does not seem to be feasible. Under the assumption of weak electric field, the number of molecules in the upper states which leave the state separator exit with a given value of M is proportional to M^2. The molecules enter and leave the separator making very few transitions between different quadrupole levels. In addition, the dependence of the focusing strength on M causes a substantial increase in the relative population of the higher energy quadrupole levels. If the change in the relative population of the quadrupole level is very large due to the strength of the electric field, this allows the possibility of producing direct quadrupole transitions of the active molecules in the region between the focuser and the cavity. Thus, the cavity can be considered as a detector, the quadrupole resonances being observed by the changes in intensity of the quadrupole satellite of the microwave transitions (Gordon 1955).

At intermediate fields, the stationary states have a one to one correspondence with low or high-field states. When

the electric field is increased slowly, the state of the molecule with a specified quantum state will progress through the intermediate configurations and at high field will be found in a particular high-field state. In taking into account the effect of the hydrogen spins, each of the quadrupole levels will undergo further splitting in zero electric field by the magnetic interactions of the hydrogen spin with the molecular magnetic field. The zero field magnetic hyperfine splitting is of the order of 50 kHz.

According to equation (1.11) molecules with quantum numbers $F_1 = 3$ have the highest energy states, followed by $F_1 = 4$ and $F_1 = 2$ states respectively. From figure (2.3) it can be seen that molecules in a weak electric field tend to go to the lower energy states of the high field region. A closer look at this configuration shows the quantum states $F_1 = 3$, $F_1 = 4$, $F_1 = 2$ and hence the corresponding M_F states undergo changes in their states as follows:

(1) $F_1 = 3$: with seven M_{F_1} low-field states
- 4 go at high field to $M_J = 3$ states
- 2 go at high field to $M_J = 2$ states
- 1 goes at high field to $M_J = 1$ state

(2) $F_1 = 4$: with nine M_{F_1} low field states
- 2 go at high field to $M_J = 3$ states
- 4 go at high field to $M_J = 2$ states
- 3 go at high field to $M_J = 1$ state

(3) $F_1 = 2$: with five M_{F_1} low field states
- 3 go at high field to $M_J = 0$ state
- 1 goes at high field to $M_J = 1$ state

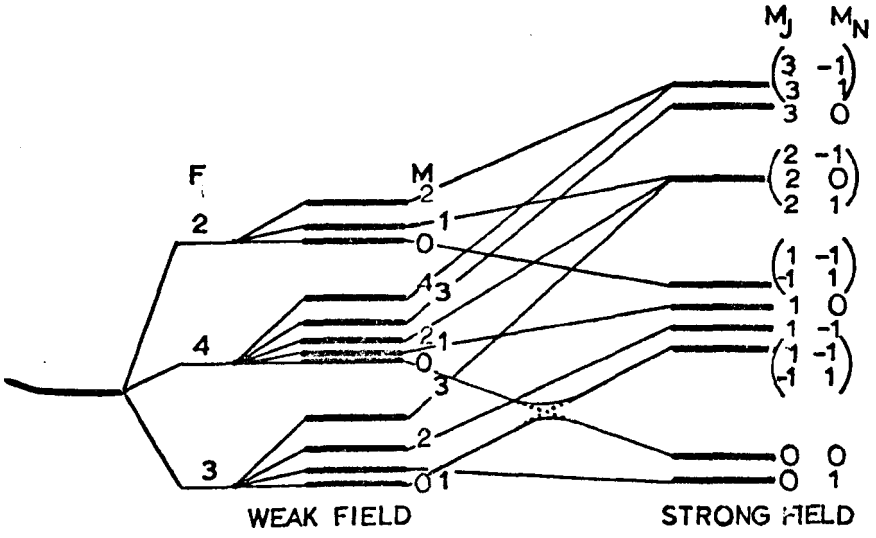

STARK SPLITTING OF UPPER ENERGY STATES IN AMMONIA INVERSION LINE J=K=3 FOR WEAK AND STRONG INHOMOGENEOUS ELECTRIC FIELD.

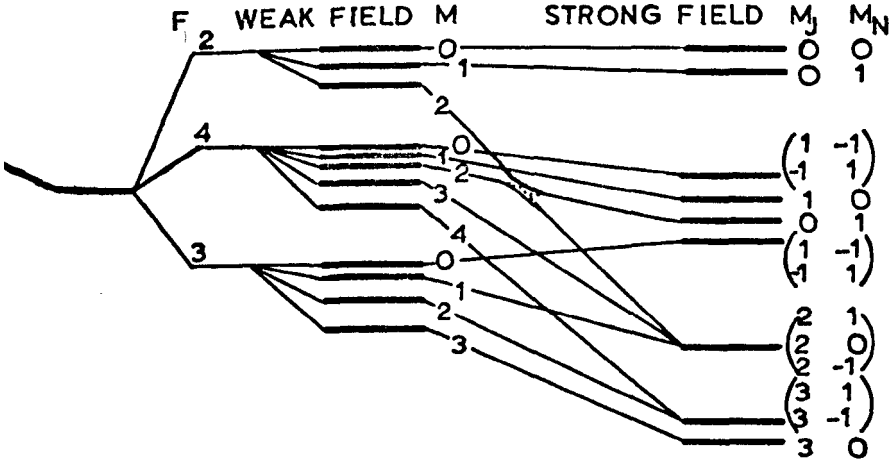

Fig (2.3) STARK SPLITTING OF LOWER ENERGY STATES IN AMMONIA INVERSION LINE J=K=3 FOR WEAK AND STRONG INHOMOGENEOUS ELECTRIC FIELD.

2.4 Influence of the separator field on the intensity of the hyperfine structure lines

In zero, or a weak electric field such that $(E|\mu_{12}| \ll eqQ)$ the energy of the $^{14}NH_3$ molecule is determined by the quantum numbers F_1 and M_{F_1}. The population of energy levels of the molecules entering the separator are equal. Within the separator the energy levels undergo strong Stark splitting $(E|\mu_{12}| \ll eqQ)$. The relation $F_1 = J+I_N$ is violated, thus to each level F_1 and M_{F_1} in the weak field there will be a corresponding definite strong field level, M_J and M_I.

If we consider the transition from weak to strong electric field as an adiabatic process, and the separation of the molecules proceeds statistically independently for all molecular energy states, then the populations of the F_1 and M_{F_1} states on leaving the separator depend only on the appropriate value of M_J in the strong field. The effectiveness $\phi(M_J)$ of separating the level M_J is given by:

$$\phi(M_J) = \sqrt{1 + a^2 M_J^2} - 1 \simeq a\,|M_J| - 1 \qquad (10)$$

where (a) is a factor which is proportional to the voltage on the state separator. Therefore, the population of the F_1 and M_{F_1} levels on leaving the state selector are proportional to the applied voltage. From the assumption that the number of molecules in a given M state which reach the cavity is proportional to M^2, the population of each F_1 level in the cavity, as well as the relative intensities of various quadrupole level transitions, must be weighted according to a factor given by (Gordon 1955):

$$\frac{\sum_M N(M)\,M^2}{2F_1 + 1} \qquad (11)$$

where N(M) gives the number of low field states which go into the particular high field states with quantum number(M).

A calculation shows the value of these weighting factors for ammonia (J=K=3) inversion line with the states F_1=3, F_1=4 and F_1 = 2 are 45/7, 37/9 and 2/5 respectively (See Appexdix 1).

2.5 Separation of molecules according to inversion states

The mechanism of state separation of the molecules in an inhomogeneous electric field can be treated on the basis of quantum mechanics. If we assume that the two energy states of the molecules are W_1 and W_2 ($W_2 > W_1$), then ψ_1 and ψ_2 are the wave functions of the two energy states respectively, hence:

$$H_o\psi = W\psi \tag{12}$$

where $\psi = a\psi_1 + b\psi_2$ and H_o is the Hamiltonian of the noninteracting molecule. In the presence of an electric field, the interaction Hamiltonian takes the form of:

$$H = H_o - \vec{\mu} \cdot \vec{E} \tag{13}$$

Hence: $(H_o - \vec{\mu}.\vec{E})(a\psi_1 + b\psi_2) = W(a\psi_1 + b\psi_2)$

where W is the energy of the molecule in the field. Since ψ_1 and ψ_2 satisfy the orthogonality condition, then for a and b the following linear equations can be obtained:

$$(W_1 - \mu_{11}E)a + \mu_{12}E\,b = 0 \tag{14}$$

$$\mu_{12}E\,a + (W_2 - \mu_{22}E - W)b = 0 \tag{15}$$

From the above equations, the two values of molecular rotational energy are given by:

$$W_{A,B} = W_1 + W_2 - \mu_{11}E - \mu_{22}E \pm \sqrt{W_2 - W_1 + (\mu_{11} - \mu_{22})E^2 + 4\mu_{12}^2E^2} \tag{16}$$

Then the wave functions which correspond to these energies are:

$$\psi_1 = a\psi_1 + b\psi_2 \tag{17}$$

$$\psi_2 = a\psi_1 - b\psi_2 \tag{18}$$

where

$$a = \left[\frac{\sqrt{h^2\nu_{21}^2 + 4|\mu_{12}|^2 E^2} + h\nu_{21}}{2\sqrt{h^2\nu_{21}^2 + 4|\mu_{21}|^2 E^2}}\right]^{\frac{1}{2}} \tag{19}$$

$$b = \left[\frac{\sqrt{h^2\nu_{21}^2 + 4|\mu_{12}|^2 E^2} - h\nu_{21}}{2\sqrt{h^2\nu_{21}^2 + 4|\mu_{21}|^2 E^2}}\right]^{\frac{1}{2}}$$

$|a|^2 + |b|^2 = 1$ and $W_2 - W_1 = h\nu_{21}$

From the above equations it can be seen that the external electric field creates two energy states as a result of interaction between the field and the dipole moment of the molecules.

In many practical interacting cases $\mu_{11} = \mu_{22} = 0$, then:

$$W_A = -\frac{h\nu_{21}}{2}\left(\sqrt{1 + \frac{4|\mu_{12}|^2 E^2}{h^2\nu_{21}^2}} - 1\right) \tag{20}$$

$$W_B = \frac{h\nu_{21}}{2}\left(\sqrt{1 + \frac{4|\mu_{12}|^2 E^2}{h^2\nu_{21}^2}} - 1\right) \tag{21}$$

Equations (20) and (21) show, when E is increasing, the magnitude value of both W_A and W_B increases. Thus the molecules in the upper states will be deflected to the region of minimum inhomogeneous electric field and those in the lower state to the region of maximum field.

In a calculation of the number of excited molecules in the sorting system many factors should be taken into account such as Maxwellian velocity distribution, the angles of capture and the energy states of the molecules. Two equations of motion for the molecules in the electric field

of the sorting system are required. The Lagrangian for the molecules in upper and lower states under the action of an electric field is dependent on the potential energies W_A and W_B of the molecules, located initially in the lower state ψ_1 and in the upper state ψ_2.

The minimum length for the state separator can be calculated by solving the equation of motion for a molecule in the separator field. The potential barrier of a ring separator is a parabola which may be taken as different from zero only close to the rings and the minimum length of the ring separator must be calculated from the mean angle of capture. The maximum angle of capture is given by the relation(Shcheglov 1961):

$$W_m = \frac{m \bar{v}^2 \sin^2 \theta_{max}}{2} \qquad (22)$$

where W_m is the maximum interaction energy of a molecule in the separator field, $\bar{v}$ is the average speed of the molecules in the beam and θ_{max} is the maximum angle of capture between the direction of the beam and the state separator axis. The minimum length for the ring state separator is:

$$L_{min} = 3 R \cot \theta_{max} \qquad (23)$$

where R is the radius of the ring.

The number of the separated molecules according to the inversion states in an inhomogeneous electric field is given by:

$$(N_{JKM_J})_{sep} = N_{JKM_J} \frac{W}{kT} \qquad (24)$$

where $W \ll kT$ at room temperature, N_{JKM_J} is the number of molecules in the level characterized by the quantum numbers J,K and M_J. W is the maximum displacement of the inversion level of the molecules in the field which is:

$$W = \frac{h\nu_{21}}{2} \left(\sqrt{1 + \frac{4 |\mu_{12}|^2 E^2}{h^2 \nu_{21}^2}} - 1 \right) \qquad (25)$$

where $h\nu_{21}$ is the energy of the inversion interaction, E is the maximum field intensity of the state separator, $|\mu|$ is the matrix element of the dipole moment which is equal to:

$$\mu_0 \left| \frac{KM_J}{J(J+1)} \right| \qquad (26)$$

In the case of ammonia inversion lines the factor $2|\mu_{12}|E/h\nu_{12} \ll 1$, therefore, equation (25) can be reduced to:

$$(N_{JKM_J})_{sep} \simeq N_{JKM_J} (|\mu_{12}|E)^2 / h\nu_{12}kT \qquad (27)$$

For the ring state separator which was used for the investigations described in this thesis (r = 2 mm and l = 2 mm) with the maximum field intensity of $E_{max} = 1.74 \frac{V}{l}$, (l is the distance between two successive rings). The expression for the number of separated active molecules has the following form:

$$(N_{JKM_J})_{sep} = (N_{JKM_J} h\nu_{21}/2kT)\left(\sqrt{1+4\left(\frac{1.74V/l|\mu_{12}|}{h\nu_{12}}\right)^2}-1\right) \qquad (28)$$

where:

$$N_{JKM_J} = \frac{\pi \bar{v} R}{4\sqrt{2}\sigma} \qquad (29)$$

R is the radius of the beam source, $\bar{v}$ is the average velocity of the molecules in the beam and σ is the collision cross section of the molecules.

2.6 Ring-type state separator

Comparative investigations of different type of sorting systems (quadrupole, ring-type, bifilar, parallel ladder, tapered quadrupole and non-parallel double ladder) have been made by many investigators (Lainé 1970). It was established experimentally that the ring or bifilar helix focusers are the most effective sorting systems (with the same parameters such as length and voltage) and are about 4 times more

effective than a quadrupole focuser. According to Mednikov and Parygin (1963) a greater electric field intensity is obtained for the same voltage applied to their electrodes. This efficiency is also, in part, due to the longitudinal electric field between the ring electrodes which is parallel to the resonator field. Since those molecules which have maximum projection of molecular moment on the direction of electric field possess a larger angle of capture, therefore the interaction energy of the molecules with the field will be a maximum. By employing a cylindrical resonator tuned to the E_{010} resonance, the emission of the molecules inside the resonator is also at a maximum because of the highest possible projection of molecular moment on the direction of the electric field in the resonator. Furthermore, the width of the spectral line will be narrower due to the minimum Doppler effect in E_{010} mode excitation.

According to Becker (1963), the diameter D of the molecular beam of upper state molecules is given by:

$$D = \frac{eB}{a}\left[1 - \frac{a(e-a)}{ef}\right] \qquad (30)$$

where e is the distance between the nozzle and the diaphragm, B is the internal diameter of the separator, a is the distance between the nozzle and the centre of the separator, f is the focal length of the separator which is given by:

$$f(cm) = \frac{B}{bmV} \qquad (31)$$

where V is the potential on the rings, m is the number of the rings, and $b = 0.87 \times 10^{-6}$ per volt for ring focusers.

According to equation (30), calculation shows that for a given ring type focuser it is possible to obtain a narrow and highly directional beam.

For other type of oscillations in the resonator where the electric field is perpendicular to the beam axis, multipole capacitors may be preferable. However, this conclusion concerning mutual orientation of the fields in the sorting system and resonator should not be considered absolutely categorical. The reason for this is the possibility of pre-orientation of the sorted molecules in space which can cause a disturbance in the distribution of the molecules with respect to the projections of their angular moments into a certain direction in space.

In conclusion, multipole capacitors and other types of sorting systems with a constant cross section are not the optimum design for efficient state selection. A comparatively long sorting system is required because, when the molecular beam is on the axis of the sorting system, molecules travel a great distance along a curvilinear trajectory in a relatively weak field and only when the distance from the axis is sufficient do the molecules enter a high field.

Several techniques for obtaining beams of slow molecules by reflecting the molecules from a potential barrier as well as by employing ring type focusers have been proposed by Basov and Oraevskii (1959), White (1959), Gordon (1960) and Kazachok (1965). These methods are: Slowing down the molecules, removal of the molecules with large velocity and lowering the effective temperature of the molecular beam. Strakhovskii and Tatarenkov (1964) using a curved state separator of the ring type were able to select slow molecules from the beam. Kazachok in his theoretical treatment showed the feasibility of slowing down the molecules by means of a tapered ring focuser using weak and strong electric fields.

Enhancement of the frequency stability of a maser depends on the production of a narrow spectral line . If the dependence of the oscillation frequency of a maser upon Doppler broadening, unresolved hyperfine structure and non-uniformity of the emission of the molecules along the length of the resonator are eliminated, then the main factor which determines the frequency stability of the maser will be the time of flight of the molecules through the resonator. The time of flight can be increased either by lengthening the resonator or by decreasing the average speed of the molecules in the beam.

In a ring separator the molecular beam passes through a series of equally spaced rings which are alternately charged positive and negative (Figure 3.7). The expression for the potential of a number of rings has the form (Kazachok 1965):

$$\phi(y,z) = \frac{0.6\ V}{I_0(\frac{\pi R}{l})} I_0(\frac{\pi y}{l}) \sin\frac{\pi z}{l} + \frac{0.1\ V}{I_0(\frac{3\pi R}{l})} \sin\frac{3\pi z}{l} \qquad (32)$$

where V is the potential difference between two neighbouring rings, l and R, the distance between, and the radius of the rings respectively, y is the radial co-ordinate in the cylindrical co-ordinate system, z is the axis along the separator. The field inside the rings separator can be given by:

$$E = \frac{V \sin\frac{\pi}{2}(1-\frac{2\delta}{l})\frac{2\pi}{l}}{I_0(\frac{\pi R}{l})\frac{\pi}{2}(1-\frac{2\delta}{l})} \left[I_0^2(\frac{2\pi y}{l})\cos^2(\frac{2\pi y}{l}) + I_0^2(\frac{2\pi y}{l})\sin^2(\frac{2\pi y}{l})\right]^{\frac{1}{2}} \qquad (33)$$

where δ is the thickness of a ring and $I_0(x)$ is the modified Bessel function of the first kind of zero order, which may be written as:

$$I_0(x) = 1 + \frac{x^2}{4} - \frac{x^4}{2^4(2!)^2} + \cdots \qquad (34)$$

If it is assumed that the quantity $\frac{R}{l}$ is small then, $I_0(x) \simeq 1 + \frac{x^2}{4}$. If it is assumed that $\delta = 0$ and considering a paraxial case ($y=0$), then the magnitude of the field on the axis of the system will be:

$$E = \frac{4V\phi}{\left[1 + \left(\frac{\pi R}{l}\right)^2\right] l} \qquad (35)$$

and ϕ varies periodically from:

$$\cos(2\pi z/l)\,(1 + 4\pi^2 y^2/l^2) \quad \text{to} \quad (8\pi^2 y/l^2)$$

It is clear from the above expression that the electric field is varying periodically along the z axis, typically a variation between 0 and 15 Mvolts/m. Thus a great advantage of ring separators is that they produce an inhomogeneous electric field along the axis of the separator and the axial molecules are well separated with high efficiency.

2.7 Transition probabilities

The transition probabilities A_J for ammonia radiative transitions with $\Delta K = 0$ (neglecting hyperfine structure) can be obtained from:

$$A_{J \to J} = \frac{K^2}{J(J+1)} \quad \text{and} \quad A_{J+1 \leftarrow J} = \frac{(J+1)^2 - K^2}{J(J+1)(2J+1)} \qquad (36)$$

If hyperfine structure is taken into account, however, the transition probabilities will differ according to the projection of F_1 on the intramolecular electric field on its z-axis (Jauch 1947). Two possible transitions should be considered: Longitudinal transitions (electric field parallel to the z-axis): The selection rules are: $\Delta F_1 = 0, \pm 1$, $\Delta M = 0$, then the transition probability for $\Delta F_1 = 0$ (central line) is:

$$A = \frac{K^2}{J^2(J+1)^2} M^2 \frac{\left[J(J+1) - I(I+1) + F_1(F_1+1)\right]^2}{4 F_1^2 (F_1+1)^2} \qquad (37)$$

and for $F_1 = F_1 + 1$ (satellite):

$$A = \frac{K^2}{J^2(J+1)^2}\left[(F_1+1)^2-M^2\right]\frac{(F_1+1+I+J)(F_1+1+I-J)(I+J+2+F_1)(I+J-F_1)}{4(F_1+1)^2(2F_1+1)(2F_1+3)} \quad (38)$$

Transverse transitions (electric field perpendicular to the z-axis): The selection rules are: $\Delta F_1 = 0, \pm 1$, $\Delta M = \pm 1$ and $\Delta F_1 = 0$, $M \rightarrow M \pm 1$, then accordingly the transition probability is:

$$A = \frac{1}{4}\frac{K^2}{J^2(J+1)^2}(F_1 \mp M)(F_1 \pm M+1)\frac{\left[J(J+1)-I(I+1)+F_1(F_1+1)\right]^2}{4F_1^2(F_1+1)^2} \quad (39)$$

and for $F_1 \rightarrow F_1 + 1$, $M \rightarrow M \pm 1$:

$$A = \frac{1}{4}\frac{K^2}{J^2(J+1)^2}(F_1 \mp M+1)(F_1 \mp M)\frac{(F_1+1+I+J)(F_1+1+I-J)(I+J+2+F_1)(I+J-F_1)}{4(F_1+1)^2(2F_1+1)(2F_1+1)} \quad (40)$$

An additional complication in the ammonia inversion spectrum is that the M states are degenerate in zero field; M^2 should therefore be summed over all the initial and final states according to the formula:

$$\sum_{-F}^{+F} M^2 = \frac{1}{3}F_1(F_1+1)(2F_1+1) \quad (41)$$

Then, for the total transition probabilities (central line):

$$A_{J,J} = \frac{K^2(2J+1)}{3J^3(J+1)^3 Q(J)} \quad (42)$$

where $Q(J) = (J+1)^4 + J^4 + \left[J(J+1)-1\right]^2$ (43)

and for the satellites:

$$A_{J-1,J} = K^2(2J-1)/3J^3(J+1)^3 \qquad (F_1 = J-1 \rightarrow J) \quad (44)$$

$$A_{J,J+1} = K^2(2J+3)/3J^3(J+1)^3 \qquad (F_1 = J \rightarrow J+1) \quad (45)$$

The magnitude of these quantities for different values of J and K must be multiplied by a statistical weight factor = 1 for K = 1, 2, 4, 5, ... and = 2 for K = 3, 6, 9 ... and the Boltzmann factor $\exp\left[-E(J,K)/kT\right]$.

From the matrix element of the dipole moment for the inversion transition: $\mu = \mu_0 \frac{KM}{J(J+1)}$, it is clear that its

maximum value is when K = J. Since the intensity of the line is proportional to $|\mu|^2$, the lines with K = J possess greater intensity than other lines. It is possible from the above formula to show that the most intense inversion line of the ammonia molecule at room temperature is obtained with J = K = 3.

The transition probabilities for the three components of the central line ($F_1 = 2$, $F_1 = 3$ and $F_1 = 4$) for the ammonia inversion line J = 3, K = 3 may now be calculated (Appendix 1) from equations (37 and 41). The result for the transition probabilities is that:

$$A_{F_1=3} : A_{F_1=4} : A_{F_1=2} = \frac{847}{576} : \frac{1215}{576} : \frac{640}{576}$$

The relative intensities (R) of the satellites to the intensity of the central line can also be evaluated (Appendix 2) from the following relationships:

$$R_{J-1,J} = \frac{A_{J-1,J}}{A_{J,J}} = \frac{(J+1)^2(2J-1)}{(2J+1)\,Q(J)} \qquad (45)$$

$$R_{J,J+1} = \frac{A_{J,J+1}}{A_{J,J}} = \frac{J^2(2J+3)}{(2J+1)\,Q(J)} \qquad (46)$$

CHAPTER 3

SOME DESIGN CONSIDERATIONS AND EXPERIMENTAL APPARATUS

3.1 Introduction

A lot of attention has been given by many investigators to the problem of large beam intensities, narrow velocity distribution and high signal-to-noise ratio in molecular beam experiments. For this purpose, effusive, multiparallel cylindrical holes, converging-diverging nozzles and conical converging nozzle sources have been developed and found to be helpful but still have left much to be desired. Thereafter, suitably shaped diaphragms called "skimmers" were employed in conjunction with different types of nozzles.

In 1951, Kantrowitz and Grey made an important suggestion which seemed to promise beam intensities orders of magnitude greater than could be achieved by any effusion technique. Basically, this method consists of transfering the core portion of a molecular beam flow into a high vacuum region by means of a skimmer. This proposal was investigated by Kistiakowsky and Slichter (1951), Becker and Bier (1954), Campargue (1964) and others.

In 1971 Lainé suggested the application of the nozzle beam skimming device to an ammonia molecular beam maser. He pointed out that with such an arrangement it might be possible to obtain very strong oscillations even for many weak ammonia inversion lines, without the aid of cryogenic pumping.

Thus the present molecular beam maser system was designed and constructed on the basic principles of nozzle-skimmer techniques. The initial results showed that there was a large increase in the amplitude of oscillation for the same value of focuser potential relative to the amplitude of oscillation when a conventional nozzle-diaphragm was employed. Ammonia inversion lines such as $J = K = 2$ and $J = 3$, $K = 2$ can oscillate strongly at threshold values of 12 and 24 kV respectively without cryopumping. With the aid of cryogenic pumping, the thresholds are 9 and 18 kV respectively. For the strongest ammonia inversion line $J = 3$, $K = 3$ the threshold voltage for oscillation is as low as 9.8 kV without cryopumping and 4.8 kV with cryopumping. In addition, the operation of this device with the ammonia (3,3) line has revealed many new results and phenomena which stem from the hyperfine structure of the ammonia molecule.

However, the conclusions that can be drawn at the present time are few, and the questions raised are many. The most definite conclusion is that the nozzle-skimmer technique provides a powerful tool central to the beam formation problem, with greatly reduced scattering and increased signal-to-noise ratio of the detected signal. The results obtained are such that further investigations are encouraged. However, more experimental data is needed. It is possible that the technique could be improved in the present work by a second stage of beam skimming. Consideration of this point also may contribute to the improvement of the theory of molecular beam formation.

In spite of all the effort that has been expended in forming an intense molecular beam, it must be recognized that

there is still much to be done before the technique can be regarded as perfected. What is really involved is the engineering development of a principle into a useful tool. Therefore, a careful procedure, involving iterative improvements of knowledge of the gas flow properties and skimmer operation seems to be necessary and must be accompanied by conclusive proof of the perfection of the beam-skimming process.

3.2 Basic principles and some design considerations

In the development of a molecular beam apparatus several unforseen difficulties in design might arise because of insufficient knowledge of certain physical phenomena. Therefore it is necessary to conduct preliminary studies to obtain large molecular beam intensities up to 10^{19} molecules cm^{-2} sec^{-1} with very low background pressure and with narrow velocity distribution. It is appropriate to discuss the function of the characteristic features of the nozzle beam system in the light of both theory and experience. The main features are; pumping requirements, the nozzle flow complex and the skimmer.

According to Kistiakowsky and Slichter(1951)(using ammonia as the test gas), it was found that beam intensification was possible up to a factor of 30 compared with the intensity from the conventional molecular effusive source. Therefore the total gas flow in a nozzle beam system was of an order of magnitude greater than in a typical effusive beam apparatus. Most of the gas which was introduced initially through the nozzle was removed upstream from the skimmer and did not contribute to the pumping load after the skimmer. The ratio of axial beam intensity to skimmer mass flow is considerably

higher than the ratio of the beam intensity to effusive mass flow in a conventional effuser. Therefore, for an optimum total intensity, the pumping speed required in the high vacuum region is substantially lower for a nozzle beam than an effuser. On the other hand, for a usable beam intensity with a particular velocity interval and hence narrow velocity distribution, the nozzle source demands a lower pumping speed of the high vacuum system than for an effusive source. In contrast, the situation upstream near the skimmer is entirely different. The effusive systems require no fast auxilliary pumping but the nozzle exhaust chamber in a nozzle beam system must be provided with enough pumping capacity to remove all of the total nozzle flow except a small fraction which passes through the skimmer to the next chamber. Thus the first stage pumping plays an important role in a nozzle beam system.

Experimental evidence has shown that the higher the pumping speed in the nozzle exhaust chamber, the more effectively can molecular beams be produced. Cryogenic pumping with liquid nitrogen has been used with great success and it was found that it provides extremely large pumping speeds.

There are a number of special considerations that apply to nozzles designed for molecular beam systems. The advantage of high intensity and narrow velocity distribution predicted by theory are a consequence of the absence of collisions between molecules in the nozzle exit and after they have passed through the skimmer. This implies a low density in the beam flow at the skimmer entrance and in the nozzle

exhaust chamber. To minimize the necessity of fast vacuum pumping, the nozzle mass flow must be relatively low, thus the nozzle diameter and its width must be small provided that the pressure behind it is adjusted so that a free jet flow of the beam can be obtained.

If the thickness of the nozzle throat is less or equal to λ_m (mean free collision path distance inside the source) then every molecule which reaches the aperture passes through and will not suffer a change in its direction. This implies that the spatial velocity distribution of the molecules inside the source is not affected by the emerging molecules. With nozzles of large diameter and thickness larger than the mean free collision path, it was found that as the source pressure reached a certain value above threshold, the detected beam intensity starts to fall rapidly instead of increasing. This limitation is due to an increasingly large fraction of the effusing molecules colliding with each other in the source exit. In this way a cloud of scattered molecules (instead of the source aperture) serves as the effective source of the molecules and as the source pressure is further increased, scattering increases more rapidly than molecular intensity.

In employing a nozzle source with small dimensions with a given pumping speed and gas flow in the first low pressure stage, the expansion ratio P_o/P is proportional to $1/d^2$ (where P_o and P are the nozzle source and nozzle exhaust chamber pressures respectively). Decreasing the nozzle diameter (d) will yield an increase in the intensity of the molecular beam (Bier and Schmidt 1961) and the resulting molecular density from the nozzle flow is inversely

proportional to the square of the distance from the nozzle exit (Parker et al 1960).

3.3 Nozzle source and condensation phenomenon.

In the generation of molecular beams there are some essential gas parameters as well as the geometry of the nozzle that have to be considered (Kantrowitz and Grey 1950, Becker et al 1962).

For the nozzle source it can be assumed that all the molecules have the same mass flow velocity, v, and the random velocities are negligible compared to v. Thus, for a given effective expansion ratio (P_o/P), the resulting speed ratio or the flow mach number (M) can be determined. (Hence, $M = \frac{v}{s}$, where s is speed of sound just ahead of the nozzle).

The other parameter is the real nature of the gas which determines the conditions for the condensation phenomena within the expanding flow of gas under the action of given nozzle dimensions and geometry.

In the present investigations, a condition for ammonia molecular beam condensation has been obtained in the maser system. The nozzle employed was made from very thin stainless steel (0.10 mm) with a hole of 0.05 mm in diameter. This hole was made by the aid of YAG laser.

The maser was operated at an optimum condition for strong oscillation with a voltage of 26 kV on the state separator and a gas pressure of 460 torr behind the nozzle. A steady amplitude of maser oscillation was obtained and displayed on the oscilloscope screen. After running the maser for approximately $\frac{1}{2}$ hour, a reproducible and continuous

fluctuation (between zero and maximum amplitude) was observed in the oscillation signal, continuing without time limit. An average periodicity of about 52 seconds was observed for the amplitude to fall from maximum to zero.

The onset of the condensation can be explained as follows: As the gas expands isentropically, the enthalpy of the molecule is converted to net translational mass motion. The most probable velocity will be higher and narrower than for an effusive source. Owing to the very low static temperature reached during the adiabatic expansion in the flow, the translational temperature for the molecules will be much lower than the nozzle source temperature. Consequently, the number of collisions decreases and eventually, a transition from hydrodynamic flow to a free molecular flow would prevail at a distance of a few nozzle diameters downstream from the source. Thus a considerable gain in the beam intensity can be obtained on the account of molecular rotational cooling and consequent higher population of the low J states. In contrast, under such conditions when the gas expansion is non-isentropic, all the enthalpy of the molecules which is converted to translational energy will be frozen (Anderson et al 1966). The molecules thereafter, become highly supersaturated with respect to their equilibrium condensed phase. Under such critical conditions small aggregates of molecules, even dimers might pass unnoticed. However, when a substantial degree of supersaturation is reached, the onset of the condensation manifests itself as an observable effect when the molecules in the condensed phase have grown to a microscopic size and

hence, this will appear as an abrupt change in the beam intensity.

3.4 Skimmer geometry and performance

It is convenient to consider that the second defining element in a nozzle beam system is the "skimmer" and that it plays a role analogous to the "diaphragm" of a conventional maser apparatus.

The characteristic geometrical quantities in designing a skimmer are: mouth radius, lip radius, internal and external angles and length. Under continuum gas dynamical beam performance caused by the skimmer itself, operation has been ascribed to an oblique shock wave on the skimmer cone apex (Bier and Hagena 1966, Deckers and Fenn 1963). The shock wave in the core stream is caused by the finite thickness (t) of the skimmer edge, provided that the gas kinetic mean free path (λ) is small compared to (t). If at lower gas density, (λ) is comparable to (t) or even larger but still small compared to the diameter (d) of the skimmer, a similar shock wave can occur in the core stream due to a boundary layer at the skimmer walls which might extend as a deleterious effect into the molecular beam region.

The influence of skimmer on the molecular beam generation has been investigated experimentally. Three skimmers of different diameters (1.2, 1.4, and 1.6 mm) and equally sharp leading edge of the skimmer, but equal cone angles (inner angle 35°, outer angle 45°, Figure 3.1) were employed. Various characteristics have shown that the skimmer with 1.6mm in diameter was best suited for ammonia

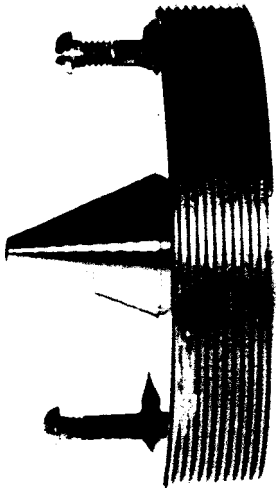

SKIMMERS

NOZZLES

FIGURE (3.1)

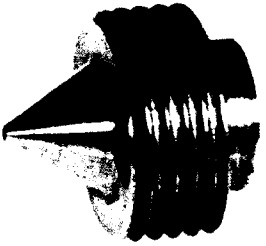

beam maser operation in conjunction with different nozzle sources. It was found that the relative maximum of molecular beam intensity at a certain optimum inlet pressure depends on the given nozzle-to- skimmer distance. The decrease of beam intensity following a maximum in varying the optimum nozzle-to-skimmer distance is very marked for the skimmer of diameter 1.2 mm. This effect is somewhat smaller than those for skimmers with 1.4 and 1.6 mm in diameter. This difference can be attributed to a disturbance of the core stream by molecules reflected from the outer skimmer wall.

In addition, the influence of the diameter of the skimmer on molecular beam performance was investigated. It was recognized that for the two skimmers with similar geometry but with different diameters of 1.2 and 1.6 mm, for the skimmer of 1.6 mm in diameter the intensity of the molecular beam was higher by an average factor of about 1.4. At this point it should be noted that the possibility of increasing molecular beam intensity by increasing the diameter of the skimmer is limited of course, by the maximum gas flow into the working chamber. However, this can be tolerated by increasing available pumping capacity.

From theory and experiment in continuum gas dynamics there is a well-established relationship between the Mach number of the free molecular flow and the maximum included angle of skimmer cone apex (Bier and Hagena 1966). If the cone angle is greater than a critical value for a particular Mach number a shock wave will be detached. Therefore, the cone angle must be such that the shock wave is as close as

possible to the cone apex. According to experience with the present maser system, skimmers with cone angles less than 60° (i.e. $40\text{-}60^{\circ}$) is a convenient design criterion for molecular beam formation. Figure(4.1) shows the dimensions of a typical nozzle-skimmer assembly used in the present investigations. However, there is still much to be done before the skimmer design can be considered fully developed.

3.5 Experimental apparatus

(i) General

Figure (3.2) shows the main maser chamber with its associated microwave and electronic equipment. The apparatus is mounted on a table such that the molecular beam axis is horizontal. The two cylindrical cans with insulating jackets are liquid nitrogen reservoirs. The pumping system, ammonia reservoir and the ammonia purification traps are mounted below and beside the table. Electronic equipment was mounted on standard Post Office racks.

(ii) Maser vacuum system and gas supply

Figure (3.3) is a block diagram of the maser vacuum system.

(a) First chamber (nozzle chamber)

This chamber consists of an $8\frac{1}{2}$" high, $10\frac{1}{2}$" internal diameter rolled stainless steel cylinder, Figure(3.4). It is fitted with 9 flanged windows, 4 of $4\frac{1}{8}$" internal diameter, 5 with $2\frac{1}{8}$" internal diameter and a liquid nitrogen trap. The base holds a stainless steel disc, $10\frac{1}{2}$" outer diameter, $6\frac{1}{2}$" internal diameter, supporting a 6" diffusion pump. The top flange holds a 12" perspex plate of thickness 1". All 11 openings are sealed by rubber "O" rings. The weight of the nozzle chamber is taken by the 6" diffusion pump which has its upper flange supported by a wooden bench.

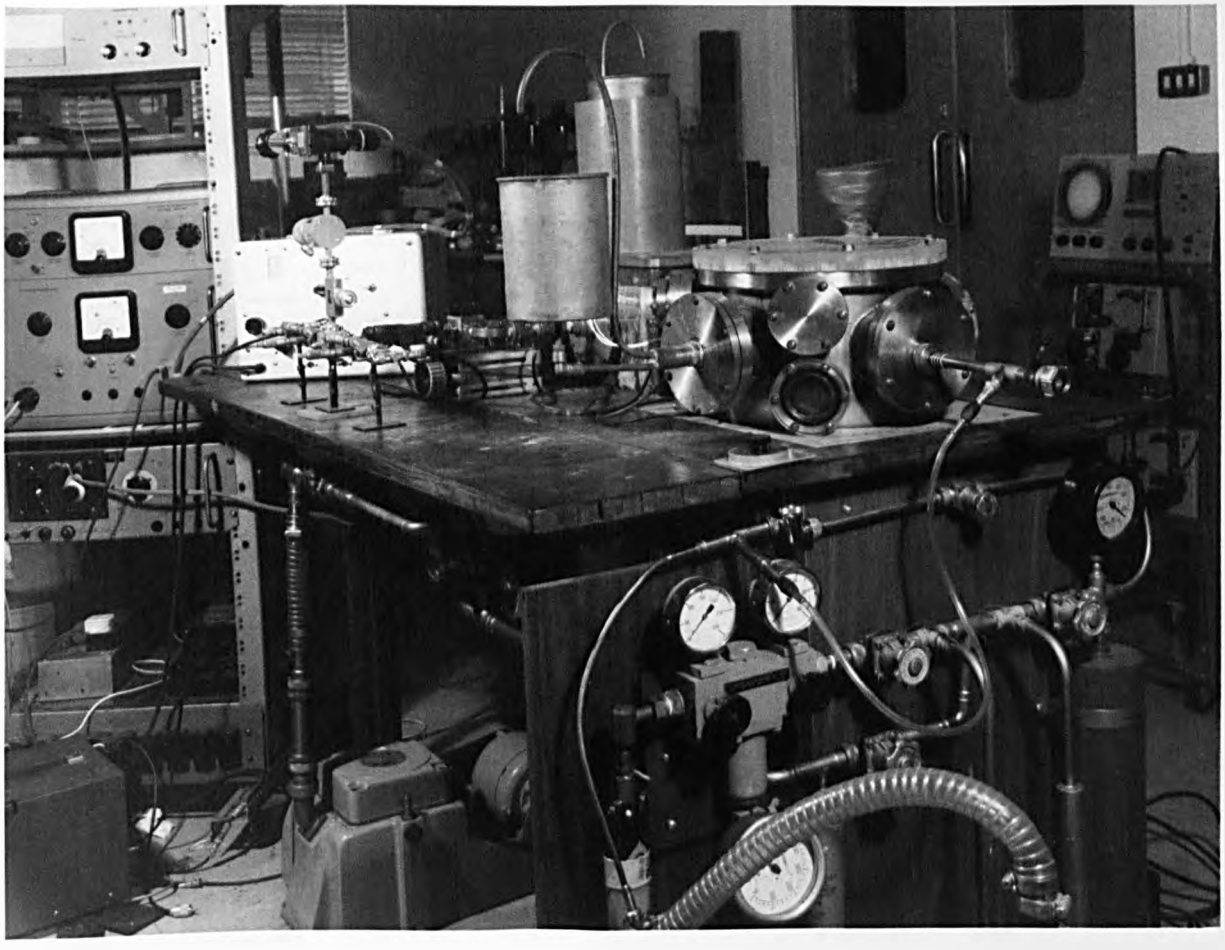

FIGURE(3.2) TWO VIEWS OF THE MASER ASSEMBLY.

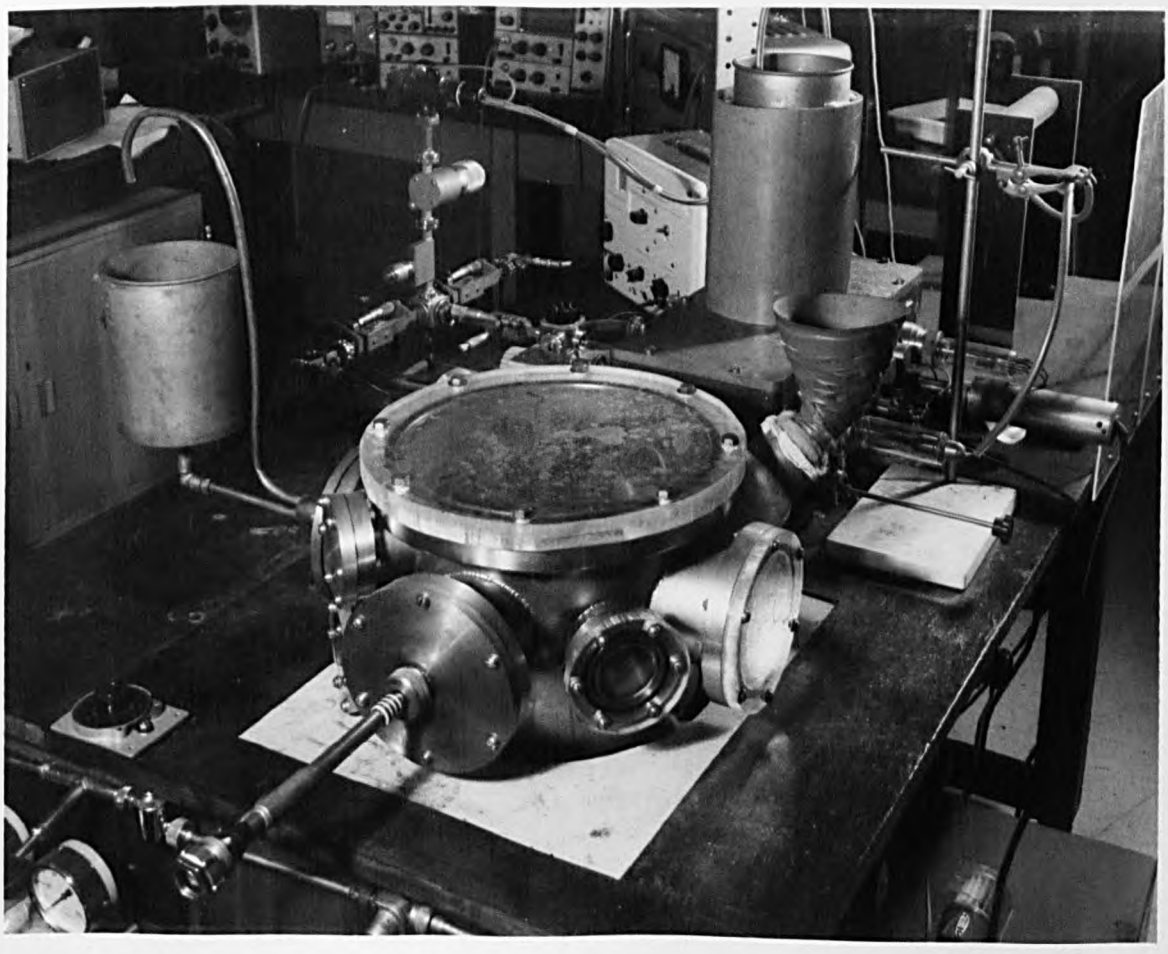

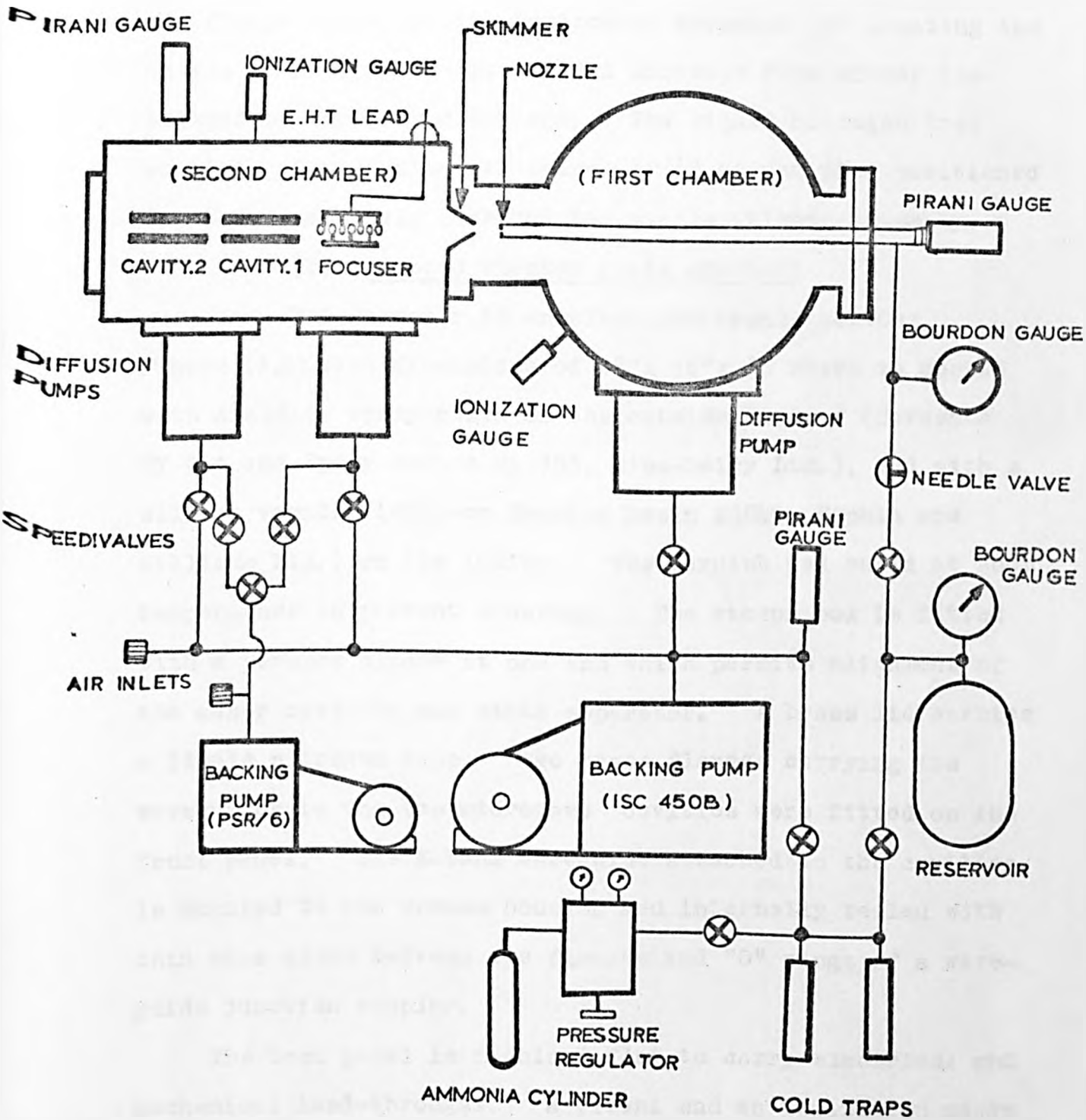

Fig (3.3) BLOCK DIAGRAM OF THE MASER VACUUM SYSTEM.

The ammonia supply is through a copper tube $\frac{1}{2}$" diameter, holding the nozzle, which runs across the chamber. This tube is held in position by an adjustable support at the nozzle end. The other end is attached via an "O" ring to the flange which permits horizontal movement for locating the nozzle at an optimum operational distance from either the skimmer or the iris diaphragm. The liquid nitrogen trap consists of a 2" diameter spiral of $\frac{1}{4}$" copper pipe positioned so as to completely surround the nozzle-skimmer assembly.

(b) Second chamber (main chamber)

This chamber is an aluminium-bronze casting, Figure (3.5) with dimensions of 18"x 18"x 8" which is coated with Araldite epoxy resin on the outside surface (Hardener HY 951 and Epoxy Resins My 753, Ciba-Geigy Ltd.), and with a silicon varnish (Silicon Bonding Resin M5840, Hopkin and Williams Ltd.) on the inside. The varnish was cured at room temperature to prevent cracking. The vacuum box is fitted with a perspex window at one end which permits alignment of the maser cavities and state separator. A brass lid carries a liquid nitrogen trap. Two brass flanges carrying the waveguides to the two microwave cavities were fitted on the front panel. The K-band waveguide attached to the cavities is mounted to the vacuum housing and internally sealed with thin mica discs between the flanges and "O" rings of a waveguide junction coupler.

The back panel is machined flat to carry electrical and mechanical lead-throughs. A pirani and an ionization gauge were mounted on the same panel. All flanges and lead-throughs are sealed with rubber "O" rings.

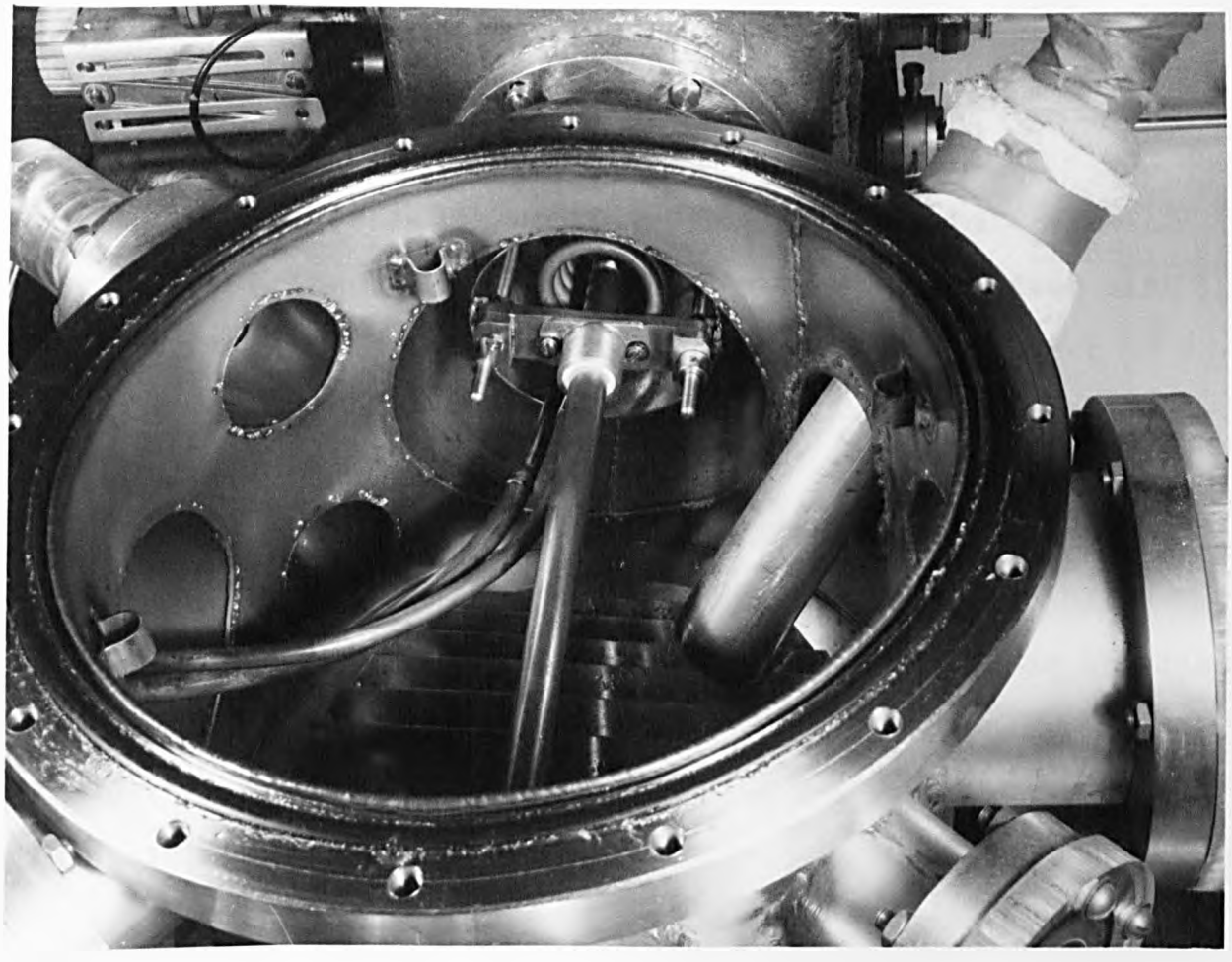

FIGURE(3.4) NOZZLE-SKIMMER CHAMBER

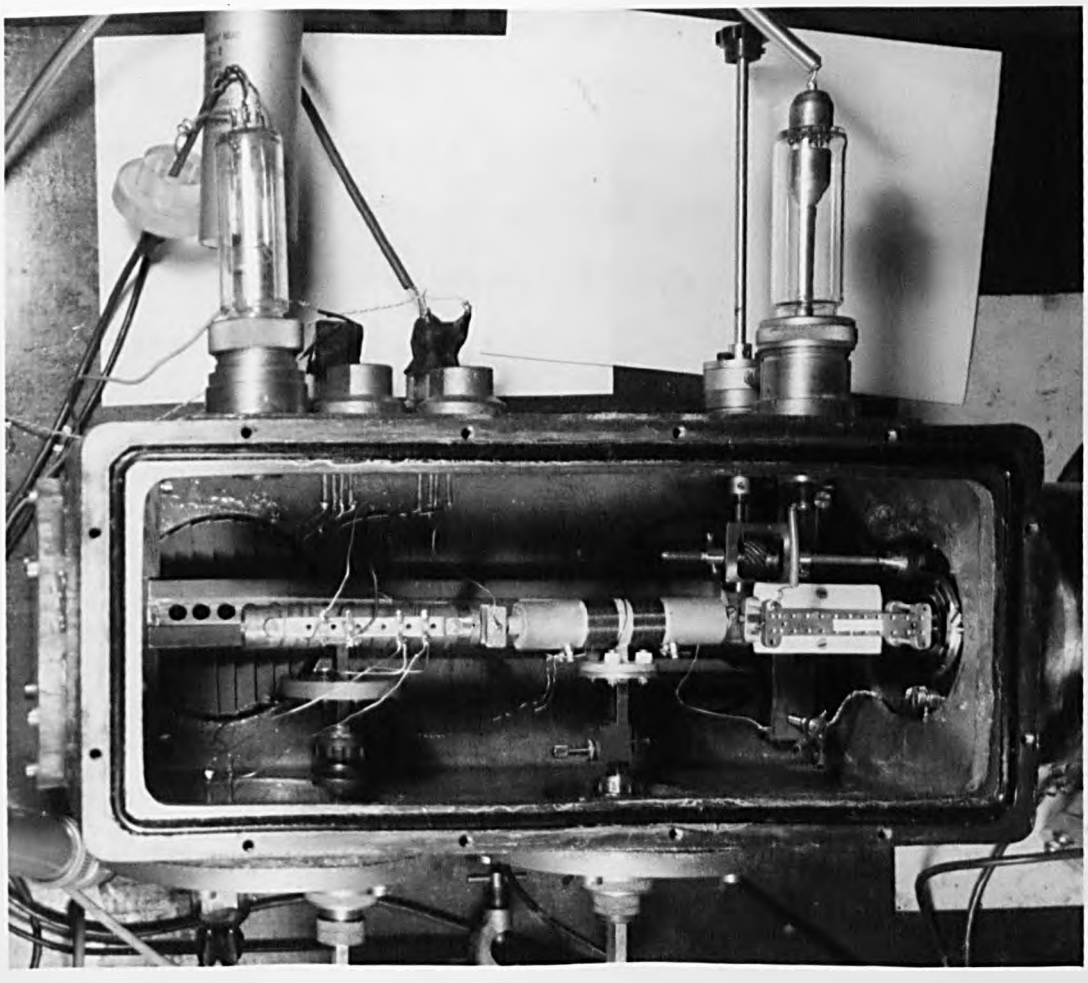

FIGURE(3.5) MAIN CHAMBER

(c) Maser vacuum assembly

The vacuum system is constructed with differential pumping of the two chambers. These are separated from each other by a screw threaded holder which can accept either a diaphragm iris of variable diameter or a skimmer of the type used in supersonic molecular beam work. The aperture of this iris is controlled from outside the second chamber with a rotary drive lead-through, directly coupled to a gear box assembly Figure (3.5) . This assembly consists of two bevelled screws mounted in a brass cube which permits the transfer of the external rotational motion to drive the variable iris aperture as required.

The first chamber is pumped with a 6" Edwards oil diffusion pump type (E04), and the main chamber by two 4" Edwards oil diffusion pump types (403A) Figure (3.6) . Each is charged with an appropriate quantity of 704 silicon oil which has a limiting vapour pressure of 10^{-7} torr. The total pumping speed for both chambers is about 1200 ℓs^{-1}; each chamber of capacity 600 ℓs^{-1}. The 6" and the two 4" diffusion pumps are backed by an Edwards Model ISC450B and an NGN Model PSR/6 rotary pump respectively. The two rotary pumps are vacuum coupled to the equipment by means of flexible couplings to minimise the vibration with the main pumping lines of 1" copper tubing. The background pressure in each chamber is monitored with Edwards IG6G and IG6M ionization gauge heads operated by Edwards power supply unit Model (Ion7).

The pressure in the nozzle chamber and second chamber was 4×10^{-6} torr and 1×10^{-5} torr respectively without cryogenic pumping after about one hour pumping. Addition of

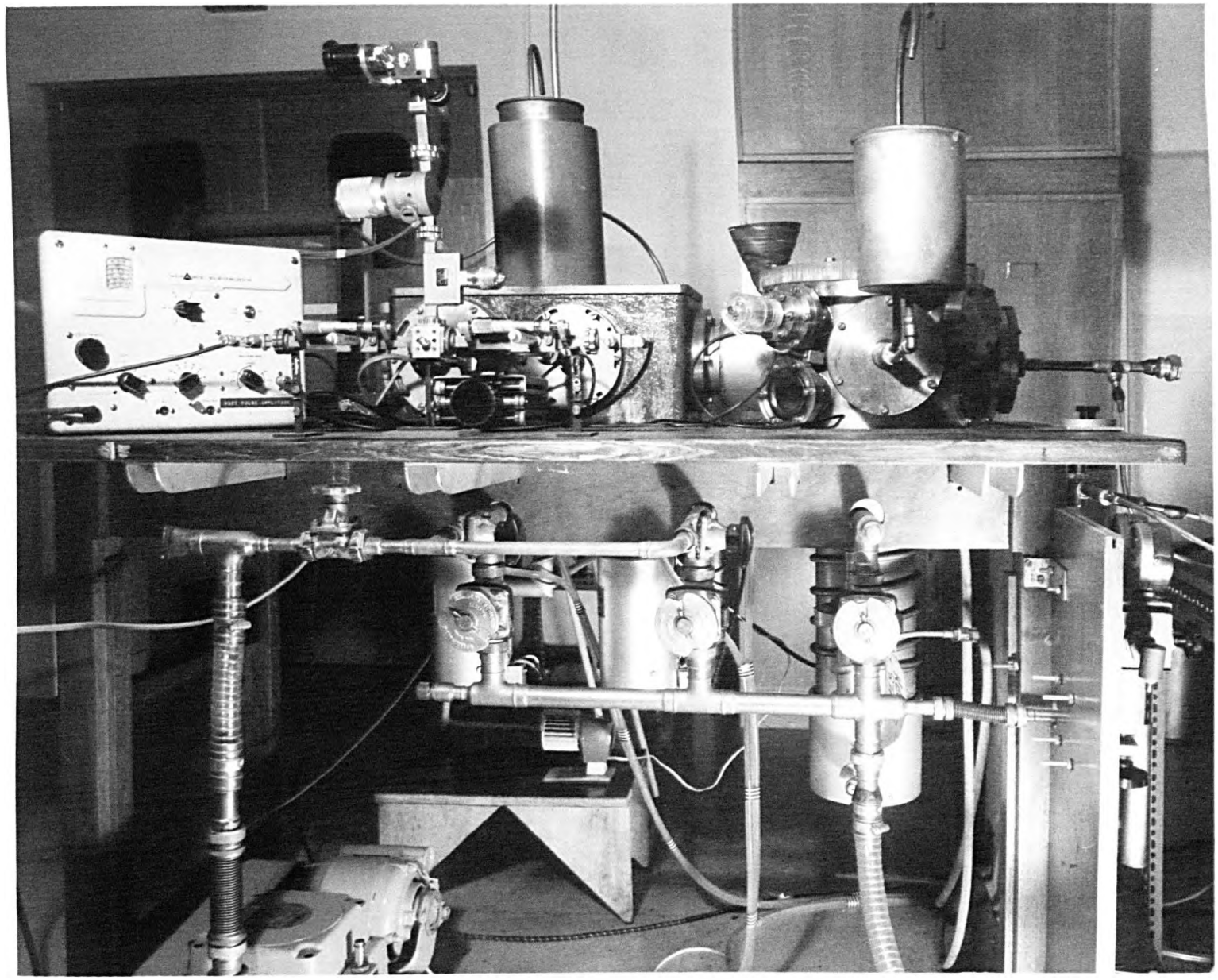

FIGURE(3.6) FRONT VIEW OF THE MASER SYSTEM SHOWING PUMPING SCHEME.

liquid nitrogen to the traps in both chambers reduces the pressure to about 4×10^{-7} torr in the first chamber, 7×10^{-7} torr in the second chamber within 2 hours.

(d) Ammonia source and supply line

Figure (3.2) shows the ammonia source, control valves, traps, reservoir and pressure gauges. The ammonia source is a lecture size cylinder of anhydrous liquid ammonia which is controlled by a pressure regulator valve adjusted to an output pressure of about 950 torr. The gas flow from the lecture cylinder to the nozzle is controlled by four $\frac{1}{2}$" speedivalves and one finely adjustable needle valve. The pipe line is of $\frac{1}{2}$" copper tubing. The needle valve is coupled to the nozzle holder tube by thick walled flexible P.V.C. tube. This thickness is sufficient to prevent wall collapsing under the action of the atmospheric pressure. Two Bourdon gauges with appropriate ranges 0 - 760 torr and 0 - 100 torr are used to monitor the gas pressure in the reservoir and behind the nozzle respectively.

In order to increase the pumping efficiency of the liquid nitrogen trap which is used in the working chamber, a thick flat copper plate with channels milled into it, is used in order to increase its effective surface area. This plate is soldered to a length of $\frac{1}{4}$" copper tubing. Then a single continuous copper tube is soldered at the opposite face of the channeled surface. The two ends of the copper pipe are soldered to the flange by employing a thin nickel silver tube as the connection between the trap and the flange, because of its low thermal conductivity which in turn prevents the "O" rings from cracking due to cooling cycling. Silver solder is used for all high vacuum joints.

3.6 Resonant cavity

The cylindrical cavity is an important component of the complete maser apparatus. The tolerance is such that a cavity has to be of the highest order due to the possibility of multi-mode cavity operation, and high Q value required for strong oscillation. The natural frequency of oscillation is determined by the geometry of the resonator and depends on the type of wave excited in the resonator.

The maximum interaction between molecules and radiation field is obtained by an appropriate choice of mode in a resonant system. Thus modes generally favoured are those with a single maximum field in the transverse direction. If a parallel beam of univelocity molecules passes through a cavity of length L operated in the E_{010} mode, the total linewidth at half-maximum is 0.9 v/L, and the emitted power is a maximum at the molecular resonance frequency. Such narrow spectral line width typically of the order of 6 kHz can be obtained with cavities operated in this particular mode which eliminates much of the Doppler effect.

With cavities operated at higher modes of the type E_{01n} ($n = 2,3,...$) a larger linewidth is obtained because of the field E varies along the length of the resonator and a line splitting on account of the longitudinal Doppler effect is produced (Gordon et al 1955, Krupnov and Skvortsov 1964). Various modes of cavities have different Q factors and different distributions of electric field. Therefore, the choice of modes and type of cavity for molecular beam maser operation has to be considered. Shimoda, Wang and Towns (1956) had introduced a measure for such choice in terms of a "figure of merit" M for the maser resonator:

$$M = \frac{L Q_o}{A} \left(\frac{8}{\pi 2}\right)^n \qquad (1)$$

where n is zero for a uniform field along the cavity axis (E_{010} mode) and unity if the distribution has a maximum at the centre (E_{011}, H_{211}, H_{011}, H_{111} modes). L, Q_o and A are the length, the quality factor and the cross sectional area of the resonator respectively. The parameter LQ_o is a measure of sensitivity for resonator design.

According to the above formula, in the case of a broad beam filling the cavity with E_{010} mode, the value of M = 7.7, whereas for E_{011}, H_{111} and H_{011} the value of M is 6.0, 5.9 and 4.1 respectively. For a narrower beam the advantage of the E_{010} mode is even higher. Hence, the larger value of M is obtained for the E_{010} mode i.e. the larger the value of M, the smaller the number of molecules required for maser oscillation. In practice it is found that a cavity length of about 10 cm at λ = 1.25 cm wavelength is an optimum value for a strong maser oscillation requirement with a loaded Q factor of 6000 - 7000 for the E_{010} mode.

In the cylindrical cavity two types of modes may exist, these are:

(a) Transverse Magnetic (TM or E); where the electric field is parallel to the axis of the resonator (no magnetic field parallel to the axis). This permits a long time for interaction between the molecules and the electric field.

(b) Transverse Electric (TE or H); where there is no electric field parallel to the axis of the resonator.

The dimensions of a cavity required to produce resonance

for different wavelengths can be derived from the waveguide theory (Harvey - Microwave Engineering). A cavity can be regarded as a length of waveguide such that the electric and magnetic fields are oscillating in space and time and an integral number of half-wavelengths with a complete standing wave existing inside.

The resonant wavelengths (λ) for TM modes can be given by (Montgomery, 1947):

$$\lambda = 2 \left\{ \left(\frac{2X_{lm}}{\pi d}\right)^2 + \left(\frac{n}{l_c}\right)^2 \right\}^{-\frac{1}{2}} \qquad (2)$$

where:

n is an integer equivalent to the number of half period variations of the wave along the resonator axis.

l_c is the length of the resonator

d is the diameter of the cavity

X_{lm} is the m^{th} root of the 1^{th} order Bessel function $J_1(X) = 0$. For TM (E_{01n}) and TE (H_{01n}) modes, X_{lm} has the values 2.4048 and 3.832 respectively. In case of the E_{010} mode excitation, equation (2) takes the form,

$$\lambda = 2 \left(\frac{2 X_{lm}}{\pi d}\right)^{-1} \qquad (3)$$

from which:

$$d = \frac{v X_{lm}}{\pi f_o} \qquad (4)$$

where v is the velocity of light (2.997925×10^{10} cm/sec) and f_o is the resonance frequency of the transition under consideration.

The cavity diameter for the different transitions of $^{14}NH_3$ inversion lines (J = 3, K = 3), (J = 3, K = 2), (J = 2, K = 2) and (J = 1, K = 1) were calculated from

equation (3) and all constructed in a similar manner as described in the following section. These cavities were tested and found to be in excellent agreement with the above calculations for each transition frequency involved.

Transition (J,K)	Cavity diameter (cm)	(in)
(3, 3)	0.961004	0.378333
(3, 2)	1.004602	0.395497
(2, 2)	0.966979	0.380685
(1, 1)	0.968127	0.381137

3.7 Cavity design and fabrication

Methods of fabrication of cavities for molecular beam masers have been discussed by a number of investigators (Gordon et al 1955, Helmer 1957 and Vonbun 1960).

In the present work, cavities for different transitions (J,K = 3,3 , 3,2 , 2,2 , 1,1) inversion lines of $^{14}NH_3$ were all constructed in a similar manner with the dimensions being the only variable. Taking various critical conditions into consideration, the construction of the cavity was evaluated for each transition (see the previous section) and thereafter the following procedure was followed:

The cavity was fashioned by electrolytic deposition onto a mandrel made of stainless steel type (S 80). The diameter of the mandrel was ground on a lathe to a precision of 10^{-4} inches . (The coefficient of variation of frequency with diameter is about 6 MHz per 0.0001 inch)

An acidic copper sulphate solution composed of 200 gm of $CuSO_4 \cdot 5H_2O$ (copper sulphate), 12 gm of potassium aluminium

sulphate, 56 gm of pure sulphuric acid (s.g. = 1.84) and 1 litre of distilled water was used. The anode was oxygen free, high conductivity copper. A synchronous motor was employed to rotate the mandrel slowly.

In order to minimise the possibility of uneven deposition of copper on the mandrel, the current flowing through the solution was reversed for about one third of the one cycle time. The current had to be within the limit of 100 to 200 ma at the beginning of the deposition period of about 48 hours. If the current exceeds 200 ma, the smoothness of the initial layer on the mandrel could not be guaranteed because of the possibility of deposition of bubbles of the solution in the copper which would affect the resonator Q.

When the electroform had reached a thickness of about one to two millimeters, the current was increased to 750 ma and plating continued for about three weeks until the electroform diameter was about 2.5 cm. Then the electroform was machined on a lathe to an outer diameter of about 2 cm, The waveguide mount was machined with the mandrel still inside to prevent cavity deformation. The mandrel was then removed carefully from the cavity by slight heating the two together in an oil bath. Differential expansion took place and the mandrel was easily removed.

Next, the coupling hole was centrally drilled. The coupling hole parameters were; hole diameter 0.096", diaphragm thickness 0.012".

The quality factor (Q) for each cavity was increased by inserting end caps made from brass and fitted tight in each end, so that the cavity ends are beyond cut-off frequency .

Maximum Q was obtained for each cavity by positioning the end caps but the physical length of the cavity was reduced to an effective length somewhat less than the physical length.

All the cavities are undercoupled and have a loaded Q between 6500 - 7000. Heater coils (glass covered Eureka wire or copper insulated wire) are bifilar wound round each cavity for stabilized tuning. Figure (3.8) shows the cylindrical cavity, complete with vacuum flange and input waveguide.

3.8 Ancillary equipment

Two E.H.T. units have been used to operate the state separator; one with reversible polarity from 0 - 30 kV (Brandenberg Model 800) and the other (negative polarity) from 0 - 60 kV (Brandenberg model 907). Both are radio frequency units with a stability of better than 0.25%. The lead-through to the state separator was made from a disused ion gauge after removing all electrodes, except the pins. A brass hemisphere of diameter $\frac{1}{2}$" had 7 holes of diameter $\frac{1}{8}$" drilled in it at positions corresponding to the pins on the gauge. These holes were then filled with solder and accurately drilled to the pin diameter. The pins on the gauge could then be inserted into the hemisphere with very good electric contact. A similar hemisphere was constructed for the pins on the inside of the gauge and threaded in its center to accept a screw ended resistor of 375 MΩ. This high resistance was connected in series with the supply to the state separator in order to reduce the current which can be drawn when a spark occurs in the separator, hence protecting the separator from any possible breakdown. This ion gauge

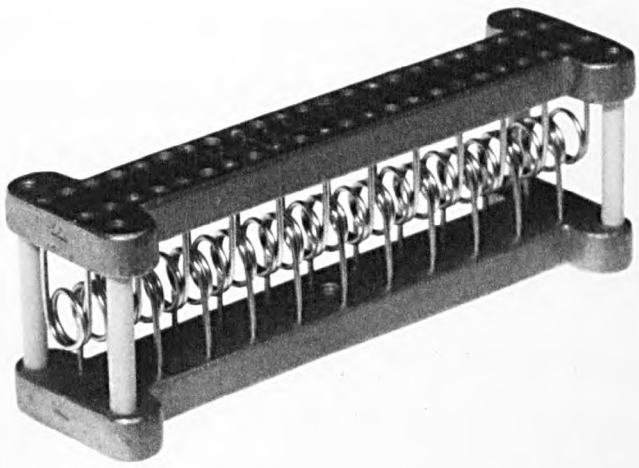

FIGURE(3.7) RING FOCUSER

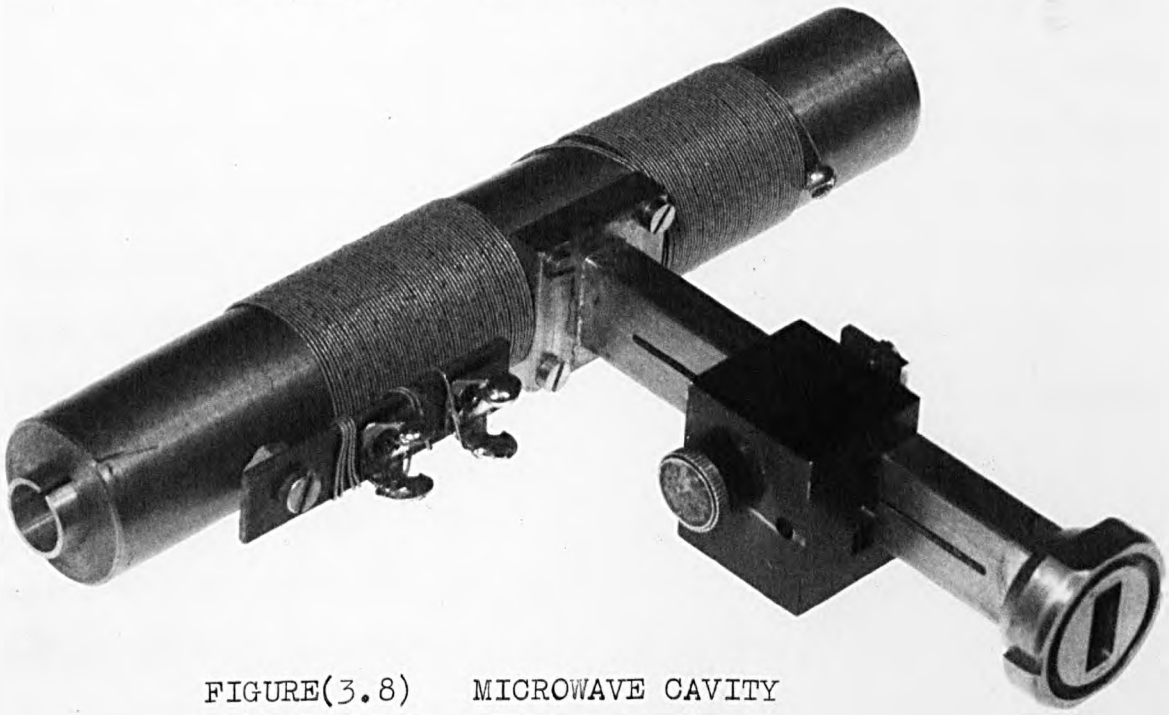

FIGURE(3.8) MICROWAVE CAVITY

lead-through was found to be very efficient in comparison with the conventional spark plug lead-through often used. The lead-through (Figure 3.5) is capable of withstanding potentials higher than 50 kV without any breakdown whereas the spark plug type starts to break down at about 25 kV.

The Klystron power supply is a Mid-century microvegear type EE/4-289 unit. The power units used to supply the D.C. potentials for intermediate frequency amplifiers are stabilised by a Farnell A15 power supply. The 30 MHz. I.F. amplifier has a gain of 55 dB and a band width of about 2.5 MHz. A local oscillator Advance E2 was used to generate two 30 MHz side-bands of the central frequency. An oscilloscope is used for visual display and measurement (Telequipment type D53).

In order to tune the cavities and also to prevent their frequencies from drifting due to temperature variation, two temperature control units are used. Stabilisation of the first cavity temperature to better than 1/10th C^{o} is effected with a commercial temperature control unit, whereas the temperature of the second cavity was controlled by an Airmec N.299 temperature control unit.

The two cavities are thermally heated until they are tuned by expansion to the desired ammonia transition. They are designed to be stabilised between 25 to 30^{o}C and their resonant frequency changes by 0.4 MHz per degree C. The heater coils on both cavities are bifilar wound to avoid magnetic effects in the vicinity of the cavities. The first cavity is heated by a current flowing in a 2.5 ohm bifilar wound coil of copper insulated wire round it. For the second cavity, the input potential is switched on and off by

the Airmec N.299 operated by a copper resistance thermometer of 8.89 ohm at 20°C (S.W.G. 32) bifilar wound to the cavity.

All the electronic units are powered via a 750 watt harmonic filter, 240 volts (50 Hz) mains constant voltage transformer type Advance CVH 750 A. This provides a constant voltage output of 230 ± 5 volts from an input anywhere between 140 and 270 volts with a true sinusoidal waveform with harmonic content of less than 5%. Various earth connections between units and frames have been adjusted to minimise 50 Hz mains pick-up.

3.9 Ring Focuser

The ring focuser is made from domestic stainless steel safety pins with their ends clipped off. The ring section has a smooth profile which decreases the possibility of electrical breakdown. The internal diameter of the rings is 3.4 mm and the diameter of the wire is 1 mm. At the widest part of the spiral, each ring has a thickness of 2.02 mm. The length of the focuser is 83 mm.

Figure(3.7) shows the focuser. There are 23 rings mounted in two rows. 12 rings are in one row (upper) and 11 rings in the other (lower) such that the two sets of rings interleave. The two sets are separated by four sintox ceramic tubes. The spacing between the adjacent (oppositely charged) rings is of the same order as the ring diameter.

This is an optimum spacing which represents a compromise between the high field strength and the transparancy of the ring focuser (Krupnov 1959).

Alignment of the device was made with a metal rod passed through the rings, with the ends of the rings placed in the

holes of the brass strips. When the rings were so aligned, the pins were secured with solder in their final positions. Later the four sintox tubes were araldited to the brass strips and finally the aligning rod was withdrawn. All surfaces were then rounded and smoothed.

The completed focuser was then mounted on a sliding carriage and positioned axially between the exit of the skimmer and the entrance of the maser cavity. The E.H.T. supply was connected to the upper set of rings and the lower set of rings were earthed. This focuser has permitted the operation of the maser with voltages in excess of 45 kV between the rings. A detailed analysis for ring focusers has been given in Section 6 of Chapter 2.

3.10 Microwave Bridge

Figure (3.9) is a schematic representation of the basic microwave bridge employed with the electronic detection system. An essential element of the microwave bridge (Magic-T) is the junction between the four waveguide arms. The arm No. 1 introduces the input power from the Klystron. Arm No 4 which is connected to the cavity via a matching unit and a microwave switch, acts as the detecting arm, while the arms No. 2 and No. 3 are the comparison arms of the bridge. The comparison arms have the property that when the two arms are matched and terminated by equal admittances then the input admittance at the first arm is independent of the output admittance of the fourth which means that the power fed into the first arm will be transmitted equally to the second and third arms and no power is transmitted to the fourth.

In practice the T-junction is not perfect and a certain amount of asymmetry or cross-coupling exists, and this has to be balanced out by a slight mismatch introduced by means of matching units in the arms 2 and 3.

3.11 Microwave power and crystal detector

In order to obtain a signal of high signal-to-noise ratio with a reasonably high sensitivity, the microwave power in the cavity should be made as large as possible. But this is subject to limitations due to the properties of the detecting crystal.

The output power from the cavity to the waveguide will have an optimum value, and hence, a certain fraction of the power concentrated in the cavity will be coupled out to the detecting crystal. The power level in the cavity and the power falling on the detecting crystal are therefore, not independent of one another and increasing the power level in the cavity to produce a larger amount of absorption creates too much noise in the detecting crystal and reduces the overall sensitivity.

The cause of these drawbacks is due to the properties of the detecting crystal. The first of these properties is the conversion loss which is a measure of the efficiency of the crystal in converting the incoming microwave radiation to d.c. or low frequency modulation. The conversion loss and thus the inefficiency of detection is very high at low values of input microwave power and mean crystal current but falls rapidly as these increase. Consideration of this parameter by itself therefore, suggests that the crystal detector should always be operated with a fairly large amount of microwave power falling on it.

The second property of the crystal is the excess noise which the crystal itself produces over and above the random thermal noise of its equivalent resistance. This noise also varies with the frequency of detection and with the amplitude of the mean detected current flowing through the crystal. The noise level rises linearly with increasing magnitude of the flowing current in the crystal. Consequently, as a result of both of these effects, there is an optimum crystal current in which the conversion loss has to fall to a reasonably low value and the excess noise has not become too large.

The other basic requirements for a low noise and thus sensitive detecting system is to employ an intermediate frequency of about 30 MHz. As it has already been seen that the crystal detector itself is the main source of noise and the employment of a balanced bridge can ensure that the crystal is operated at an optimum level of mean detected current. But on the other hand, the excess noise itself varies inversely with the frequency over a wide range, Figure (3.10). This figure shows the characteristic behaviour of the noise level in the crystal and the amplifier over the frequency range of detection, with a broad minimum centered on about 30 MHz in which the noise level of the detecting system is at a minimum. Therefore, for a maximum signal-to-noise ratio an intermediate frequency of about 30 MHz has to be employed and the smaller the bandwidth the higher will be the sensitivity of the detecting system.

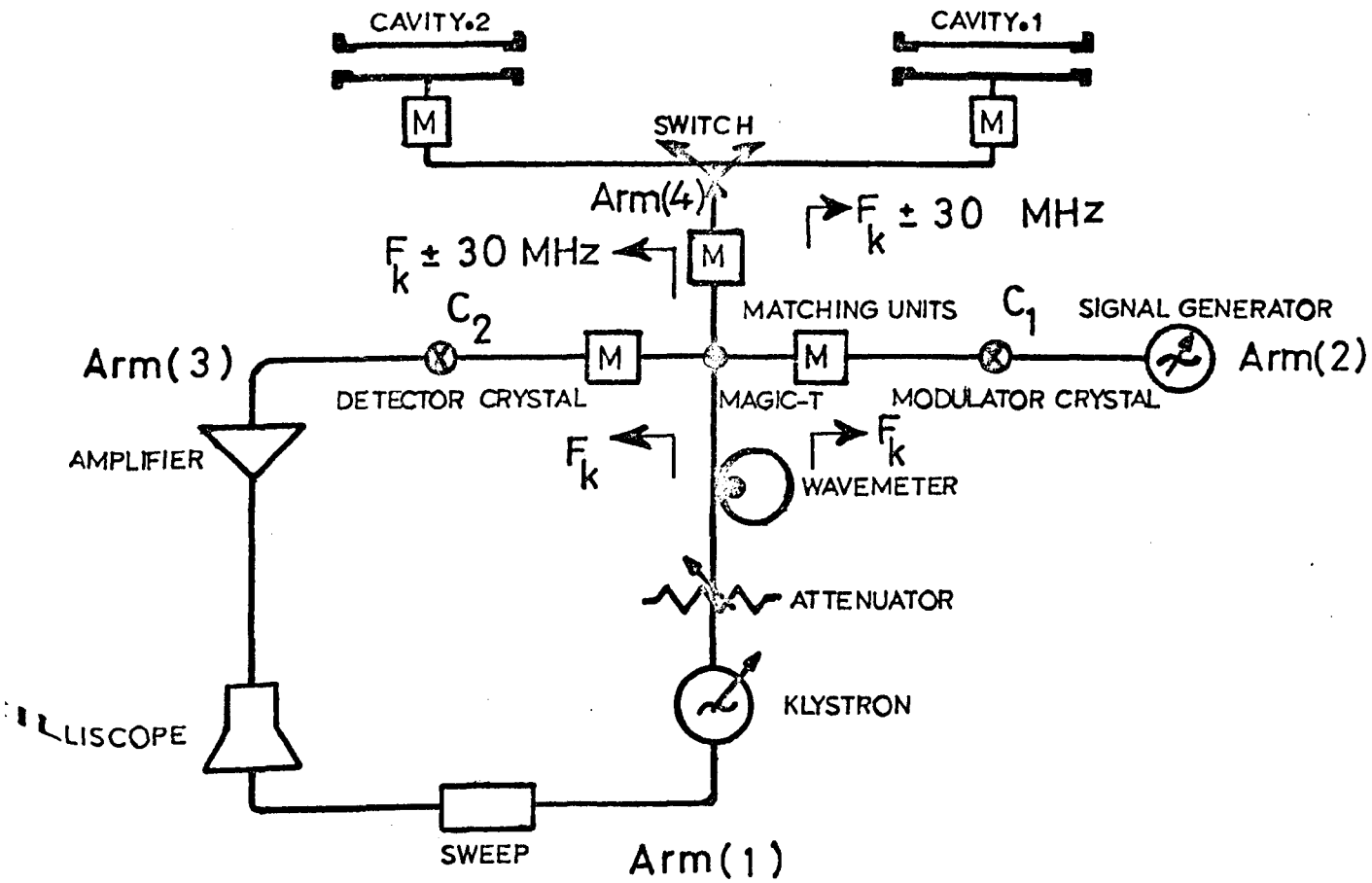

Fig (3.9) MICROWAVE BRIDGE & DETECTION COMPONENTS.

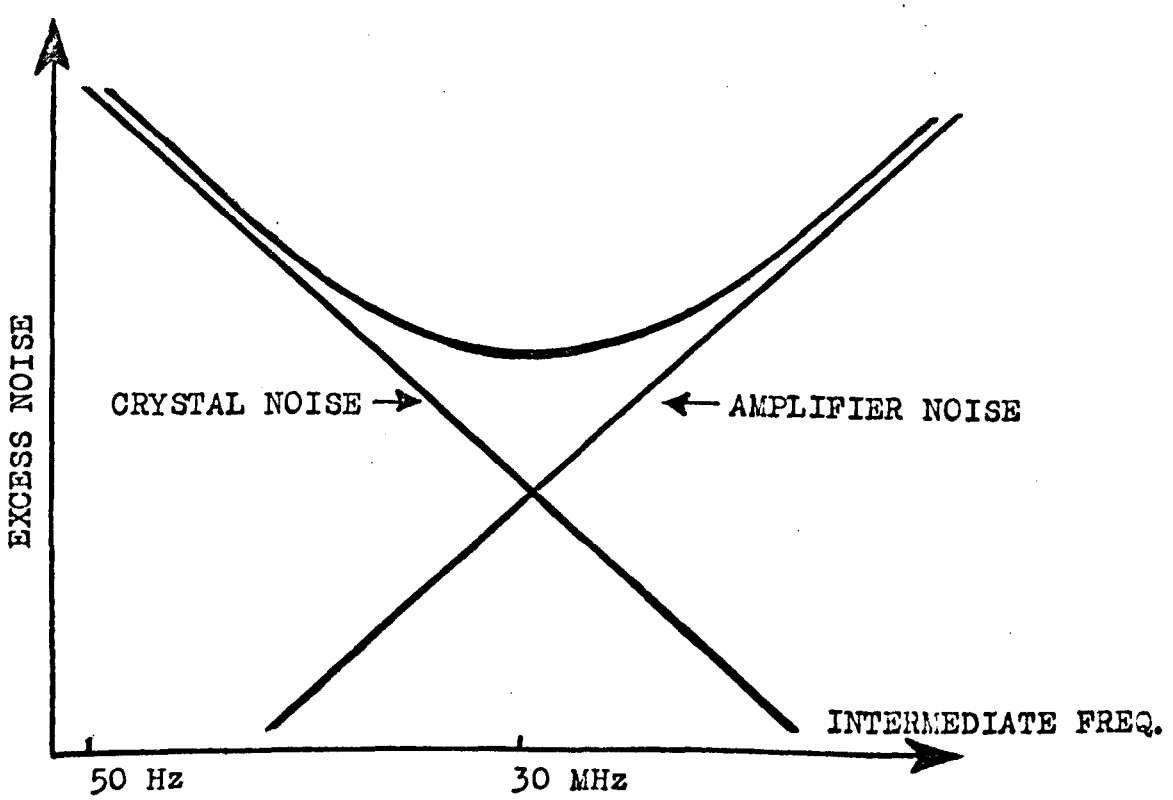

Fig(3.10) CRYSTAL AND AMPLIFIER NOISE.

3.12 Mode of operation

There are three modes of operation of the microwave system: crystal video, frequency swept superheterodyne and superheterodyne detection with zero sweep. The last two methods have the great advantage that they do not produce spectral line broadening.

(i) Crystal video

The simplest method of microwave detection is the crystal video technique which is used only in setting up procedures, such as cavity tuning. Microwave power passes from the Klystron type (Mfg No. 2443 OKI Electric Ind.) through the attenuator to the magic T. (See Figure 3.11 and 3.9). Here, the power is divided between the second and third arms. Power is reflected back down the second arm and passed into the fourth arm, entering the resonant cavities via a matching unit, followed by a microwave switch. Some of the power then will be reflected from either cavity through the third arm to pass to the detector crystal C_2 (Sylvania 1N26A). When the microwave signal f_k within the resonant cavity is at the transition frequency of the molecules in the cavity, the associated signal is transmitted by reflection to the magic T and along the third arm to C_2 , where the resonant signal is detected.

If the resonant signal is passed directly to the audio frequency vertical amplifier of an oscilloscope, the output power can be displayed. When the microwave cavity is tuned to the appropriate ammonia inversion line frequency, the mode of the Klystron and a small dip corresponding to the microwave cavity absorption can be seen on the oscilloscope. Any

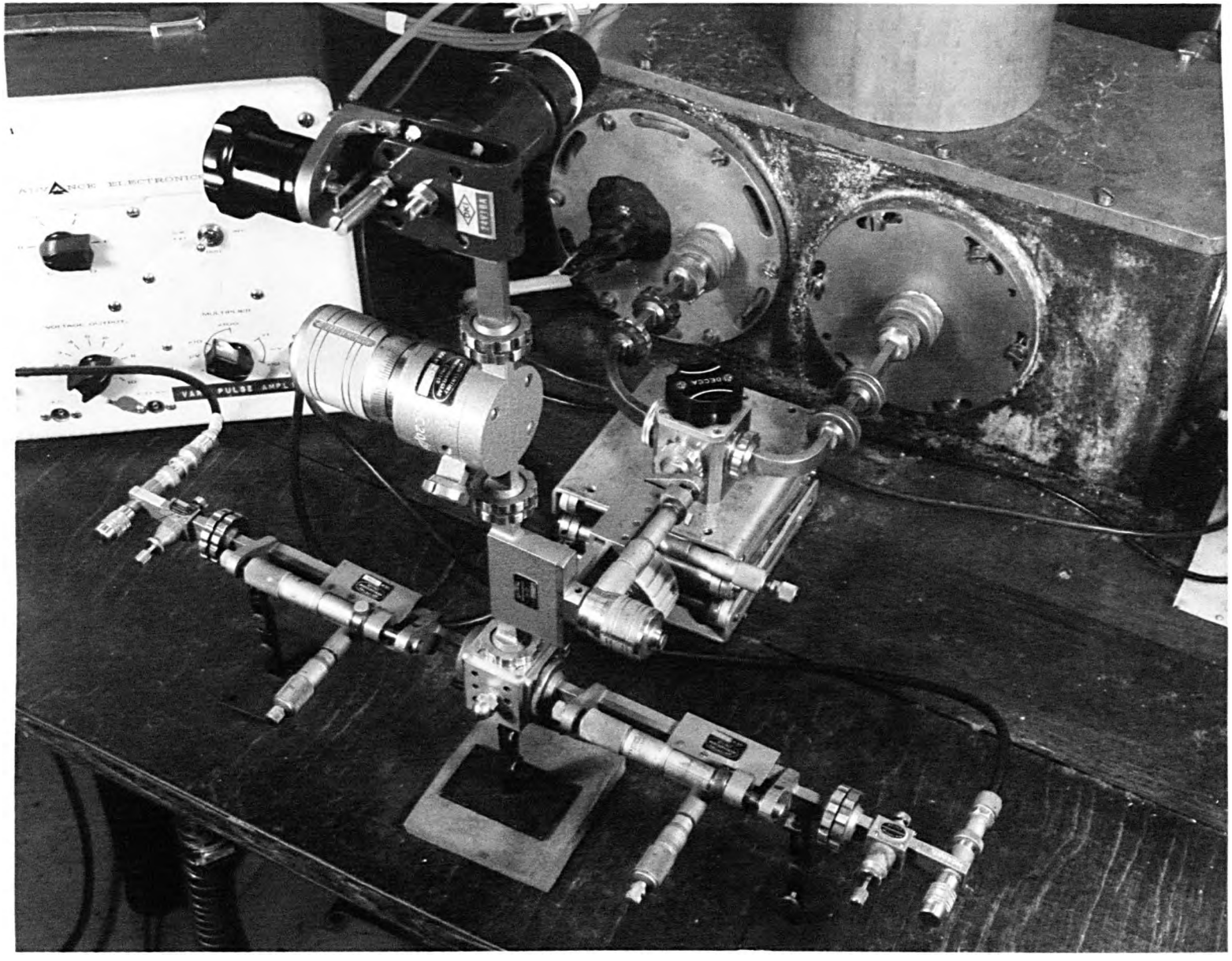

FIGURE(3.11) THE MICROWAVE BRIDGE

absorption of power due to the ammonia molecules in the cavity will then be displayed as a dip superimposed on the cavity absorption dip.

Having obtained the above conditions, the cavity resonance can be made to coincide with the molecular resonance by means of the cavity temperature controller and maximum absorption can be attained by precise matching of the microwave system.

With this crystal video mode of operation, the Klystron was swept over its electronic frequency tuning range by a saw-tooth waveform of about 100 volts peak potential. This was applied to the reflecter of the Klystron which swept the output of the Klystron through a complete mode and the frequency of the Klystron was varied at 50 Hz about the mean frequency of 23,870 MHz.

(ii) Frequency swept superheterodyne detection

Having determined that the cavity is tuned to the molecular resonant transition as already described above, the frequency swept superheterodyne mode of operation is obtained by inserting the 30 MHz preamplifier and main amplifier between the crystal detector C_2 and the oscilloscope. A 30 MHz signal is fed into the mixing crystal C_1 at an appropriate power level. The exciting signal is one of the two sidebands produced by amplitude modulation of the local oscillator power.

The Klystron frequency is offset by a frequency of 30 MHz from the resonant frequency of the ammonia line transition. As in the crystal video mode of operation, the signal of frequency f_k splits equally (under optimum matching

conditions) between the second and third arm. The signal f_k and the injected 30 MH_z signal from the sideband generator are mixed in the crystal C_1. The compound signal $f_k \pm 30$ MHz then passes to the cavity resonator via the magic T, the matching unit and the microwave switch. One of the components either $f_k + 30$ or $f_k - 30$ will interact with the molecules in the resonant cavity and the associated signal is reflected back via the fourth arm to the magic T and through the third arm to the second mixer C_2. Then, as the Klystron is swept over a small frequency range, the 30 MHz beat signal which results is passed into the I.F. amplifier and a spectroscopic signal is then displayed on the oscilloscope.

(iii) Unswept frequency superheterodyne detection

This mode of operation is similar to the frequency swept mode except that the sweep to the klystron reflector is switched off and hence, a steady D.C. output from the maser oscillation can be displayed on the oscilloscope.

CHAPTER 4

OPERATION OF J=3, K=2, $^{14}NH_3$ MOLECULAR BEAM MASER OSCILLATOR WITHOUT CRYOPUMPING OR TIME LIMIT

4.1 Introduction

Since the late 1940's scientific interest has been aroused in quantum frequency standards (atomic and molecular clocks) because they promise high frequency stability. High-precision frequency and time measurements are required for many applications in satellites, missile guidance systems in space, navigation and terrestrial communication systems.

Quantum standards of frequency developed in the microwave regions include the following: The caesium beam device, and quantum oscillators based upon either rubidium, hydrogen or ammonia.

Indeed, the unit of time was redefined by the "International Committee of Weights and Measures" in October 1967, in terms of the frequency of the caesium hyperfine spectral line. Two factors influenced the adoption of this system: The high accuracy (1 part in 10^{12}) of the resulting atomic time unit, and the technical simplicity of the caesium atomic beam device. Furthermore, the caesium hyperfine line is only symmetrical at resonance (9.192631770 GHz), so this provides an accurate check for the absence of any perturbing effect.

The rubidium vapour cell atomic standards are based on the same type of spectral line but employ different techniques. To obtain a sharp resonance the bulb containing the metal vapour utilizes a buffer gas at a pressure of about 1 torr.

Since this gas causes a frequency shift of a few kilohertz, the gas cell must be calibrated. In addition there is another shift due to the intensity and spectral distribution of the optical pumping light from the discharge lamp. Therefore, this type of device is useful as a secondary rather than primary standard of frequency.

The hydrogen maser is also a frequency standard of high accuracy and excellent long and short term frequency stability. However, it is subject to a technical difficulty which has not yet been fully overcome: the presence of a frequency shift associated with atom-wall collisions, as in the rubidium cell. When the two hyperfine levels of the hydrogen atom in zero magnetic field are shifted under the action of a strong magnetic field, those atoms in two of the three substates of the higher level pass into a bulb whose inner surface is coated with teflon. Inside the bulb, the atoms make thousands of bounces before undergoing a transition and therefore, a small frequency shift will usually occur. This shift is much smaller in the hydrogen maser oscillator than in the rubidium maser device, the former being of the order of 3 parts in 10^{11}, but its presence makes it impossible up to the present time to define frequency in terms of the hydrogen spectral line with a precision which exceeds that possible with the caesium atomic beam frequency standard.

Much attention was once given by workers in this field to developing a frequency standard based upon the $J = 3$, $K = 2$ inversion line in ammonia, both because ammonia beam masers are relatively simple to operate, and because a

successful conclusion of this work would have provided a very useful laboratory frequency standard with an accuracy of approximately 1 part in 10^{11}. However, this precision has only been obtained by intermittent operation as a consequence of freezing of the ammonia on the state selector and elsewhere.

Nevertheless, it was not until the present experimental programme was undertaken that the aim of operation without cryopumping or time limit was achieved. Since ammonia beam masers of conventional design require cryogenic pumping on weak inversion lines, such as the inversion line $J = 3$, $K = 2$ this necessarily imposed a time limit to their operation. A maser based upon stronger inversion lines of ammonia, for example $J = 3$, $K = 3$, has been freed from this restriction, by operation without cryopumping. For this particular line, the threshold condition is much more easily satisfied than for other lines, especially the $J = 3$, $K = 2$ transition which is particularly stable for laboratory frequency standard.

In practice, it is hard to find a spectral line which consists of only one component; the presence of hyperfine interactions in many molecules leads to splitting of the main transition into a number of hyperfine structure components and with line width obtained in practice many of these are not resolved. The line $J = 3$, $K = 3$ of the inversion spectrum of $^{14}NH_3$, which is usually used in masers, has a rich hyperfine structure caused by electric and magnetic interactions in the molecule. The strongest of these (the electric quadrupole interaction of the ^{14}N nucleus with the

field of the molecule) is of order of magnitude 4 MHz. The weakest interactions are those of the magnetic type. They include the spin-spin interaction between hydrogen and nitrogen nuclei, and the interaction of the spins of these nuclei with the magnetic field of the molecule caused by its rotation. They are of the order of (25-100) kHz. The frequency of the oscillation is given by:

$$\omega = \omega_L \left[1 - \frac{\omega_L - \omega_o}{\omega_L} \quad \frac{Q_o}{Q_L} \quad f(\phi)\right] \qquad (1)$$

where $f(\phi)$ is proportional to the potential on the focuser and to the saturation parameter (γ), i.e. $f(\phi) = f(V, \gamma)$ where $\gamma = (\mu E/\hbar)$. As can be seen from this formula, the function $f(V, \gamma)$ determines the variation of the oscillation frequency of the maser, as it depends on the tuning of the natural frequency ω_o of the resonator relative to the frequency ω_L of the spectral line.

The fractional change of the frequency caused by the presence of hyperfine structure when the saturation parameter (γ) is varied, is a quantity of the order of 2×10^{-9}; when the voltage is changed from 5 to 25 kV, the fractional change of the frequency is about $(3-5) \times 10^{-9}$. Therefore, to secure a high stability of the oscillation frequency of a maser better than 10^{-10}, it is necessary to use emission lines in which there is no hyperfine structure. A line of this sort is the inversion line of $^{14}NH_3$ (J = 3, K=2), for which there is no quadrupole hyperfine structure, but only magnetic hyperfine splitting. The magnetic splitting is small and the frequency shift is of order of magnitude one part in 10^{-11}.

A disadvantage of this line is its relatively weak intensity (the condition for self oscillation is less well satisfied than for the line $J = K = 3$ by a factor of about 135). According to Basov (1961) the statistical weight of of the inversion levels ($J = 3$, $K = 2$) is only half of that for levels ($J = 3$, $K = 3$) and the matrix element of the dipole moment for inversion transition $J = 3$, $K = 2$ is smaller by a factor of 1.5 than that for the transition $J = K=3$, which means that there is less effective sorting of molecules which are in the level $J = 3$, $K = 2$.

According to Barnes (1958), the percentage density and focusing force constant for $J = K = 3$, ($M = 2$) are of the order of 6% and 5.6×10^{-37} Farad. meter^2 respectively, while in case of $J = 3$, $K = 2$, ($M = 2$) they are of the order of 2% and 2.64×10^{-37} Farad.meter^2.

From equation (1.11) it can be seen that for lines of $^{14}NH_3$ with K not a multiple of 3, the magnetic constants which determine the hyperfine interaction are 3 in number. Therefore it is necessary to have the results of tunings for 3 lines. But all the inversion lines of $^{14}NH_3$ except $J = 3$, $K = 2$ have quadrupole splittings in the first order of perturbation theory which are much larger than the magnetic splitting, and the effect of the magnetic satellites on the tuning will be smeared out by the stronger influence of the quadrupole structure of the line. Thus, this line ($J = 3$, $K = 2$) is a special case in the respect that the factor $J(J + 1) - 3K^2$ vanishes and so the only interactions which should be non-zero are the nitrogen and hydrogen magnetic interactions with molecular rotation.

4.2 Stability and reproducibility

Masers operated on the J = 3, K = 2 line of $^{14}NH_3$ have been constructed by several workers (Bonanomi et al 1958, Shimoda 1961, and Strakhovskii et al 1963). They have been found to be more stable and reproducible than those on the J = K = 3 line. Dependence of the frequency of oscillation on the source flux, focuser voltage and small magnetic and electric fields between the focuser and the entrance of the resonator have been investigated. The results of Strakhovskii et al attest to the fact that the electric and magnetic fields affect the maser frequency not only indirectly, through the varying intensity of emission, but also directly by shifting the frequency of the peak of the emission line. They found that the weak nonuniform stray electric field which is always present in the space between the resonator cavity and the end of the sorting system has a substantial effect on the frequency stability of the maser on J = K = 3 line, especially with ring and helical types of focuser. But for a maser operated on the J = 3, K = 2 inversion line the effect of stray fields on the absolute stability was considerably weaker, since in this case the peak of the emission line is practically unshifted. The effect of the electric and magnetic fields within the maser operating on the line J = 3, K = 2 may be used to tune the maser to the peak of the emission line. Tuning by the magnetic perturbation method can be successfully applied to the 3,2 line maser if sufficient care is taken. The reproducibility of tuning can be within a fraction of 1Hz.

This is probably the best result obtained so far concerning the resettability of any molecular frequency standard.

Since the weak field Zeeman effect of the 3,2 line of $^{14}NH_3$ is now throughly understood, the magnetic perturbation method can be employed as a precise method of tuning the cavity of the maser oscillator. A system of automatic cavity control with a time constant of less than a second was built by Shimoda (1961) and operated in the Tokyo Astronomical Observatory. A precision in tuning the frequency within $\pm 5 \times 10^{-12}$ and a stability of $\pm 1.2 \times 10^{-11}$ was obtained, when the focuser and the flow rate of ammonia was kept constant within several percent.

It was found that the frequency of the maser tuned by the magnetic perturbation method varies with the earth and other magnetic fields in the vicinity of the resonator. The inhomogeneity of the magnetic field as well as its magnitude and direction has been found to shift the centre frequency determined by magnetic perturbation method.

In contrast to the hydrogen maser, it should be noted that the effect of a magnetic field upon frequency is several orders of magnitude smaller than in the hydrogen maser. The frequency shift due to the longitudinal Doppler effect is larger in the ammonia maser than in the hydrogen maser, but the transverse Doppler effect is larger in the hydrogen maser. However, the frequency shift due to longitudinal Doppler effects can be reduced by using two beams in opposite directions. A system of automatic beam balancing which compensates for the effect of slight asymmetry of the cavity and the focuser may permit an absolute accuracy of the order

of one part in 10^{-12} provided the maser is magnetically shielded.

4.3 OPERATION WITHOUT CRYOPUMPING

In the maser one of the important parameters is the power delivered and the length of time of operation. These characteristics are directly related to the construction of the basic elements of the maser; the molecular beam source, the selection system, the background pressure and the cavity resonator. Increasing the power of a maser (strong oscillation) means increasing the number of active molecules entering the cavity resonator. This number can be enhanced by increasing the total number of molecules moving in the direction of the cavity or by increasing the molecular capture angle in the selector system. The directivity of a molecular beam entering the sorting system and then the cavity plays a major role for high power output. In the present work this has been achieved by employing a nozzle-skimmer configuration. Consequently, a larger number of molecules can be obtained for the same background pressure conditions in the system. However, the question of stability of the maser with such a source (Nozzle-skimmer), remains open because the gas flow is in the form of a jet causing an increase in the molecular velocity which leads to a broadening of the emission linewidth.

In view of the interest in maser oscillators as frequency standards of high stability and reproducibility, work on the operation of the maser without cryopumping has been carried out by various workers (White 1959, Skvortsov et al 1960,

Griger'yants and Zhabotinskii 1961 and Bardo and Lainé 1971) on an ammonia beam maser ($^{14}NH_3$ $J = 3$, $K = 3$ line) without liquid nitrogen cryopumping and by Krupnov and Skvortsov with the $1_{01} \rightarrow 0_{oo}$ line of formaldehyde (CH_2O) which has no unresolved hyperfine structure.

It was found, neither of these transitions is satisfactory for frequency standard applications, because of the presence of unresolved quadrupole hyperfine structure in the $J = K = 3$ line of $^{14}NH_3$, and unsatisfactory control over the beam intensity as a consequence of the preparation of CH_2O gas from the polymer.

Owing to the success of the maser operation on the $J = K = 3$ inversion line of $^{14}NH_3$ without cryopumping, extension of the technique to the same transition of $^{15}NH_3$ is possible. But this isotopic species of ammonia is very expensive, thus gas recycling is necessary, which is both inconvenient and difficult on account of gas purity problems over a period of time. Therefore, it appears that the $J = 3$, $K = 2$, line of $^{14}NH_3$ is the preferable one for frequency standard applications without cryopumping.

In fact, the present apparatus was designed with a view to obtaining oscillation on several weak spectral lines of $^{14}NH_3$ without the aid of cryogenic pumping and therefore, capable of continuous oscillation. Particular attention has been paid to the 3, 2 inversion line of $^{14}NH_3$ in view of its properties as a molecular frequency standard. For the first time, strong and continuous oscillation without time limit on this line (3,2) was readily obtained without

cryopumping. Subsequently, strong and continuous oscillation also was obtained on the (2,2) line of $^{14}NH_3$.

4.4 Experimental setup

Owing to the fact that the spectral line of the $J = 3$ $K = 2$ line of $^{14}NH_3$ is rather weak and state selection efficiency poor, to reach the oscillation threshold condition an increase in gas flux over that commonly employed in a $J = K = 3$ inversion line of ammonia maser by a factor of 135 is needed (Bonanomi et al 1958). The present maser technique is capable of fulfilling this requirement and attaining the conditions for strong oscillation on this line in the absence of the usual cryopumping facility, without time limit.

This has been made possible by the use of differential pumping, a molecular beam skimmer separating the two vacuum chambers and a nozzle type of gas source. The maser was constructed with differential pumping of the two main chambers. The first chamber housed the molecular beam source, the second the state separator and the maser cavity resonator. The gas source chamber was pumped by a 6" Edwards oil diffusion pump type E04 and the state separator-cavity chamber by two 4" Edwards oil diffusion pumps type 403A. The 6" and the two 4" pumps were respectively backed by Edwards ISC 450B and Metrovac GDR1 rotary pumps. The pumping speeds in the nozzle and cavity chambers were both of the order of 0.6 $m^3.s^{-1}$, to make a total pumping speed of 1.2 $m^3.s^{-1}$. The wall separating the two chambers was drilled and screw threaded to accept a diaphragm iris of

variable diameter which could be adjusted by means of reduction gearing from outside the vacuum chamber, or a skimmer of the type conventionally used in supersonic molecular beam work (Zapata et al, 1961).

The skimmer cone angles of 35° inside and 45° outside were machined to form a cone apex with a very sharp leading edge in order to reduce molecular beam scattering. The nozzle source used was constructed by machining a 45° cone into a brass disc, to within about 0.1 mm of breaking through. A hole of 0.2 mm in diameter was then made by using a jeweller's drill. The nozzle source was vacuum sealed into the screw threaded end of a 12.7 mm diameter copper pipe. The axial position of the nozzle could be varied externally. The nozzle-skimmer geometry and dimensions are shown in Figure (4.1). The state separator was of the ring type as in Figure (3.7).

4.5 Experimental results

One objective of the experimental work was to oscillate on the $J = 3$, $K = 2$ line of $^{14}NH_3$ pumped solely by diffusion and mechanical pumps. The maser was first set up to oscillate on the $J = K = 3$ inversion line of $^{14}NH_3$ with a cavity of 10 cm long. The variable iris diaphragm between chambers was set to an optimum diameter of 2.0 mm. The ammonia maser was operated with an optimum oscillation threshold voltage of 9.8 kV without cryopumping, and a pressure of 17.5 torr behind the nozzle. When the variable iris diaphragm was replaced with the molecular beam skimmer, the oscillation threshold fell to 7.2 kV with an optimum

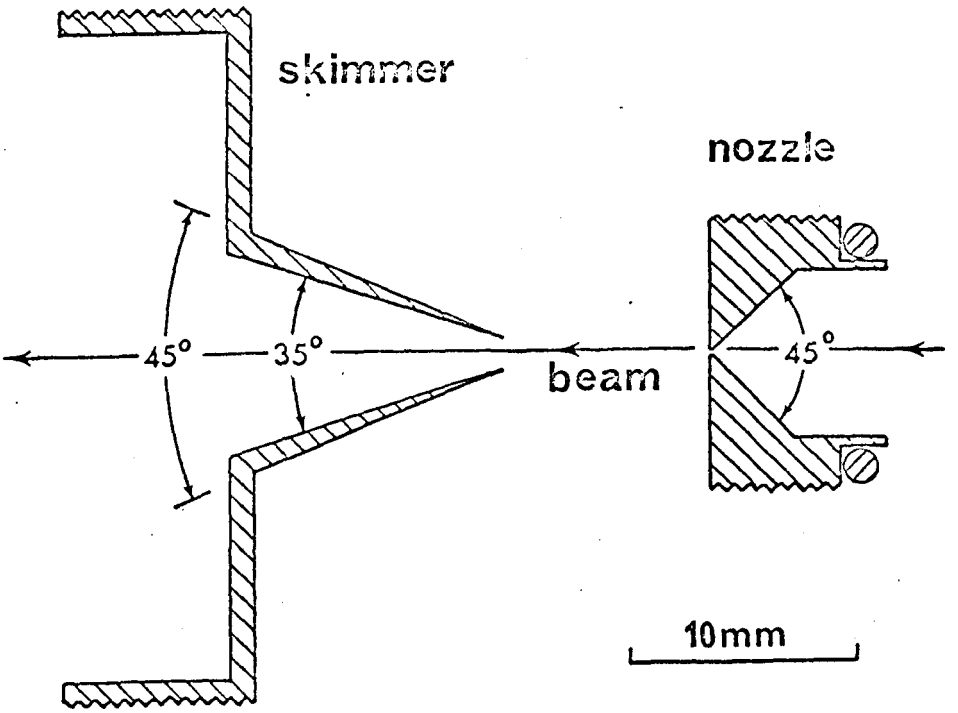

FIGURE(4.1) SECTION THROUGH MASER GAS NOZZLE AND SKIMMER.

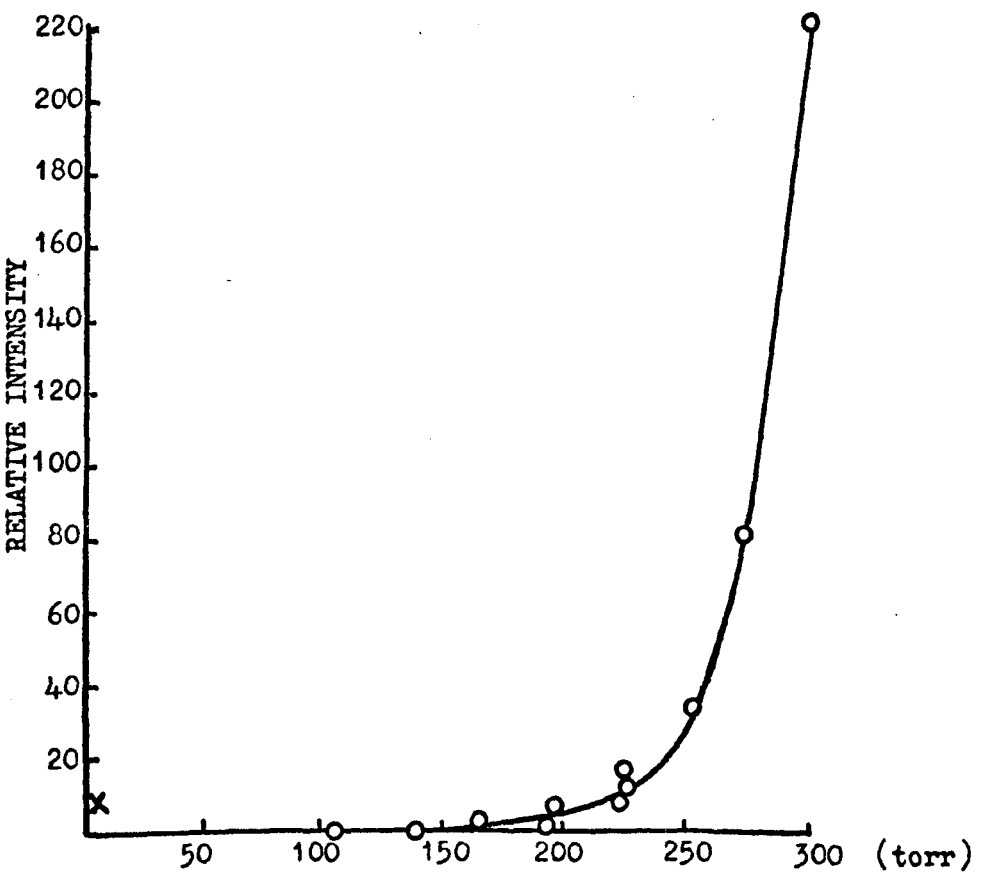

FIGURE(4.2) BEAM INTENSITY AS A FUNCTION OF THE INLET AMMONIA GAS PRESSURE (After Kistiakowsky and Slichter 1951).

pressure of 30 torr behind the nozzle. When both chambers were cryopumped with liquid nitrogen, the threshold for oscillation fell to 5.2 kV with an optimum nozzle pressure of 40 torr.

The maser was then set up on the $J = 3$, $K = 2$ inversion line of $^{14}NH_3$ by employing a cavity of 130 mm long with a loaded $Q = 7300$ (Figure 3.8) with the same state separator, nozzle and skimmer as before. The maser was operated with an oscillation threshold of 25 kV without cryopumping with a nozzle pressure of 12.5 torr. Then, with cryopumping, the oscillation threshold fell to 18 kV at an optimum gas pressure of 25 torr behind the nozzle.

In comparison, other $J = 3$, $K = 2$ cryopumped ammonia beam masers have been operated with threshold of 8 kV and 175 mm respectively (Bonanomi et al 1958), and 6 kV and 400 mm (Shimoda 1961). The focuser length was determined by the relatively short mean free path for molecules without cryopumping. It appears that the relatively high focuser voltage required to reach the threshold of oscillation with cryopumping was due to a short focuser (83 mm) employed for the present investigations. Therefore, it is quite possible that even lower oscillation threshold voltage could be obtained by designing a focuser with an optimum length and transparency provided that the same nozzle-skimmer combination is used.

In view of the emphasis placed on the threshold conditions for oscillation, it should be noted that the maximum amplitude of oscillation without cryopumping was sufficient to give strong oscillation transients on the $J=K=3$

spectral line (Lainé and Bardo 1969) and an aperiodic transient on the J = 3, K = 2 inversion line. With cryopumping an oscillation transient was also observed on the latter line.

A summary of the operation parameters of the maser operated without cryopumping is given in table (4.1). Clearly, the above results represent a substantial improvement over those obtained previously by Bardo and Lainé (1971) where the lowest focuser voltage for oscillation with J = K = 3 inversion line was 21 kV.

4.6 Conclusions

The present apparatus showed the feasibility of operation of a molecular beam maser based on the J = 3, K = 2 inversion transition of $^{14}NH_3$ with only oil diffusion pumps and associated backing pumps. This has been made possible by the use of a skimmer to collimate the molecular beam and a fairly high pressure of ammonia behind the miniature nozzle source.

The maximum attainable intensity in the collimated beam in a conventional molecular beam source "effuser" is limited by several factors:

a) the geometry of the effuser

b) the number of molecules per unit volume behind the exit of the effuser

c) The unfavourable geometrical factors encountered in selecting the collimated beam from the Maxwellian distribution of initial velocities.

Ammonia inversion transition (J , K)	3,3	3,3	3,2
Single hole nozzle diameter (mm)	0.20	0.20	0.20
Gas pressure behind nozzle, optimum, (torr)	17.5	30.0	12.5
Background gas pressure, nozzle chamber (torr)	$\sim 1 \times 10^{-7}$	7×10^{-7}	$\sim 1 \times 10^{-7}$
Iris separating two vacuum chambers optimum diameter (mm)	2.0	-	-
Skimmer separating two vacuum chambers diameter (mm)	-	1.6	1.6
Separation between nozzle or iris and entrance to skimmer	9.0	9.0	9.0
Background gas pressure focuser/cavity chamber (torr)	1.0×10^{-5}	1.0×10^{-5}	1.4×10^{-5}
Length of cavity (mm)	100	100	130
Loaded cavity Q	$\sim$ 9000	$\sim$ 9000	$\sim$ 7300
Threshold voltage for oscillation (kV)	9.8	7.2	25.0

TABLE (4.1) COMPARISON OF OPTIMUM THRESHOLD CONDITION FOR AMMONIA MASERS OPERATED WITHOUT CRYOPUMPING.

If the diameter of the effuser is larger than the mean free path of the molecules, the beam from the source will be changed from free molecular flow to a process called "cloud formation", such that the molecules spread out evenly into a hemispherical profile. The radius of this profile is of the order of magnitude of the distance between the effuser and the second slit "diaphragm". This leads to a reduction in the intensity of the molecular beam at the detector.

By the use of a "nozzle source" most of the random translational and internal energy of the gas is converted into directed mass motion, which provides an initial collimation. This improves the effusion rate and the geometrical profile of the gas flow. Therefore, the molecules spread out within a narrow elliptical profile, mainly along its major axis which is several times the distance between the nozzle source and the skimmer. As a consequence the molecular velocities in the beam would be partially monochromatized.

Since, the molecules in the beam are grouped about the initial mass motion the skimmer provides an additional partial velocity selection among the velocities of the molecules in the beam. This depends on the skimmer geometry, diameter, internal and external angles, leading edge thickness and the distance between the leading edge and the nozzle source. On the vacuum side those molecules which enter the skimmer and strike its walls should be pumped away fast enough to minimise beam scattering. The flow deflection caused by

the skimmer should not be large enough to form a shock wave upstream which would destroy the molecular flow. This can be overcome by adjusting the distance between the nozzle source and the skimmer. The required high ratio of the nozzle source pressure to the nozzle exit pressure, causes lags in the internal molecular energy due to the rapid temperature drop in the nozzle source as the result of a sudden expansion by the nozzle. Under such conditions, it can be assumed that nearly all the molecules leaving the nozzle have the same mass flow velocity, thus all the thermal energy should be converted into energy of directed mass motion. Consequently, the internal molecular energies (temperature) in the beam would be reduced from their previous values. According to Kantrowitz (1950) the temperatures which are attainable by nozzle source expansions are very low (0.24 x gas supply temperature for the sample design) and it should be possible to attain a molecular beam with a large number of the molecules in the lower rotational states.

Kistiakowsky et al (1951), had employed a nozzle-skimmer type device with ammonia as a test gas. They found that the maximum intensity obtained exceeded by more than a factor of 20 that which is obtainable from the ordinary effusion system under optimum conditions. They suggested that still greater enhancement of molecular beam intensity is possible with an apparatus of refined design.

Figure (4.2) represents a typical result obtained for the beam intensity of ammonia gas as a function of the inlet

gas pressure. It was observed that for relatively low pressures, the beam intensities obtained were small. At higher pressures the intensity of the beam began to rise far more rapidly with respect to the pressure. For pressures above 170 torr a marked gain in the intensity is obtained, especially at a pressure of about 300 torr. The point (x) on the graph indicates the relative beam intensity to be expected with a conventional effuser source at the optimum pressure predicted by the kinetic theory. Therefore, this characteristic is not explicable by conventional kinetic theory, but on the basis that the source is functioning, as expected, hydrodynamically. Moreover, further tests with ammonia gas showed an anomalous behaviour. It was found that a sudden introduction of ammonia gas to the nozzle source caused a decrease in the intensity, while cutting off the flow resulted in a temporary large increase in the beam intensity. Similar behaviour with the apparatus discussed in this thesis has been obtained and attributed to condensation of ammonia gas in the nozzle (see Section 3 of Chapter 3).

From the results obtained, it can be concluded that the use of a nozzle-skimmer combination leads to the benefit of high beam intensity of excellent directivity. Furthermore, a univelocity beam results with cooling of the molecular rotational states which favours stronger emission lines in the present work.

CHAPTER 5

MOLECULAR OSCILLATOR WITH TWO CAVITIES IN SERIES

5.1 Introduction

Detailed experimental investigations and theoretical studies have been the subject of several papers, after Higa (1957) who was the first to conduct an experiment on two cascaded cavities employing ammonia gas ($^{14}NH_3$, $J = 3$ $K = 3$ inversion line). This is because the properties of two cavity maser systems are extremely interesting both, from a practical point of view, and for investigating radiation processes. Various points of interest may be summarised as follows:

(a) The system can manifest the fundamental properties of two quantum state systems.

(b) Such a system is a very sensitive spectrometer for observation of the hyperfine structure of the ammonia molecule.

(c) The two-cavity system can be used as a frequency standard.

(d) The system can be used as a very low-noise amplifier.

(e) The second cavity can be used for exact tuning of the first cavity to the molecular resonance frequency.

In 1957 Higa investigated the operation of an ammonia oscillator with two cavities in series. The two cavities were coupled only by the oscillating polarization carried by the beam. In Higa's experiment the two cavities were first tuned to the molecular frequency. The first cavity (C_1) through which the beam passed was then detuned. Oscillations in the second cavity (C_2) were observed to follow

precisely the frequency in C_1 up to a value a few kHz from the molecular resonance frequency. With further detuning of C_1, C_2 began to oscillate simultaneously at the molecular resonance frequency to which it was tuned, and the frequency of C_1.

Subsequently, a number of detailed experimental investigations and theoretical analyses have been put forward by many authors. The most important characteristics, such as the frequency, spectrum, intensity and general behaviour of the oscillation in C_2 were investigated (Strakhovskii and Tatarenkov 1962, Lainé and Srivastava 1963, Basov et al 1964, and others). Generally, it is found that the characteristics of such a system are rather complex. However, the gross features of the system are understood qualitatively while several aspects have not yet received an adequate quantitative explanation. Nevertheless, further attempts to obtain a more satisfactory theory have been reported by Basov et al (1967) and Lainé et al (1968, 1971, 1973).

Qualitative explanations of the dynamic state of the molecules after emerging from C_1 have been given by Wells(1958) Basov and Oraevskii (1962) and Oraevskii (1964, 1967) on the basis of quantum mechanics. Wells used a geometrical technique developed by Feynman, Vernon and Hellwarth (1957) to explain qualitatively the experimental observation of a cavity (C_2) in a maser which oscillates simultaneously at two different frequencies under certain conditions as the beam is first passed through C_1. According to Dicke (1954) the radiation field in C_1 produces states with definite coherent phase relations between the individual excited molecules

(the molecules radiate co-operately in a coherent emission field). As the molecules emerge from C_1 their phase relations are preserved, thus they are in a "super radiant" state and the molecular frequency is equal to the oscillation frequency in C_1. On entering C_2, the molecular signal will drive C_2 and an emission signal is established at a frequency of the first cavity transition.

When C_1 and C_2 are tuned to the molecular resonance, the population in the upper state reaching C_2 is insufficient to sustain an oscillation independent to that in C_1 but as C_1 is detuned its oscillation amplitude decreases and enough molecules in upper state (with a transition probability larger than $\frac{1}{2}$) enter C_2 to support an independent oscillation. Consequently, two signals may be detected in C_2 as a beat note with a frequency of the order of several kHz. Strakhovskii & Tatarenkov (1962) and Lainé and Srivastava (1963) as two independent groups have examined the oscillation characteristics in C_2 in some detail. Both groups found that if C_1 and C_2 were tuned to the molecular resonance and C_1 was strongly oscillating, then the output signal from C_2 was relatively small. When C_1 was gradually detuned, a decrease of oscillation amplitude in C_1 was observed whereas, the oscillation in C_2 grew to a maximum value at about 2 MHz from the central line. On further detuning, the output from C_2 decreased until, in the region of 4 to 5 kHz, sinusoidal Higa beats appeared and the oscillation amplitude rapidly increased, reaching a maximum, with a modulation depth of about 25%. With further detuning of C_1 (beyond 5 MHz), the beats gradually disappeared, C_1 ceased to oscillate

and C_2 performed as a single cavity maser oscillator. Lainé and Srivastava introduced a qualitative explanation of the behaviour of the spectrum and amplitude modulation in C_2 in terms of molecular ringing, amplification and saturation. A typical graph of their results is shown in Figure (5.1).

Basov et al (1964) used a quantitative theoretical analysis based on Maxwell and Schrödingers' equations to explain the oscillation amplitude characteristics and Higa beats in C_2. In their approach a classical field was assumed to arise from the polarisation of the beam. In their treatment they were able to show that when C_1 is detuned from its resonance frequency, the frequency of oscillation in C_2 follows precisely that of C_1 over a limited range from D to B or D to $\bar{B}$. They were also able to show that if C_1 is tuned exactly to the molecular resonance frequency then for a large electric field amplitude in C_1, the radiation intensity in C_2 could become zero. See figure (5.1).

Li Tie-Cheng and Fang-Li-Zhi (1964) adopted a more rigorous quantum mechanical treatment using a model similar to that employed by Senitzky (1958) where the radiation field was quantized. Their analysis predicted that when C_1 is detuned through its full range, there should be certain frequency sectors for which oscillations are induced in C_2 and other sectors would not sustain oscillations. This section of assumption seemed to be in qualitative agreement with the double maximum of the detuning pattern, but it does not offer an explanation for the single maximum pattern at low voltages on the sorting system.

It can be seen from the above argument that not all of the macroscopic effects observed in a two-cavity system can be

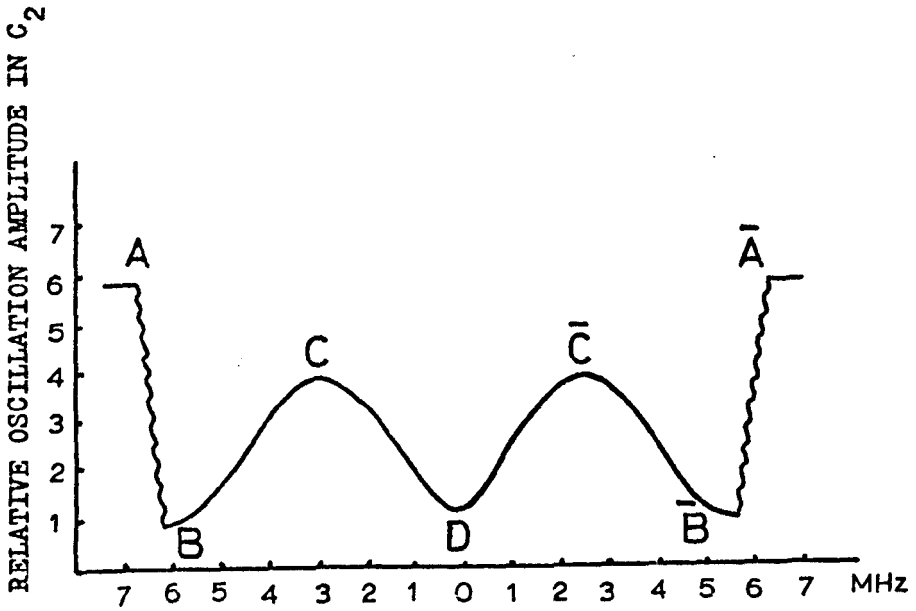

FIGURE(5.1) AMPLITUDE OF OSCILLATION IN C_2 AS A FUNCTION OF TUNING C_1 (After Basov et al 1964).

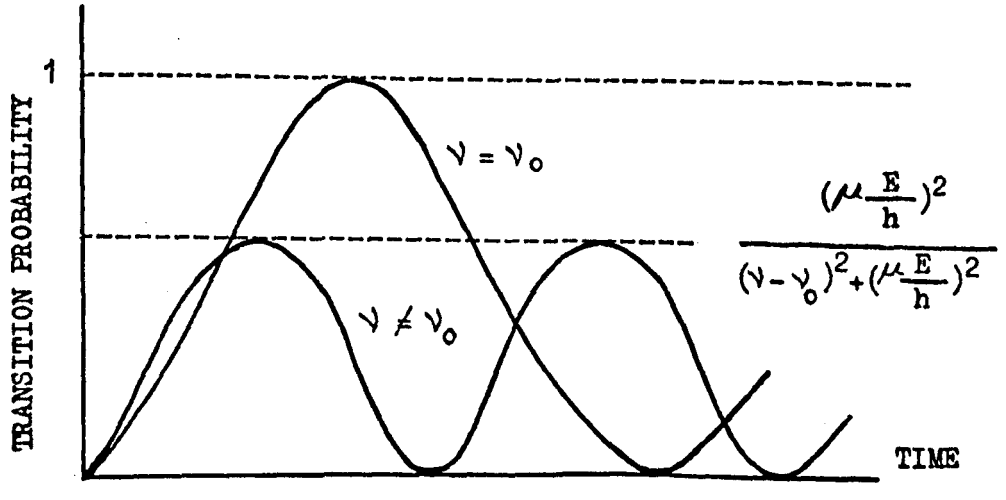

FIGURE(5.2) TRANSITION PROBABILITIES BETWEEN MOLECULAR ENERGY STATES AS A FUNCTION OF TIME.

explained clearly, especially the "two maxima with the gap in the middle". However, Basov et al (1963) reported that this effect might arise as a result of the transition probability of the molecules passing through C_2 depending on the degree of excitation received from C_1. Moreover, Basov et al (1967) suggested that the two maxima with gap might arise as a result of the interference between the emission from molecules which are moving with different velocities and radiate fields with different phases.

With the aim of providing a deeper insight into two-cavity maser phenomena, in the remainder of this chapter a critical review of the previous work will be introduced. Extensive investigation of new features obtained will be described in detail and compared with previous results. A theoretical treatment of a two-cavity problem will be given in an attempt to interpret the results obtained experimentally. From the physical principles underlying the mechanism of amplification in a two-cavity molecular beam amplifier, a simplified theory of the operation of the cascaded system is presented. Analogies between a two-cavity molecular beam maser system and a two-coil nuclear maser (n.m.r.) will be discussed.

5.2 Theoretical treatment of molecular transition probabilities

(i) Single-cavity system

In general, the state of a molecule can be described by a wave function ψ which is a linear combination of the energy eigen-functions of the system:

$$\psi = a_1 U_1 \exp(-iW_1 t/\hbar) + a_2 U_2 \exp(-W_2 t/\hbar) \qquad (1)$$

where the eigen values W_1 and W_2 are corresponding to eigen functions U_1 and U_2 and a_1 and a_2 are constants and $|a_1|^2$ and $|a_2|^2$ give the probability of molecules being in state 1 or 2 respectively in the stationary state. The frequency for the molecular transition from state 1 to state 2 is given by:

$$\omega_0 = (W_1 - W_2)/\hbar \tag{2}$$

If at time t = 0, the molecules are subjected to a time dependent perturbation (periodic perturbation of the electric field $E \cos(\omega t + b)$) which can induce transitions between two molecular eigen-states, then a_1 and a_2 become functions of time. Then the wave function ψ takes the form:

$$\psi = a_1(t)\, U_1 \exp(-iW_1 t/\hbar) + a_2(t)\, U_2 \exp(-W_2 t/\hbar) \tag{3}$$

where $a_1(t)$ and $a_2(t)$ can be obtained from the time-dependent Schrödinger equation under the initial conditions. Now ψ must satisfy the time-dependent Schrödinger equation. Therefore, the solutions are:

$$\ddot{a}_1 + i(\omega - \omega_0)\,\dot{a}_1 + (\mu E/2\hbar)^2\, a_1 = 0 \tag{4}$$

$$\ddot{a}_2 - i(\omega - \omega_0)\,\dot{a}_2 + (\mu E/2\hbar)^2\, a_2 = 0 \tag{5}$$

If the initial conditions are such that at t = 0; $a_1(0) = 1$ and $a_2(0) = 0$ and b = 0, the solution for the values of $a_1(t)$ and $a_2(t)$ are:

$$a_1(t) = \left[\cos(yt/2) + (iz/y)\sin(yt/2)\right] \exp(-izt/2) \tag{6}$$

$$a_2(t) = \left[(ig/y)\sin(yt/2)\ \exp(izt/2)\right] \tag{7}$$

Here $$y = \left[(\omega - \omega_0)^2 + (\mu E/\hbar)^2\right]^{\frac{1}{2}}$$

$$z = (\omega - \omega_0)$$

and $$g = (\mu E/\hbar)$$

The above equations represent the expression for the transition probabilities used in a single cavity maser. Hence, the transition probability that a molecule has made a transition from state 1 to 2 at time t is:

$$|a_2|^2 = \frac{(\mu E/\hbar)^2}{(\omega - \omega_0)^2 + (E/\hbar)^2} \sin^2\left[(\omega - \omega_0)^2 + (\mu E/\hbar)^2\right]^{\frac{1}{2}} \frac{t}{2} \qquad (8)$$

Figure (5.2) is a plot of equation (8). As shown the transition probability varies periodically between zero and $(\mu E/\hbar)^2/\left[(\omega - \omega_0)^2 + (\mu E/\hbar)^2\right]$ with a rate being equal to $\left[(\omega - \omega_0)^2 + (\mu E/\hbar)^2\right]^{\frac{1}{2}}$. On resonance ($\omega = \omega_0$), a molecule oscillates between the two energy states, whereas under the off resonance condition ($\omega \neq \omega_0$), a molecule which starts in one state has no certainity of reaching the other state unless the process is reversed (Wittke 1957).

(ii) Two-cavity system

The following treatment is applied to a two-cavity maser operated with both cavities tuned to the molecular resonance frequency (ω_0). The average power emitted by a molecular beam in a maser is given by:

$$P = N h f_0 |a_2(t_1)|^2 \qquad (9)$$

The power emitted in C_1 is given by:

$$P_1 = N h f_0 |a_2(t_1)|^2 \qquad (10)$$

where t_1 is the time spent by the molecules in C_1 and $\omega_0 = 2\pi f_0$.

If subsequently the molecules pass through C_2 for a time t_2, then the total power in C_1 and C_2 for the total time $(t_1 + t_2)$ can be given by:

$$P_{1+2} = N h f_o \left|a_2(t_1+t_2)\right|^2 \qquad (11)$$

Then the power emitted in C_2 is

$$P_2 = N h f_o \left[\left|a_2(t_1+t_2)\right|^2 - \left|a_2(t_1)\right|^2\right] \qquad (12)$$

The coefficients $a_2(t_1)$ and $a_2(t_1+t_2)$ are the transition probabilities for the molecules making a transition from the upper energy level to the lower energy level in time t_1 and $(t_1 + t_2)$ respectively. In order to evaluate the power P_2, the two coefficients should be determined. Consider a molecule on which the perturbation

$$H_1 = - E_1 \mu_1 \cos(\omega_1 t)$$

acts on the molecule for a time t_1 after which it enters a region where another perturbation

$$H_2 = - E_2 \mu_2 \cos(\omega_2 t)$$

acts for a time t_2, then the solutions of the two differential equations (when $a_2(0) = 1$ and $a_1(0) = 0$) yield the following expressions

$$a_1(t_1) = \left[\cos(y_1 t_1/2) + (iz_1/y_1)\sin(y_1 t_1/2)\right] \exp(-iz_1 t_1/2) \qquad (13)$$

$$a_2(t_1) = \left[(ig_1/y_1)\sin(y_1 t_1/2)\right] \exp(iz_1 t_1/2) \qquad (14)$$

$$a_1(t_1+t_2) = \left\{\left[\cos(y_2 t_2/2) + (iz_2/y_2)\sin(y_2 t_2/2)\right] a_1(t_1) + \right.$$

$$\left.\left[(ig_2/y_2)\exp(-iz_2 t_1/2)\sin(y_2 t_2/2)\right] a_2(t_1)\right\} \exp(-iz_2 t_2/2) \qquad (15)$$

$$a_2(t_1+t_2) = \left\{\left[(ig_2/y_2)\exp(iz_2t_1/2)\sin(y_2t_2/2)\right] a_1(t_1) + \cos(y_2t_2/2) - (iz_2/y_2)\sin(y_2t_2/2)\, a_2(t_1)\right\} \exp(z_2t_2/2) \quad (16)$$

Now in the case of a two cavity ammonia beam maser with both cavities tuned to the molecular resonance, the above expressions under conditions $z_1 = z_2 = 0$, $y_1 = g_1$ and $y_2 = g_2$, yield

$$a_1(t_1) = \cos(g_1t_1/2) \quad (17)$$

$$a_2(t_1) = i\sin(g_1t_1/2) \quad (18)$$

$$a_1(t_1+t_2) = \cos\left[(g_2t_2/2) + (g_1t_1/2)\right] \quad (19)$$

$$a_2(t_1+t_2) = i\sin\left[(g_2t_2/2) + (g_1t_1/2)\right] \quad (20)$$

from which the transition probabilities can be obtained, thus:

$$\left|a_2(t_1+t_2)\right|^2 = \sin^2\left[(g_2t_2/2) + (g_1t_1/2)\right] \quad (21)$$

Hence, from the equations (12), (18) and (21), the power P_2 emitted by the molecular beam in the second cavity is:

$$P_2 = N h f_o \left\{ \sin^2\left[\left(\frac{g_2t_2}{2}\right) + \left(\frac{g_1t_1}{2}\right)\right] - \sin^2\left(\frac{g_1t_1}{2}\right)\right\} \quad (22)$$

$$= N h f_o \left\{ \sin^2\left[\left(\frac{\mu E_2t_2}{2h}\right) + \left(\frac{\mu E_1t_1}{2h}\right)\right] - \sin^2\left(\frac{\mu E_1t_1}{2h}\right)\right\} \quad (23)$$

where g_1 and g_2 are given by $\mu E_1/\hbar$ and $\mu E_2/\hbar$ respectively.

Whereas, the power emitted in the first cavity is:

$$P_1 = N h f_o \sin^2\left(\frac{\mu E_1t_1}{2\hbar}\right) \quad (24)$$

A comparison of equations (23) and (24) reveals that

(a) the power output in C_2 is larger than in C_1

(b) it is seen that for small values of E_2 , the power P_2 is proportional to E_2 while P_1 in C_1 is proportional to E_1^2. This implies that with a two cavity system a self-sustained oscillation can be obtained in C_2 at a threshold value of N lower than that required for oscillations in C_1 or radiation can be obtained for any number of active molecules reaching C_2.

5.3 Experimental setup

The maser used for these experiments has been described in Chapter 3. Both the resonant cavities were operated in the E_{010} mode. The first cavity C_1 (10) cm long, the second C_2 (11) cm long are coaxially aligned and separated by a distance of 1.5 cm. C_1 and C_2 have loaded quality factors of 8,000 and 6,000 respectively. Both cavities are tuned thermally by means of copper resistance heater thermometers.

A beam of upper state molecules of ammonia $^{14}NH_3$ ($J = K = 3$) is formed by a nozzle-skimmer source followed by a ring electrostatic state separator. The two cavities are coupled unilaterally by the molecular beam (radiation leakage from one to another is avoided by close fitting each cavity with end-caps below cut-off frequency). The oscillation power in C_2 is detected with a superheterodyne receiver with a 30 MHz I.F., followed by an oscilloscope.

As an initial step in the experimental investigations, the two cavities are tuned to the molecular resonance. Accurate tuning can be achieved by the following procedure.

First, display the klystron sideband mode as a bell shape on the oscilloscope screen with a dip corresponding to the microwave cavity absorption. Adjust the microwave bridge components for maximum cavity absorption and then set the wavemeter approximately to the ammonia (3,3) line transition frequency (23.870 GHz), so that a second dip corresponding to wavemeter absorption appears on the klystron mode. Switch on the cavity heater until the two dips coincide. At this stage offset the wavemeter frequency and operate the maser with a resonable amplitude of oscillation. At this point, if the position of the oscillation signal is not exactly in the middle of the lower portion of the cavity dip then by adjusting the fine control of the cavity heater controller bring the signal to the centre of the dip. For tuning the second cavity repeat the above procedure.

As a precise check whether C_1 is tuned to the molecular resonance a second step has to be taken as follows:

Switch off the side band power generator (use i.f pass band mode display) and connect the microwave switch to the second cavity and obtain a threshold condition for oscillation by adjusting the gas pressure behind the nozzle and the voltage on the focuser. Next, increase the voltage in steps; if C_1 is tuned close to the molecular resonance, the amplitude of oscillation in C_2 must go through zero at some value of the voltage on the focuser.

5.4 Operation characteristics and results

In Section 5.1 it was pointed out that the oscillation amplitude characteristics in ammonia masers operated with two cavities in cascade coupled unilaterally by molecules which pass through them in succession, has been of some considerable interest over a period of many years.

In two cavity masers the oscillation amplitude (A_2) in C_2 has been studied as a function of (i) detuning of C_1 with C_2 tuned to ω_o and (ii) the amplitude of oscillation in C_1 or related parameters, such as focuser voltage or beam flux, with both cavities accurately tuned to the maser line centre. In the second case the molecular beam is also examined under conditions when the polarization of the emergent beam from C_1 is destroyed.

(i) C_1 detuned across ω_o and C_2 tuned to ω_o.

The oscillation amplitude characteristics of the cavity maser have been examined for the case where C_1 is tuned over the full frequency range of oscillation (across ω_o) and C_2 resonant at ω_o. A smooth variation of tuning is obtained by electrical heating of C_1 to a point well above ω_o and then allowing it to cool. Figure (5.3) gives the experimental results of the relative amplitude of oscillation in C_2 as C_1 is detuned over its full oscillation range (maser operated at 37 kV at a nozzle pressure of 21 torr, nozzle and skimmer diameter 0.2 mm and 1.6 mm respectively).

As C_1 is detuned outside its self-oscillation range (beyond A or G), self-oscillation occurs in C_2 as in a normal single cavity maser. When C_1 detuning is decreased, regeneration in C_1 increases up to the point G or A, at which

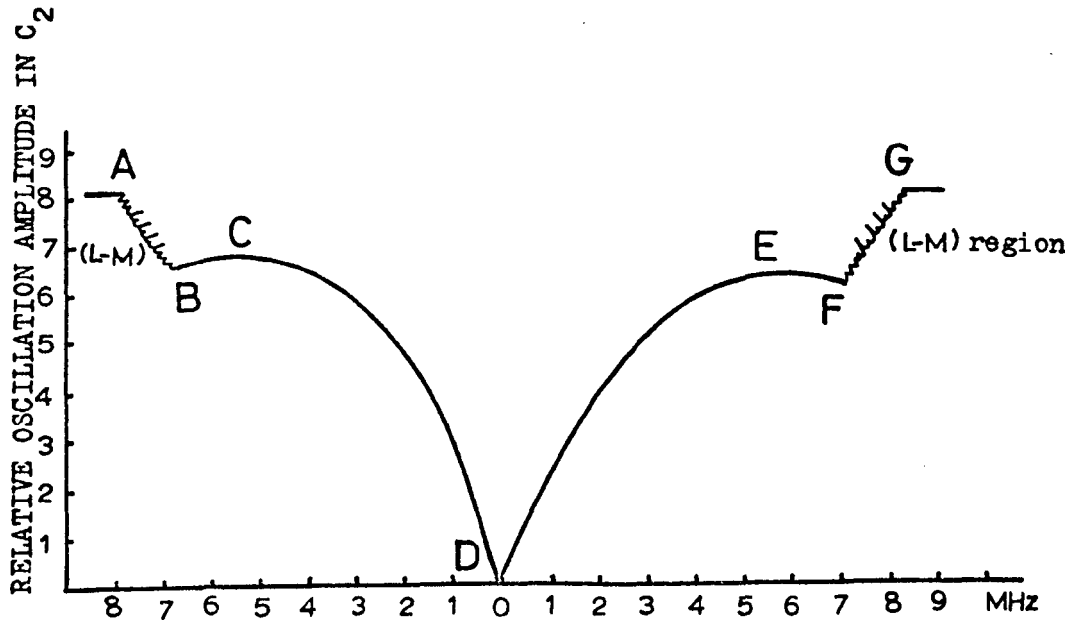

FIGURE(5.3) EXPERIMENTAL CURVE SHOWING VARIATION OF RELATIVE OSCILLATION AMPLITUDE IN C_2 WITH TUNING OF C_1(Focuser voltage 37 kV).

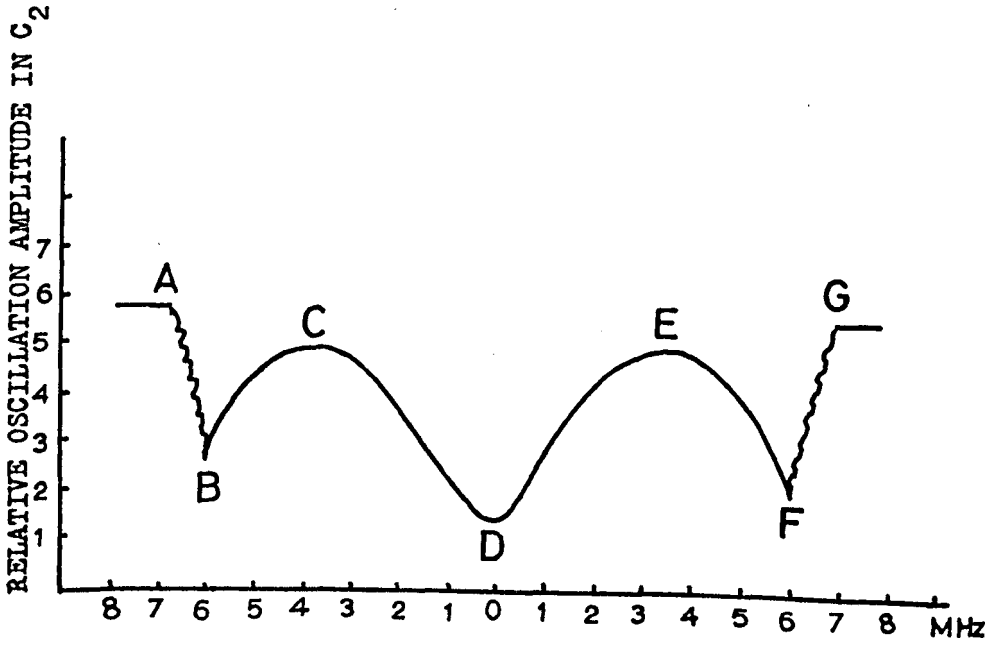

FIGURE(5.4) EXPERIMENTAL CURVE SHOWING VARIATION OF RELATIVE OSCILLATION AMPLITUDE IN C_2 WITH TUNING OF C_1(Focuser voltage 23 kV).

point self-oscillation sets in at a frequency given by the pulling equation (4.1). As a result of this oscillation in C_1 , a ringing signal appears in C_2 which mixes (through non-linearities of the detection system) with the pulled frequency signal giving rise to a biharmonic oscillation which appears (between G → F or A → B, henceforth designated the L-M region) as an amplitude modulation of the output power. Under such conditions, if C_1 is tuned closer to ω_0 the oscillation in C_1 grows in amplitude beyond the microwave electric field value for which the $\pi/2$ beam excitation condition is reached, thus the oscillation amplitude in C_2 decreases.

When the tuning of C_1 reaches F or B, C_2 ceases to self-oscillate so that the beats disappear and the ringing signal becomes the driving field of C_2 at exactly the oscillation frequency of C_1. With further detuning towards ω_0 , the ringing signal in C_2 increases towards the optimum value of a $\pi/2$ pulse, at E or C. As the detuning progresses towards D (closer to ω_0), the oscillation signal in C_1 continues to grow in strength while the signal from C_2 decreases as a result of beam excitation in C_1 in excess of the $\pi/2$ pulse condition. When C_1 is exactly tuned to the molecular resonance frequency the beam is excited at, or close to, the π pulse condition. Beyond this minimum (D), there is a reversal of the process already described as the cavity is further detuned on the opposite side of ω_0.

Figure (5.3) gives the experimental results for the maser operated with C_1 detuned through its full oscillation range and C_2 resonant at ω_0. The pattern of the double hump

detuning phenomenon is not consistent with the corresponding pattern for the same phenomenon previously obtained by several investigators (Strakhovskii and Tatarenkov, 1962, Basov et al 1964, Lainé and Srivastava 1963, Lainé and Smith 1966). Figure (5.1) shows a typical form of their results.

In comparison, the only common feature between the two sets of results is that, in the whole mode of operation the intensity of oscillation in C_2 displays an equal number of maxima and minima with a gap in the middle. But close inspection reveals a substantial difference between the corresponding sectors displayed on each curve with respect to each other. From Figure (5.3) it is seen that the relative amplitude of oscillation at F is much larger than at $\bar{B}$ in Figure (5.1), and the gap to the right of point E is almost negligible in comparison with the gap at the right side of $\bar{C}$. This distinctive feature might be considered as the effect of the establishment of oscillation on the quadrupole satellite lines owing to the fact that the cavity is nearly tuned to the latter. Moreover, a slight fluctuation in the amplitude of oscillation was noted before the biharmonic regime of operation set in. This effect has almost vanished when the E.H.T. on the state separator was reduced to 23 kV. The detuning curve obtained is shown in Figure (5.4). Furthermore, this Figure shows that the amplitude of oscillation at D, no longer falls to zero.

However, it was found that the most important sectors on Figure (5.3), are the two L - M regions. Each of these regions corresponds to a particular range of detuning C_1

($\sim$ 0.8 MHz) in which an increase in the oscillation strength in C_2 is associated with a particularly persistent non-sinusoidal biharmonic regime of 100% oscillation amplitude modulation or pulsation with a repetition frequency of 7 -14 kHz. A detailed study of this modulation/pulsation behaviour is given in Chapter 6.

As mentioned earlier in this chapter, a number of theoretical explanations have been put forward to explain the double hump detuning phenomenon. However, none has provided an entirely satisfactory explanation of the various sectors of the detuning curve. Nevertheless, it should be noted that Krause (1968) was the first to offer a reasonable theoretical explanation for much of the double hump detuning phenomena. The treatment was based on the consideration that the molecules experience a "pulse" of radiation in passing through C_1. The polarization imparted to the beam depends on the magnitude of the pulse whose magnitude is determined by the strength of the oscillating signal in the cavity. Bardo and Lainé (1971) were able to extend this treatment by a quantum mechanical analysis and by a modified Feynman diagram appropriate to the electric dipole case. Various initial levels of excitation were assumed and the detuning patterns were then computer plotted. These showed shapes not yet observed experimentally.

It was shown that as C_1 is detuned through its full detuning range, the amplitude of oscillation follows a semi-elliptical pattern given by:

$$\frac{E_1^2}{E_{01}^2} + \frac{\beta^2}{\beta_m^2} = 1 \qquad (25)$$

where E_{01} is the magnitude of the field in C_1 at ω_o, $\beta = (\omega_{n1} - \omega_o)/\omega_o$ is a detuning parameter of C_1 whose natural resonance angular frequency is ω_{n1}, and β_m is the maximum detuning parameter beyond which C_1 will not oscillate (Helmer 1957, Jaynes and Cummings 1963).

When the oscillation level in C_1 is high, no free oscillation can occur in C_2. Thus C_2 is driven by the oscillating polarization carried by the beam from C_1. Hence, the induced electric field in C_2 follows the relationship

$$\frac{E_2}{A} = \sin\left[\frac{\mu_{12}}{2\hbar} E_{01} \tau_1 \left(1 - \frac{\beta^2}{\beta_m^2}\right)^{\frac{1}{2}}\right] \qquad (26)$$

where

$$\tau_1 = \frac{\hbar}{\mu_{12} E} (2n+1)\frac{\pi}{2} \qquad n = 0, 1, 2, \ldots$$

Figure (5.5) shows computer plotted solutions for a series of pulses up to the 2π condition assuming a univelocity beam. When the maximum radiation field in C_1 (at zero detuning) is appropriate for π pulse excitation, all the molecules in the upper state which enter C_1 emerge in the lower state, for which the radiation field in C_2 is zero. In the case of a 2π pulse the radiation previously emitted by the molecules into C_1 is reabsorbed and the molecules emerge from the cavity in the upper state once more. Thus such molecules can in principle radiate in C_2. For the cases other than π and 2π ($\frac{\pi}{4}$, $\frac{\pi}{2}$, $\frac{3\pi}{4}$, ...) the emergent molecules from C_1 are in a super-position (i.e. radiative state.

Consider two maximum values of $\frac{E_2}{A}$ in Figure (5.5) which correspond to the conditions where the molecules receive

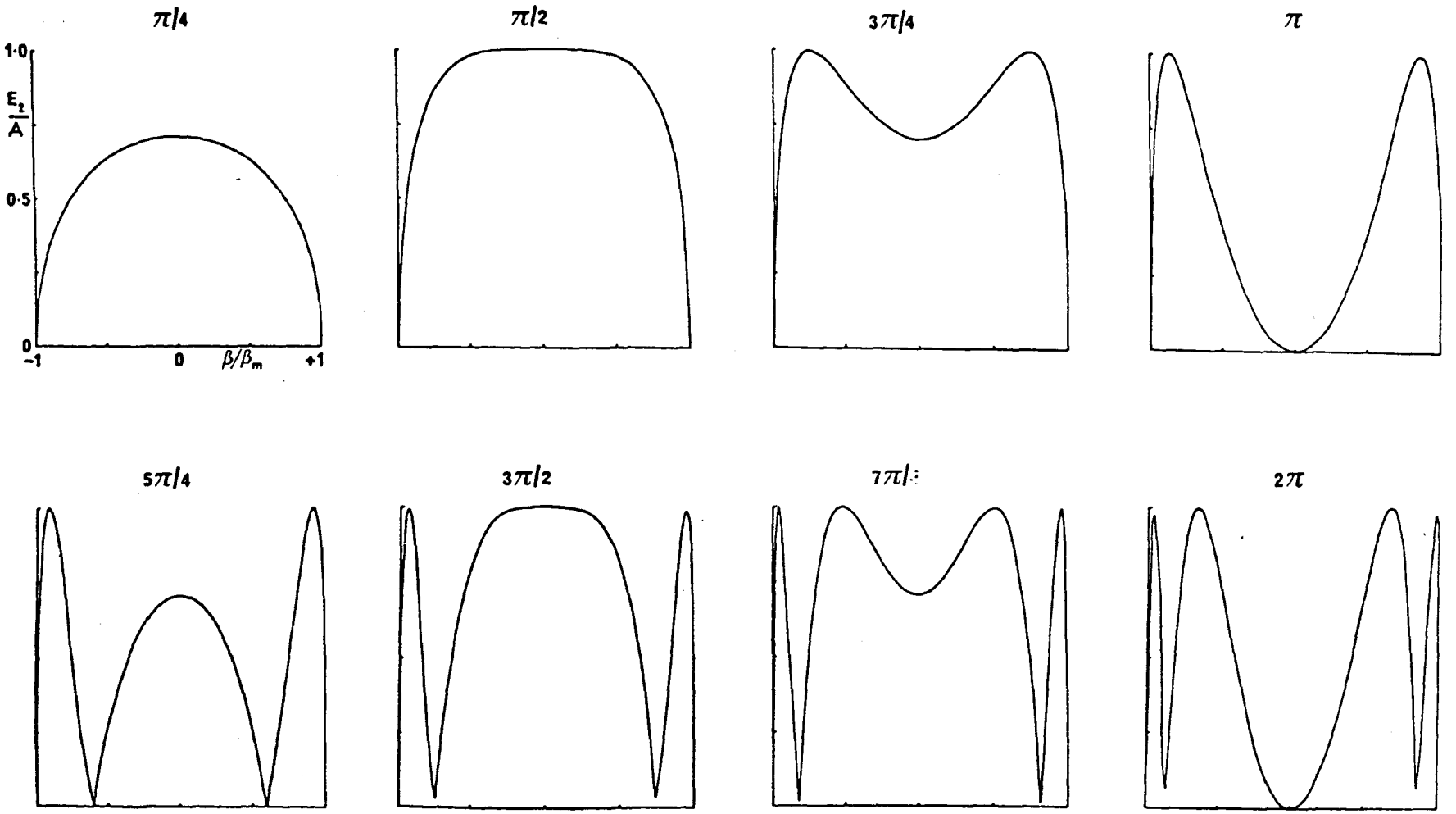

FIGURE(5.5) THEORETICAL DETUNING CHARACTERISTICS OF A MASER OPERATED WITH TWO CAVITIES IN SERIES(After Bardo and Lainé 1971).

a $\frac{\pi}{2}$ and $\frac{3\pi}{2}$ pulse in C_1. If the molecules receive a $\frac{3\pi}{4}$ pulse when C_1 is tuned to the maser line centre, then on detuning C_1 a condition could arise in which the magnitude of the radiation field in the cavity drops to a level where the molecules receive a $\frac{\pi}{2}$ pulse.

Despite the fact that the experimental results are not in full agreement with the theoretical curves, nevertheless they provide more detailed results to which a further detailed analysis can be directed at a future date. However, a comparison between Figure (5.3) and the theoretical curve corresponding to the 2π pulse, reveals a common point: the amplitude of oscillation in C_2 goes to zero at zero detuning of C_1. Therefore it can be adduced that in the present maser conditions appropriate to π and $>\pi$ pulses are possible.

However, the discrepancies observed might be attributed to several different factors as follows:

a) The detected oscillation level from C_2 is not linearly proportional to the electric field in the cavity.

b) Strong effect of the quadrupole satellites transitions and oscillation pulsations on the radiation field in the cavity.

c) Second cavity does not interrogate the beam passively, but is driven into a highly non-linear mode of operation and changes the state of molecules.

(ii) C_1 and C_2 tuned to the molecular resonance frequency

The oscillation amplitude (A_2) characteristics in C_2 measured with both cavities accurately tuned to the maser line centre ω_0, are represented in Figure (5.6) . This figure shows the variation of A_2 as a function of successive values of separator voltages at a constant gas pressure of 22 torr behind the nozzle source. At a threshold voltage of 4.6 kV on the separator, C_2 starts to sustain self oscillations. For higher voltages (5.8 kV), A_2 grows to a maximum, then falls to zero at 8.2 kV. With further increase of the voltage, A_2 increases, passing through a maximum at 22 kV and then falls to zero at 38 kV.

This sequence which is obtained by increasing the separator voltage from low to high values, differs substantially from those previously obtained by many workers. The two sets of results (previous and present) will be compared in section (5.8) . However, from the results shown in Figure (5.6), an immediate conclusion can be made: the nozzle skimmer scheme does substantially affect the performance of the molecular beam in a cascaded cavity system and provides a "fertile ground" for detailed experimental studies of radiation processes and the energy state of the molecules between and within the two cavities.

As a complementary experiment to the above investigation, the molecular beam has been examined spectroscopically under conditions where the polarization of the emergent beam prior to entering C_2 was destroyed. Detailed investigations are reported and interpretation given in the following section.

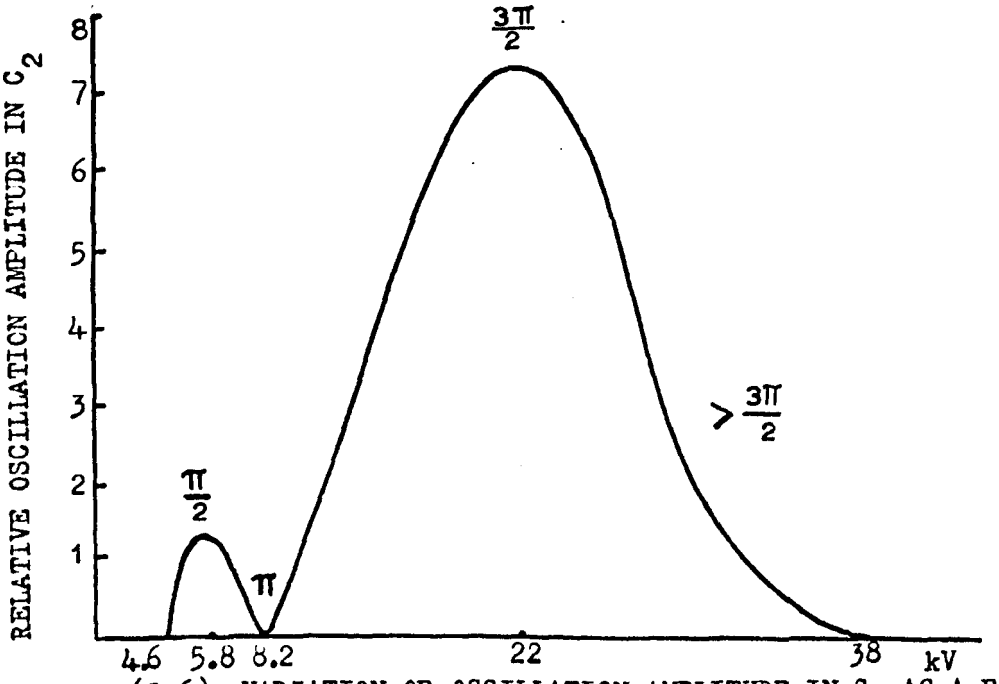

FIGURE(5.6) VARIATION OF OSCILLATION AMPLITUDE IN C_2 AS A FUNCTION OF SEPARATOR VOLTAGES WITH BOTH CAVITIES TUNED TO THE MASER LINE CENTRE .

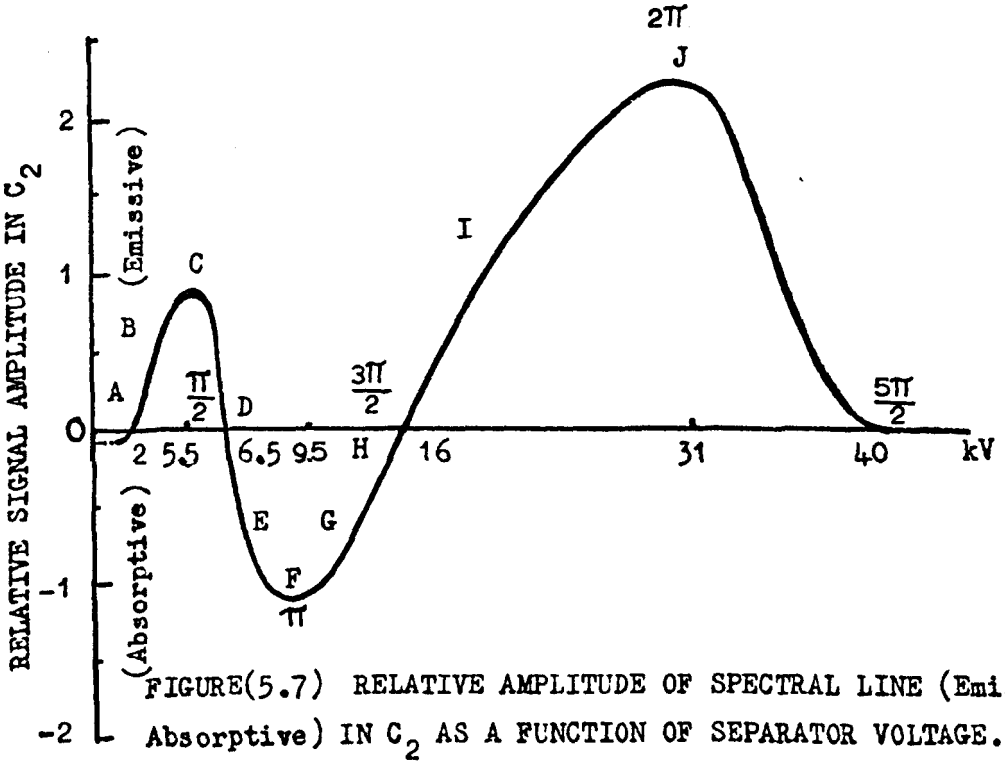

FIGURE(5.7) RELATIVE AMPLITUDE OF SPECTRAL LINE (Emissive or Absorptive) IN C_2 AS A FUNCTION OF SEPARATOR VOLTAGE.

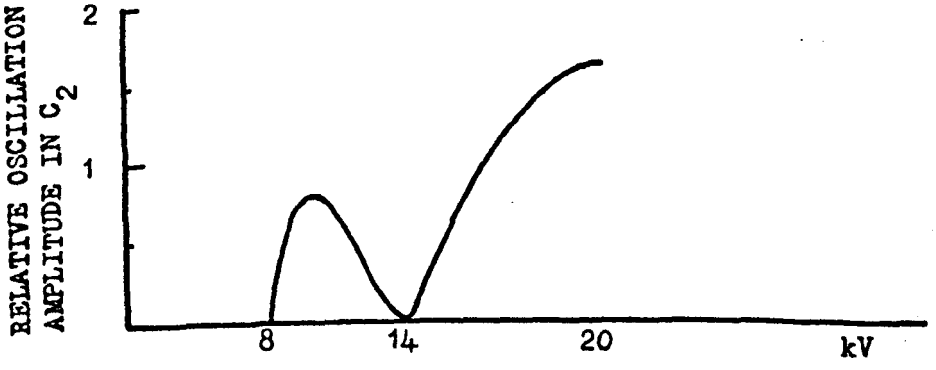

FIGURE(5.8) VARIATION OF OSCILLATION AMPLITUDE IN C_2 AS A FUNCTION OF SEPARATOR VOLTAGES (After Basov et al 1964).

5.5 Investigation of the state of emerging beam from C_1

The energy states of the beam at the exit from the first cavity is now discussed . In the case of spectroscopic investigations, it is desirable to remove the oscillating polarization carried by the beam. This is achieved by applying a small voltage across a pair of capacitor plates placed on either side of the molecular beam between C_1 and C_2. The plates are of dimensions 10 mm x 10 mm, spaced 10 mm apart. Penetration of the applied electric field into the cavities is prevented by leaving a gap of about 10 mm away from either side of the capacitor plates between the two cavities. It is preferable to maintain a low value of electric field in order to prevent any disturbance which might occur in the level population of the molecules. A useful method of reducing the strength of oscillation in C_2 is to employ either a low Q cavity or detuning the cavity slightly away from the molecular resonance frequency. Subsequently, in the experiment described below, the cavity is detuned slightly away from the line centre frequency and the forced oscillation is suppressed throughout the whole range of focuser voltage by applying a voltage of the order of 100 volts on the capacitor plates. For the arrangement used with C_1 ($Q = 8{,}000$) detuned far away (> 8MHz) from ω_o C_2 ($Q = 6000$) oscillates freely at 10 kV at an optimum nozzle pressure of 21 torr.

Figure (5.7) represents the experimental results for investigations of the spectroscopic line inversion from emission to absorption etc. The amplitude dependence of this spectroscopic signal in C_2 , is shown for various

separator voltages. Below 1.8 kV there is an absorption corresponding to a population distribution near the thermal equilibrium value. At about 2 kV, the beam emerges from C_1 in an emissive state. This emissive signal increases in amplitude (maximum at 5.5 kV), then falls and gives way to a absorptive signal at 6.5 kV. Above 6.5 kV, the absorptive signal increases (maximum at 9.5 kV), then starts to decrease and once again it turns emissive once again above 16 kV. Above 16 kV, the beam continues to be strongly emissive with an amplitude more than twice that of the emission signal at 5.5 kV. At 31 kV it reaches a maximum value, then begins to decrease and falls to zero at about 40 kV.

Throughout this process the amplitude of oscillation in C_1 was monitored. It was found that it displays a monotonic increase. At 15 kV, a condition for strong oscillation settling transients in C_1 was reached and from 31 to 40 kV, a strong pulsating character was dominant over the whole of the oscillation display.

5.6 Discussion

The state of emergent molecules from the exit of C_1 (hence the amplitude of oscillation) is strongly dependent on the various combinations of the operational parameters. These are, the molecular flux, separator voltage, time of molecular flight, nozzle-skimmer geometry, cavity tuning and consequently the degree of polarization received by the molecules within their time of flight in C_1.

The strength of the molecular polarization is determined by the number of active molecules and their spatial orientation after leaving the separator. Because the interaction between

molecules and the microwave field in C_1 depends on the molecular spatial orientation, the probability of emission in C_1 will therefore depend on the space orientation which occurs in the region between the separator and the entrance of C_1. When molecules enter C_1, the beam is polarized by the self-oscillation which then drives C_2 to oscillate at an identical frequency and with zero phase difference between the two signals if both C_1 and C_2 are tuned to the molecular line centre. By destroying the oscillation polarization of the emergent beam from C_1, the state of the molecules (absorptive or emissive) can be investigated.

When C_1 is tuned to the line centre frequency, the molecular ringing in C_2 is at maximum except for $n\frac{\pi}{2}$ excitation in C_1 ($n = 1,2,3,\ldots$). The magnitude of the ringing signal is determined by the degree of beam polarization and the population difference between the upper and lower levels. If the number of molecules in the upper and lower energy state are equalized by a strong radiation field, the polarization is at a maximum and a state of saturation can be established (Basov et al 1964 and Mukhamedgalieva et al 1965).

On the basis of univelocity molecular beam theory, the condition for maximum molecular ringing in C_2 (i.e. beam radiative, or forced oscillation in C_2) when both cavities are tuned to molecular resonance can be expressed by:

$$\frac{\mu E_1 t_1}{\hbar} = (2n + 1)\frac{\pi}{2} \qquad (n=0, 1, 2, \ldots) \qquad (27)$$

where E_1 is the electric field in C_1.

The successive magnitudes of the term $(2n + 1)\frac{\pi}{2}$ in the above equation, determines the corresponding conditions for

maximum radiation in C_2 (i.e. $\frac{\pi}{2}$, $\frac{3\pi}{2}$; $\frac{7\pi}{2}$, ...). On the other hand, the condition for maximum population inversion which corresponds to beam absorption in C_2 is given by:

$$\frac{\mu E_1 t_1}{\hbar} = (2n + 1)\,\pi \qquad (n=0, 1, 2, \ldots) \qquad (28)$$

and the solution for different values of n gives the corresponding conditions π, 3π , 5π ,... for absorption in C_2. Figure (5.9) shows a combined relationship between equation (27) and (28).

According to Bardo and Lainé (1971), the slow molecules play a role in initiating oscillations and participate in the establishment of conditions for the observation of oscillation transients. In their experiment an oscillation transient first appeared when the beam as a whole was experiencing pulse excitation in C_1 between π and $\frac{3\pi}{2}$. It was also reported that the slow molecules burn a hole in the spectral profile of the fast molecules. This appears as a small emissive going signal in the middle of the absorption line which steadily increases in amplitude and width at the expense of the absorption line until the whole line inverts into an emissive signal.

Owing to the molecular velocity distribution, the interaction time for all molecules with the radiation field is not the same. If two groups of molecules are considered such that the velocity of fast molecules is twice that of the slower, then the time of interaction between the field and slow molecules is twice of the fast molecules, $2t_s = t_f$. Accordingly, the conditions for the two cases are:

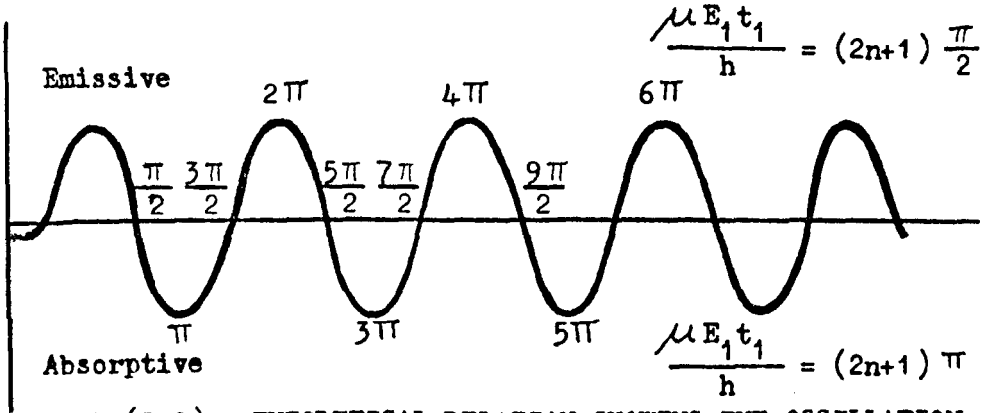

FIGURE(5.9) THEORETICAL RELATION SHOWING THE OSCILLATION BETWEEN UPPER AND LOWER ENERGY STATES FOR A UNIVELOCITY BEAM.

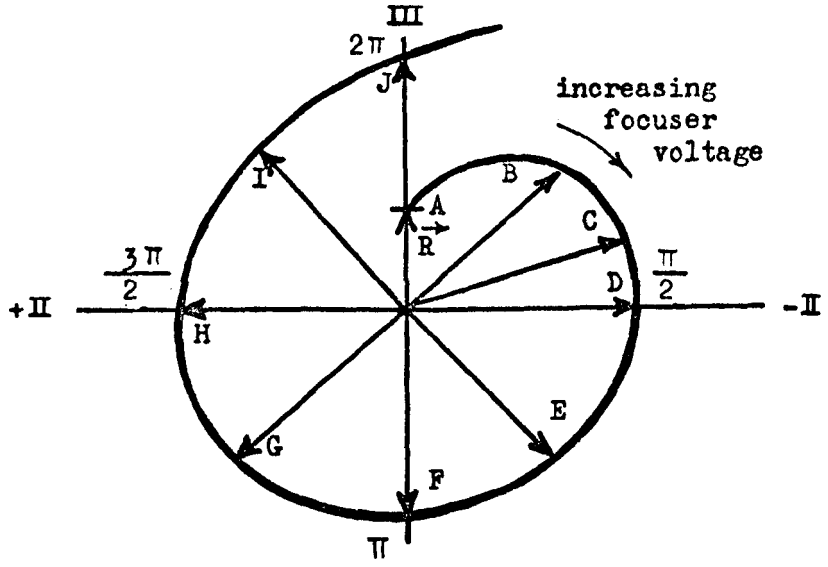

FIGURE(5.10) THE LOCUS OF $\vec{R}$ AS A PARAMETRIC FUNCTION OF FOCUSER VOLTAGE.

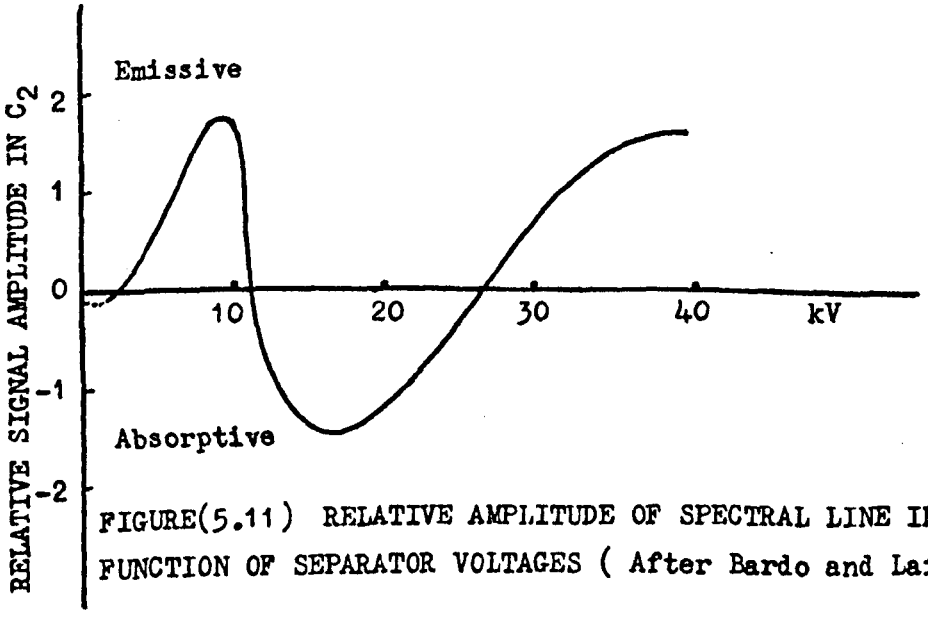

FIGURE(5.11) RELATIVE AMPLITUDE OF SPECTRAL LINE IN C_2 AS A FUNCTION OF SEPARATOR VOLTAGES (After Bardo and Lainé 1971).

$$\frac{2\mu E}{\hbar} t_s = 2\pi \qquad \text{(2 } \pi \text{ pulse excitation)}$$

and

$$\frac{2\mu E}{\hbar} t_f = \pi \qquad \text{(} \pi \text{ pulse excitation)}$$

In other words, the fast molecules receive a π pulse excitation which are absorptive and the slow molecules receive a 2π pulse, thus become emissive.

The above approach is based on the relative populations of the levels, with the polarization information carried by the beam destroyed. Further experimental and theoretical investigations have been made by Lainé and Bardo utilizing the double hump detuning characteristics. In their study the change in oscillation amplitude in C_2 as a function of the detuning of C_1 is related to the magnitude of the pulse received in C_1. This method provides complementary information to that which is yielded by the population inversion technique.

The geometrical model based on Feynman theorem (1957) has aided in the interpretation of a number of phenomena in the molecular beam maser, including the population inversion phenomenon. However, this theoretical connection, and other experimental evidence in common for magnetic (n.m.r flow masers) and electric dipole transitions (molecular beam masers) is particularly powerful in giving an intuitive insight into various processes that occur in a molecular beam maser.

Figure (5.10) shows the locus of the dipole vector R as a parametric function of state separator voltage with the cavity tuned to the molecular resonance. The vector lengthens and rotates in a clockwise sense as the molecules receive

a greater pulse in C_1. The component of the vector R along the III axis represents the population difference between the two levels and along the II axis represents the real component of the oscillating dipole moment.

At zero focuser voltage there is a small absorption due to the unsorted beam in thermal equilibrium. As the focuser voltage is increased the vector grows and when the maser oscillates, R proceeds to rotate as the molecules experience successively larger pulses in C_1. Then the growth with increasing voltage becomes slower due to the onset of saturation of the maser oscillation.

Figure (5.7) which displays the form of the amplitude of the spectroscopic line recording the state of molecules in C_2, permits the calibration of Figure (5.10) in terms of focuser voltages. Therefore, by the aid of the population inversion characteristic curve it is possible to determine the initial position of the vector R at zero detuning and establish the degree of excitation received by the molecules at a given focuser voltage. (Compare Figure 5.7 with Figure 5.10). The vector R grows and turns through position A and then through B where the population emissive component is a maximum. The vector tip continues to swing through C and then D at which the population component is zero, but the transverse component (polarization) is a maximum, after which the system becomes increasingly absorptive. As the vector transfers to position F through E, the absorption becomes a maximum and then decreases to zero at H. At H the transverse component is again a maximum. As the vector

proceeds through H to J, the system then becomes emissive once again and grows to a maximum at J when the population emissive component is at its highest value corresponding to a 2π pulse condition.

At this point, it should be emphasized that one of the fundamental requirements for pulse excitation up to and beyond the 2π condition is a very strong oscillation in C_1. In fact, the present maser device described in this thesis with its high efficiency made 2π pulse excitation and beyond possible which supports the validity of the above mentioned theory, Hence the first two maxima and two minima in Figure (5.6) appear to correspond to $\frac{\pi}{2}$, $\frac{3\pi}{2}$ and π, 2π pulse conditions respectively.

5.7 N.M.R. analogue

In 1967, Lainé proposed a magnetic maser with two spatially separated emission fields which was the magnetic resonance analogue of a two-cavity molecular beam maser. The two emission coils of the maser are arranged coaxially and the excited nuclei of water (active maser medium) passed through these coils in succession (Krause: Ph.D thesis 1969). This systematic arrangement resembles that of a two-cavity ammonia beam maser where the molecular beam passes through two resonators in series.

The population inversion of Zeeman energy levels is achieved by Benoit's liquid flow method. Distilled water as the working substance is prepolarized in a strong static magnetic field and population inversion is obtained by adiabatic fast passage through an auxiliary r.f. coil

arranged in the fringe field of the prepolarizing magnet. On leaving the field the water flows through a plastic tube into the earth's magnetic field, where upon entering a tuned coil provided with Q multiplication, the active nuclei (protons) oscillate at a frequency near to 2.04 kHz.

Apart from the different nature of the quantum transitions and different frequency of oscillation (2kHz compared with 23.870 GHz for the molecular beam maser), it is found experimentally that the characteristics of the two systems are close analogues. First some details of this study on the behaviour of the two-coil nuclear maser and its performance will be reviewed.

When the nuclear maser was operated it was observed that the oscillations occured simultaneously in both coils (both tuned to resonance) and enhanced by increasing the quality factors of the coils. When the first coil was detuned, the frequency of the oscillation of the second coil followed precisely that of the frequency of the self-oscillation in the first coil and independently of the exact frequency of tuning of the second coil. This phenomenon is in complete qualitative agreement with the corresponding effect obtained with the two-cavity ammonia system. This implies that the free coherent precession of active protons in the water flow emerging from the first emission coil is fully analogous to the condition of molecular ringing which exist in a molecular beam maser with two cavities in series.

In recording the characteristics of the two coil nuclear maser, different parameters such as the water flow rate and the quality factors of the first and second coils were adjusted.

As the first coil was gradually detuned to a critical value, the self-modulation effect was first observed as a purely sinusoidal waveform. For a certain adjustment of experimental parameters and detuning, the beat signal available at the second coil no longer appeared in the form of sinusoidal beats. The shape of the beat signal revealed the existence of a non-linearity of the system.

The two-coil maser showed another interesting feature when the modulation voltage depth across the second coil was monitored. It was found that a modulation depth of about 100% could be obtained.

It has been shown experimentally by Krause (1969) that the performance of a two-coil nuclear maser is in many respects analogous to that of a two-cavity ammonia beam maser. For the nuclear maser, the conditions for the experimental results obtained with a two-coil maser, were derived and explained using Bloch's equations. On the other hand, the analogous performances of the two different types of maser (n.m.r and m.b.m.) has been established quantum mechanically through Feynman theorem. Moreover, in the case of m.b.m. a discussion of the problem in terms of quantum mechanical probabilities led qualitatively to the same result.

However, the positive outcome of the new results (particularly, non-linearity and 100% amplitude modulation) as observed in the n.m.r. maser suggests that the two systems are indeed closely related and hence the two-cavity ammonia maser can be studied by analogous experiments with a nuclear spin maser. The experimental verification of these analogues may be regarded as a further proof of the quantum

mechanical theorem which states that the motion of any two level system to be equivalent to the motion of a spin $\frac{1}{2}$ particle in a magnetic field (Feynman et al 1957). Detailed treatment of this theorem appropriate to the dipole moment case is given by Bardo and Lainé (1971).

As the present investigation has shown, the two-coil proton maser offers flexible demonstrations of many phenomena which also occur with the two-cavity molecular beam maser. One reason is that, with the two-cavity maser, it is much more difficult to measure the operational parameters involved in absolute units than in the case of a two-coil nuclear maser in which the parameters involved can accurately be determined. Hence, for the beam maser it is more difficult to compare theoretical and experimental results. In the nuclear spin maser, the operational parameters such as flow rate and its average velocity, the quality factors of the coils are easily controlled in the audio frequency range. In contrast, in the case of molecular beam maser, the vacuum, gas scattering, quality factors of the cavities, microwave bridge and detecting techniques make the experiment more complicated and less flexible. Thus, with a well devised n.m.r. maser, various complicated phenomena obtained with the maser medium flowing from one resonant system to the other, can be examined and explained quantitatively rather than qualitatively as in the molecular beam experiments.

5.8 Comparison between previous and present results

a) As mentioned earlier, the behaviour of the two-cavity system has been investigated in detail by several research groups. With the present apparatus similar investigations on the two-cavity maser system have been undertaken, but under conditions of very strong oscillation. In both, present and previous work, the masers were operated under two sets of conditions, i.e. type (i) and (ii), which have been identified in Section (5.4).

One outcome of the present investigations is the discovery of the existence of a strong non-linearity of the maser medium. Detailed studies of the (L-M) sectors on the double hump detuning pattern, revealed such a non-linear behaviour and subsequently, several new interesting effects were obtained in association with the biharmonic regime, for example:- continuous but non-linear beats with frequency repetition of the order of (7-14) kHz, amplitude modulation depths of 100% and giant oscillation pulsations (Details in Chapter 6). On the other hand, the shape of the detuning pattern as shown in Figure (5.3), is substantially different from that in Figure (5.1) . A comparison of the corresponding magnitude of oscillation amplitude on both detuning patterns is invited.

b) The experimental results obtained under conditions of type (ii) revealed the following new phenomena: Figure (5.6) shows the variation of the amplitude of oscillation in C_2 as a function of separator voltage. Figure (5.8) represents the form of the characteristic curve obtained

previously. From Figure (5.6), it is interesting to note that the amplitude of oscillation after the second maximum falls in amplitude, and eventually reaches zero when the separator voltage reaches 38 kV. Thus, two maxima and three minima are obtained. It can be seen that the relative amplitude of the two peaks are in the ratio of 1:7 respectively in the order in which they appear with increasing separator voltage. In contrast, Figure (5.8) is typical of earlier work by Basov et al (1964) and others, shows two maxima and two minima. The two maxima are in the ratio of 1:1.5. In addition Figure (5.6) shows evidence of conditions corresponding to pulse excitation $\geqslant 3\pi/2$.

c) As it can be seen from the spectroscopic line inversion diagram Figure (5.7), the signal in C_2 shows the state of the molecules after being emissive at 31 kV, the signal amplitude falls and vanishes at 40 kV indicating a condition appropriate to, or higher than, 2π pulse excitation. Figure (5.11) typical results obtained previously by Lainé and Bardo (1970).

CHAPTER 6

PULSATION PHENOMENON IN AMMONIA BEAM MASER

6.1 Introduction

Strong oscillation amplitude pulsations have been observed to occur in the present ammonia molecular beam maser operated with a particularly intense beam produced by a nozzle-skimmer gas source configuration. Both single and cascaded cavity systems operated in a pulsation regime of operation have been investigated. The basic experimental system has already been described in Chapters 3 and 5.

6.2 Oscillation pulsations in two-cavity system

a) The characteristics of the ammonia maser with a molecular beam which passes through two resonator cavities in succession have been described in Chapter 5. A typical characteristic plot for the double hump detuning phenomenon is shown in Figure (5.3) . On this graph, attention was focused on the two (L-M) detuning regions where continuous and highly non-linear oscillation pulsations with 100% amplitude modulation were observed. The investigation procedure was as follows: When the molecular beam maser was capable of producing very strong oscillation in C_2 with C_1 gradually detuned away from the molecular resonance frequency ω_o (cavity heater switched off), a weak sinusoidal biharmonic waveform appeared on the maser oscillation, displayed in the I.F. bandpass mode. Then, the klystron power level was optimised and the microwave bridge components were carefully adjusted for maximum signal-to-noise ratio of the biharmonic maser output signal.

On further detuning of C_1 (C_2 kept tuned to ω_o), the modulation depth in C_2 gradually increased right up to 100%. Figure (6.1) displays the amplitude modulation which was detected from C_2 for successive steps of detuning of C_1. The waveform of the beat frequency is seen to progress from a simple sinusoid through to a highly non-linear region before becoming sinusoidal once again. The non-linear behaviour appears as a form of oscillation pulsation. This effect may be seen in Figures (6.1d,e,f).

Figures (6.2 a,b,c,d,e,f) represent a detailed examination of the waveforms corresponding to Figures (6.1 b,c,d,e,f), obtained under the condition of zero sweep of the klystron frequency. Inspection of this figure, reveals that the oscillation peaks alternate between large and small amplitudes, and the time interval between succesive peaks also alternate between a pair of different values. Moreover, there is a trace of a further peak near the trailing edge of the main peak (Figure 6.2 c). It is interesting to note from Figure (6.2 d) that the small peak alternates in its pulsation amplitude in a regular manner. Clearly, this occurs when the maximum non-linearity is obtained in the maser. When this pulsation gives way to the regular type by alteration of the microwave bridge, the waveform changes to that shown in Figure (6.2e), and then as in (6.2f). The repetition frequency of these pulsations covers the range 8-14 kHz.

6.3 Further investigation and interpretation

The phenomenon described above is quite sensitive to changes in any of the maser operating parameters such as gas

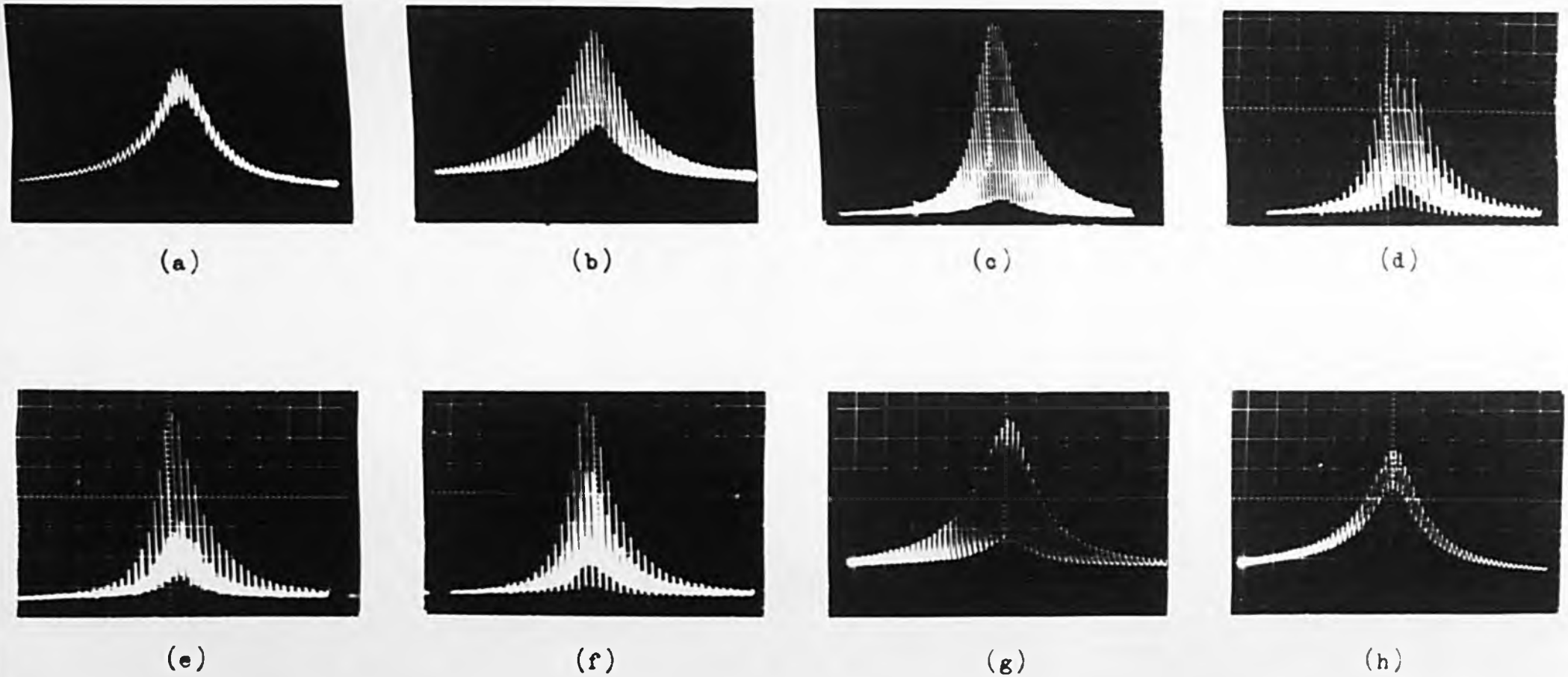

FIGURE(6.1) SEQUENCE OF AMPLITUDE MODULATION RESULTS (I.F. BANDPASS MODE) IN TWO-CAVITY MASER WITH SUCCESSIVE DETUNING STEPS OF C_1 .

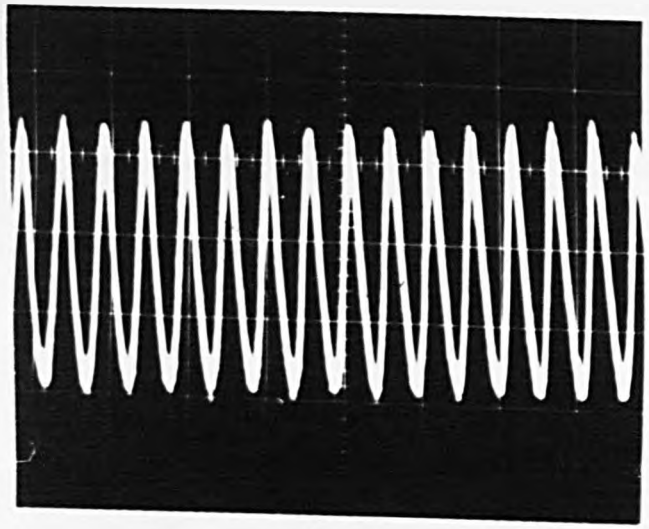

(a)

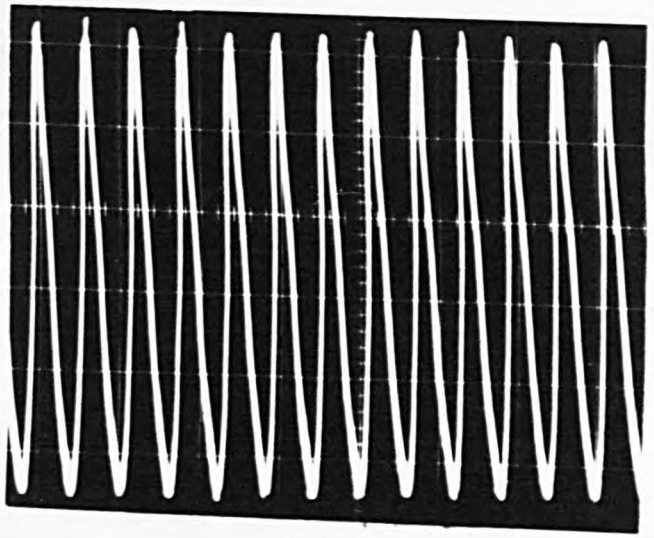

(b)

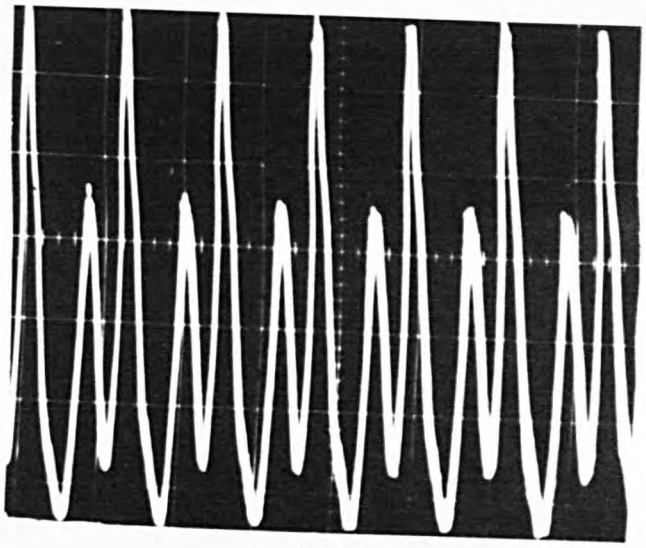

(c)

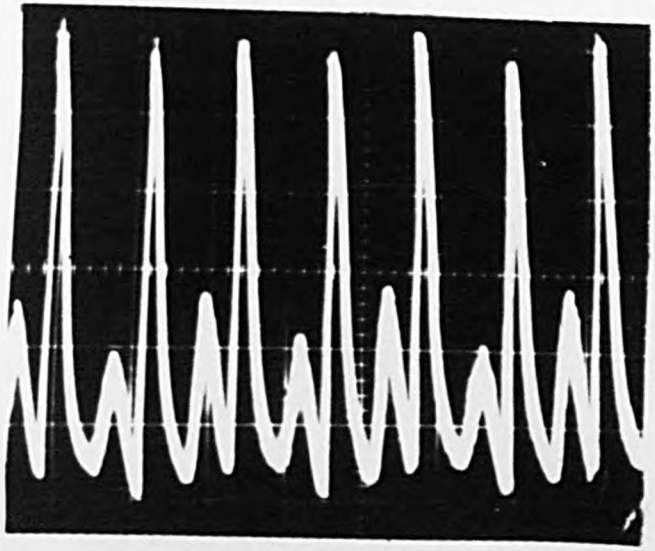

(d)

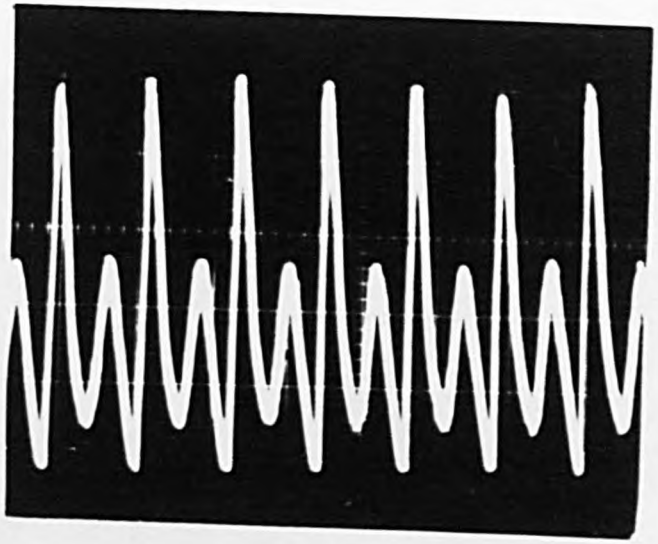

(e)

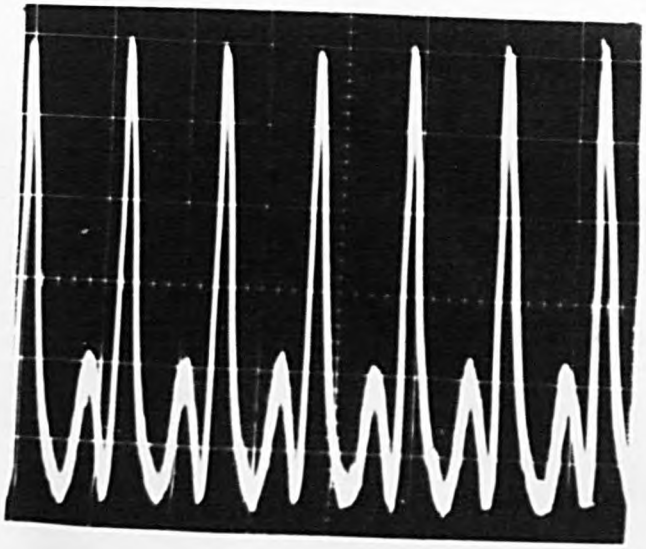

(f)

FIGURE(6.2) OSCILLATION AMPLITUDE PULSATIONS IN C_2(ZERO SWEEP MODE) IN TWO-CAVITY SYSTEM WITH SUCCESSIVE DETUNING OF C_1.

pressure, klystron power, microwave bridge loading, nozzle-to-skimmer distance, voltage on the separator and cavity tuning. In addition it is highly sensitive to either a small magnetic or electric field (particularly the latter) produced in the space between C_1 and C_2. Figure (6.3) illustrates this dependence when a sawtooth voltage of about 200 V derived from the display oscilloscope, is applied across a pair of capacitor plates situated on either side of the molecular beam and when C_1 is detuned to a frequency appropriate for oscillation amplitude pulsations in C_2. This electric field has two effects. First, as the potential between the plates is increased, the polarization carried by the beam from C_1 to C_2 is gradually destroyed (i.e. the polarization from C_1 is amplitude modulated). Secondly, spatial reoreintation of molecules prior to entering C_2 modulates the oscillation amplitude, and thus the degree of over-fulfillment of the self-oscillation conditions for which oscillation amplitude transients may be excited in C_2 (Basov et al 1964). Furthermore, since the amplitude of self-oscillation in C_2 is changed via spatial reorientation of molecules, the frequency will also be modulated through the pulling equation $\Delta\nu_m = Q_c (\nu_c - \nu_o) f(\phi)/ Q_M$ where Q_c and Q_M are cavity and molecular quality factors of C_1 respectively, ν_c the frequency of C_1 and $f(\phi)$ is a factor which is a function of beam flux, geometry of the separator system, separator voltage and gas pressure behind the nozzle. Frequency pulling occurs even when $\nu_c - \nu_o = 0$, since the J=3, K=3 line used here has a composite structure, thus $\nu_c - \nu_o$ is never strictly equal to zero.

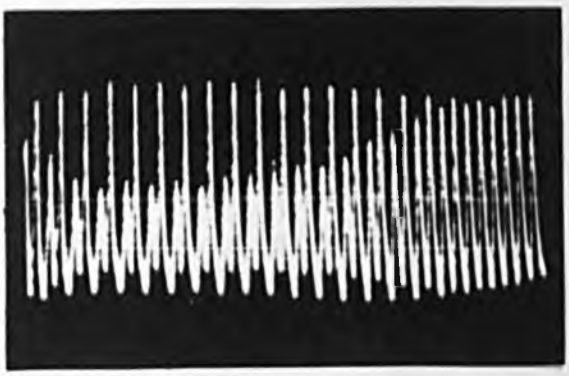

FIGURE(6.3) TWO-CAVITY PULSATIONS IN CAPACITOR VOLTAGE SWEPT MODE.

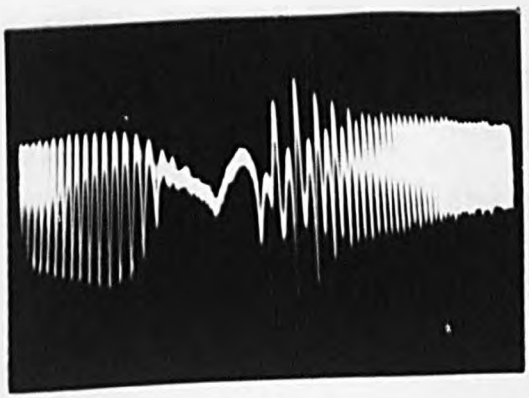

(a)

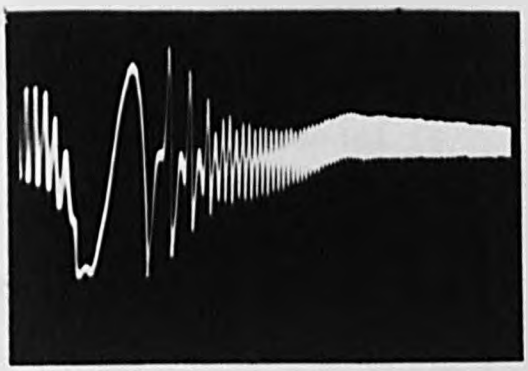

(b)

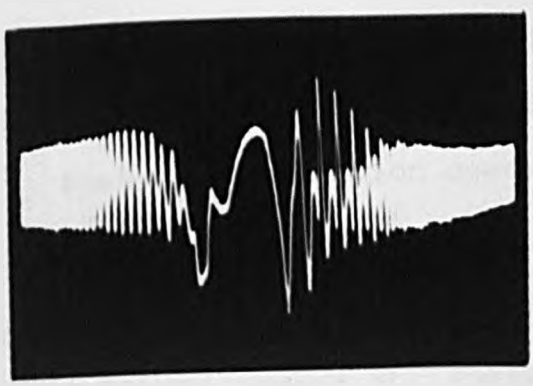

(c)

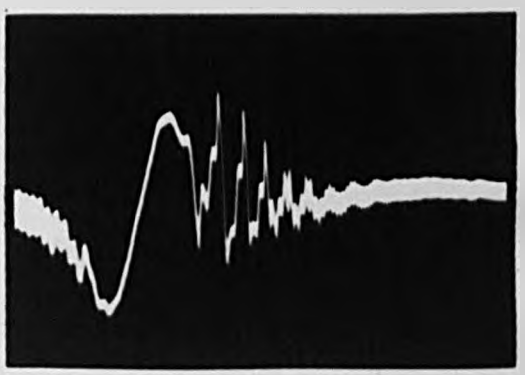

(d)

FIGURE(6.4) SINGLE-CAVITY PULSATIONS EXCITED BY EXTERNAL FREQUENCY SWEPT SIGNAL.

Basov et al (1967) have shown that if one of the oscillation parameters of a strongly oscillating maser could be periodically modulated at appropriate time intervals, oscillation pulsations can be established. If the modulation is at the natural frequency of the oscillation transient, large oscillation pulsations are produced. In such a system the maximum excitation is at the natural frequency of the transient ν_t given by $\mu_{12}E/h$, or at multiples of $\nu_t, (2\nu_t, 3\nu_t, \ldots)$ where μ_{12} is the matrix element of the dipole moment and E the cavity field. Thus, giant pulsations would be evoked at ν_t, $2\nu_t$, $3\nu_t$, ... As an example, if the beat frequency is twice that of the natural amplitude transients, the oscillation amplitude transient becomes phase-locked to the periodic perturbation. Therefore, the following model is proposed to account for the gross phenomenon observed.

The large beam flux produced by nozzle-skimmer beam maser gas source, permits a particularly strong oscillation to be observed in C_2 at a distance of about 150 mm away from the state separator. This oscillation is sufficiently strong for an oscillation transient to occur in C_2 as well as in C_1. This is confirmed by excitation of C_2, by means of a fast passage technique, with C_1 so far detuned away from ν_o that no oscillation occurs in it.

In the case of a single cavity maser operated under conditions of strong oscillation with a strong exciting signal swept slowly across ν_o, free oscillation of the maser is suppressed over a portion of the trace near ν_o. On either side of the zero beat region, beats of varying frequency are

observed as in Figures (6.4 a,b,c,d). A comparison between Figures (6.4 a,b,c,d) and (6.3) and (6.2 c,e) reveals a marked similarity of the waveforms, in particular the spiky behaviour or pulsation waveform with peaks of high amplitude followed by ones of low amplitude. Thus it appears that the phenomenon for a two-cavity maser is closely related to the one cavity maser system with a frequency swept injected signal.

If the maser is operated under very strong oscillation conditions, an amplitude pulsation appears both before and after the region of quenching. These oscillation pulsations can also be associated with oscillation amplitude transients synchronously sustained by an amplitude modulated microwave field of frequency $2\nu_t$, $3\nu_t$, or higher multiple. Examples of such pulsations are shown in Figure (6.4d).

In both cases, oscillation amplitude transients are evidently evoked by modulation of a parameter of the system. In the two-cavity case, the beat frequency between free oscillation in C_2 and driving signal from C_1, parametrically excites the oscillation amplitude transient in C_2, whereas in the one-cavity case, the external signal beats with the maser oscillation signal in C_1. Consequently, the oscillation amplitude transient is parametrically excited to produce oscillation pulsations synchronously sustained by the amplitude modulated microwave field of frequency $2\nu_t$ (which falls in the range 8-14 kHz), $3\nu_t$ or higher multiple.

b) In this case, the experiment is similar to that described in Section (6.2) but with a different detecting

technique. A spectroscopic mode of display is used in which the klystron sideband frequency is swept across the quadrupole structure on the higher frequency side of the main line. The experiment was performed as follows:

When a condition for very strong oscillation was met in C_1, the microwave detection system was connected to C_2 via the microwave switch and the I.F. bandpass response was displayed on the oscilloscope. Then, C_1 was detuned until a sinusoidal biharmonic oscillation with 100% amplitude modulation was obtained. Under such conditions, a weak stimulating klystron sideband signal was injected at the quadrupole transition frequency and the klystron frequency swept such that the sideband signal scanned across the quadrupole structure. No change in the overall sinusoidal beat waveform was observed except in the locations of the two quadrupole satellites. Figure (6.5b) shows the amplitude modulation of the sinusoidal beats at only the two positions of the quadrupole satellites (Figure 6.5a shows clearly the two quadrupoles locations just before the biharmonic regime is reached).

On further detuning of C_1 closer to the quadrupole satellites (1.6 and 2.2 MHz respectively away from the main line centre), substantial changes in the shape of the wave pattern started to originate from the exact locations of the quadrupole satellites. Consequently, the beat frequency underwent changes in amplitude, frequency and in addition, a condition similar to the pulsation phenomenon was obtained. A sequence of such modulations corresponding to the degree of detuning of C_1 is shown in Figures (6.5 c,d,e,f).

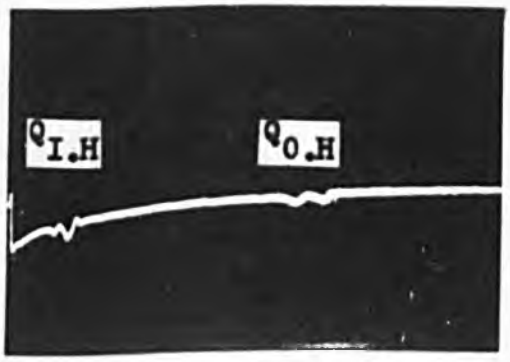

(a)

(b)

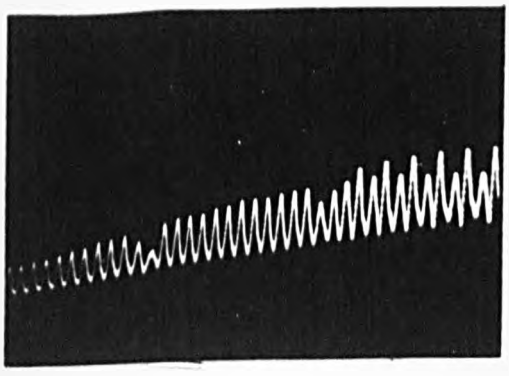

(c)

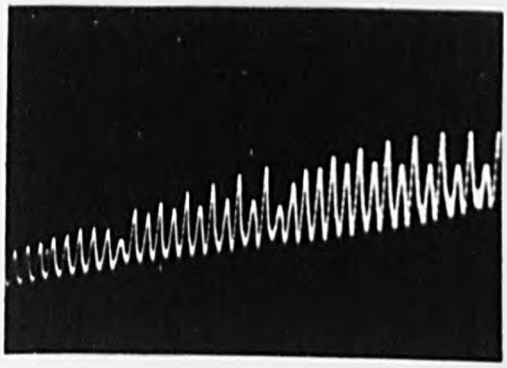

(d)

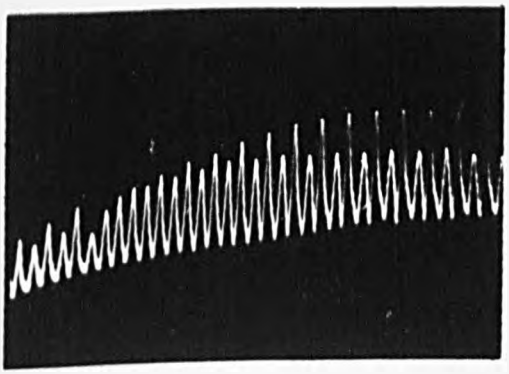

(e)

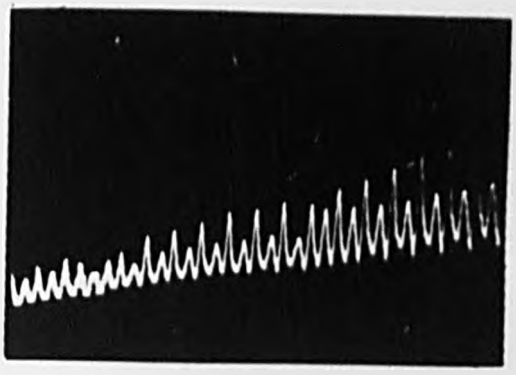

(f)

FIGURE(6.5) SEQUENCE OF TWO-CAVITY PULSATIONS WITH SUCCESSIVE DETUNING STEPS OF C_1 AND EXCITED BY SWEPT EXTERNAL SIGNAL ACROSS THE QUADRUPOLES LINE STRUCTURE .

6.4 Discussion and comments

From the above experimental results, it is surmised that the evolution of the sinusoidal biharmonic regime is strongly related to the excitation of the quadrupole satellites line structure. Figure (6.5c) shows that, as C_1 is tuned closer to the inner quadrupole transition frequency, a signal superimposed on the main trace appears at the inner quadrupole location giving rise to a waveform which is strongly modulated. This modulation can be noted between the two quadrupoles and more strongly to the right of the outer quadrupole. Thus three distinct types of modulation can be distinguished over the original biharmonic beats pattern i.e. to the left of inner quadrupole (L), between the two quadrupoles (M) to the right of the outer quadrupole (R).

Figure (6.5d) illustrates the evolution of strong non-linearity by further detuning of C_1 in the three sectors with strong pulsation oscillations in M and R sectors. Figure (6.5e) is a detailed photograph of M and R sectors. Close inspection of the R region shows a trace of a further peak near the foot of the highest peak. Yet with further detuning of C_1 a condition was obtained as in Figure (6.5f) where pulsation oscillations were dominant over the whole trace. Again, three types of amplitude modulation could be recognized according to each sector but the repetition frequency for these pulsations is the same ($\simeq$ 8kHz). Examples of such pulsations are shown in Figures (6.5f) and (6.2 c,e,f). A comparison is invited.

From these experimental results, it is evident that the non-linear behaviour of the maser and pulsation characteristics are certainly caused by (or at least strongly related to) the quadrupole satellite line structure. Since the maser system is oscillating under very strong conditions, it is possible that two or more closed-spaced lines of the resolved superhyperfine lines of the quadrupole satellites are simultaneously oscillating. As a result, a beat frequency will modulate the original sinusoidal biharmonic beats and give rise to a pulsation character when both are mutually phase-locked. It is interesting to note that this behaviour takes place only at the locations of the two quadrupole lines which may be considered to be the "locus" of this phenomenon.

6.5 Oscillation pulsations in a single-cavity system

It has also been possible experimentally, to obtain pulsations in a single-cavity maser operated under exceptionally strong oscillation conditions. Pulsations are realised under quite different conditions from that previously described in section (6.2).

Pulsations are now found to occur, when the local oscillator power is set at a high level, the cavity resonator is offset by about 1.6 to 2.2 MHz on one side or the other of the main line frequency, and without an auxiliary injected signal from the sideband oscillator.

When the molecular beam maser was capable of producing very strong oscillation, and C_1 gradually detuned from the molecular resonance ω_o (cavity heater switched off), sinusoidal biharmonic beats appeared on the I.F. bandpass mode

as shown in Figure (6.6a) over a range of detuning. As the detuning closer to the quadrupole satellites region continued, these beats progressed from a sinusoidal waveform to a highly non-linear type which appeared in a form of strong oscillation pulsations before becoming sinusoidal once again. Figure (6.6) demonstrates a sequence of amplitude modulations corresponding to detuning of C_1 close to the quadrupole satellites on the higher frequency side of the main line. The repetition frequency of these pulsations covers the range 7-14 kHz.

Close inspection of this set of results, shows the effect of tuning C_1 closer to the quadrupole satellites. Figures (6.6 b,c,d) demonstrate how the evolution of the pulsation is related to the cavity tuning closer to the quadrupoles line structure. Figures (6.6 e,f) show two other conditions for further detuning of C_1 in which giant pulsations can be seen over the two traces. It is interesting to note that three distinct types of pulsation waveforms can be seen in Figure (6.6g) similar to those which are obtained with a two-cavity system as shown in Figure (6.5 e). This waveform corresponds to a condition when C_1 is tuned somewhere between the two quadrupole satellites (about 2 MHz from the main line). Figures (6.6 h,i) show giant pulsations when the cavity is tuned closer to the outer quadrupole satellites. Close inspection of the waveform in Figure (6.6i) reveals evidence of a further peak near the bottom of the main peak. Figure (6.6j) corresponds to a further stage of detuning C_1 which shows that the pulsations character is reduced and the maser oscillation less non-linear. In Figure (6.6k) yet

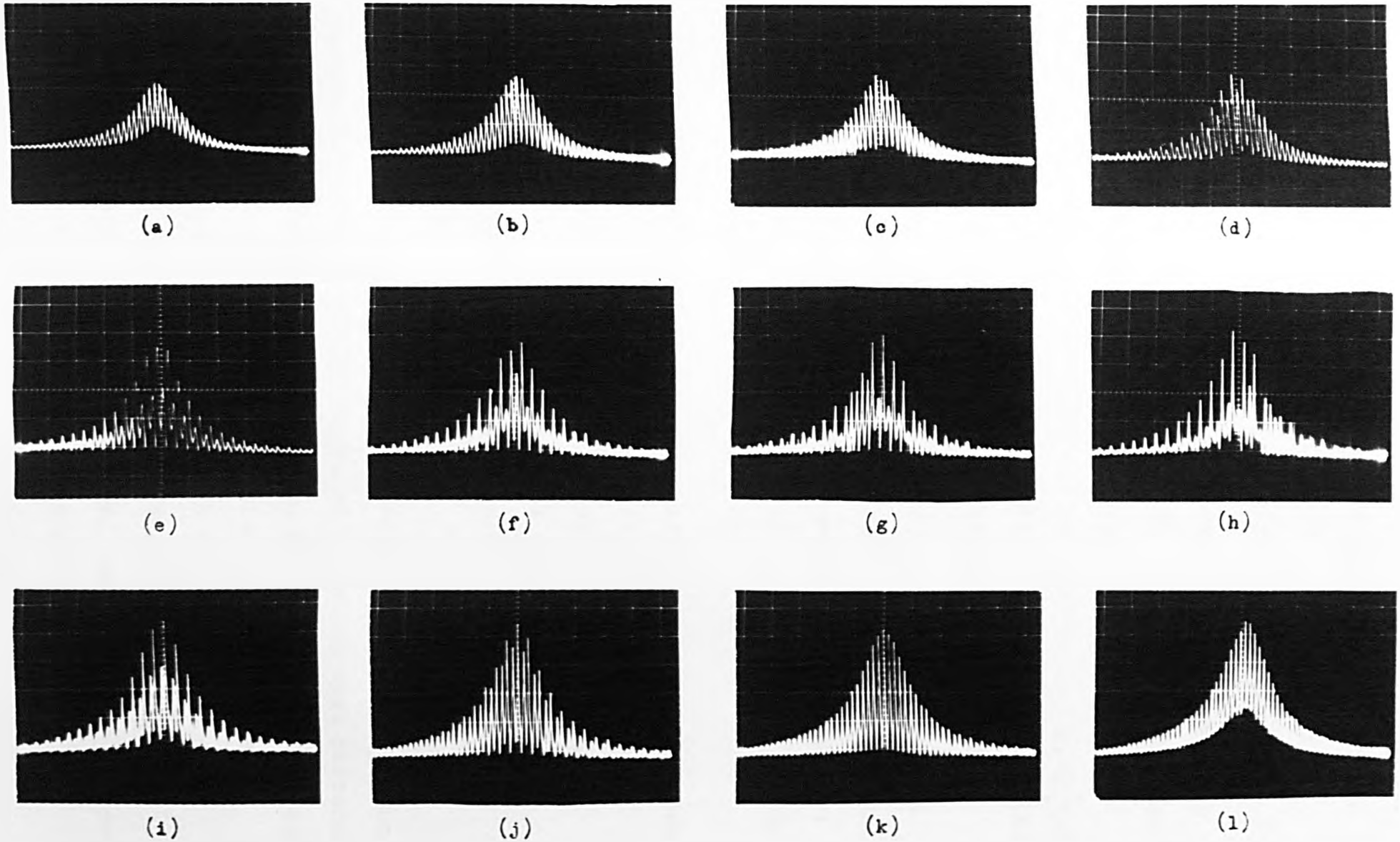

FIGURE(6.6) SEQUENCE OF AMPLITUDE MODULATION PULSATIONS IN C_1 CORRESPONDING TO THE DEGREE OF ITS DETUNING .

less non-linear pulsations, non sinusoidal in form with a modulation depth of 100% are obtained, whereas as in Figure (6.6 1) sinusoidal beats reappear as in Figure (6.6b).

Investigation of these pulsations using a zero sweep technique of the local oscillator has yielded the waveforms shown in Figures (6.7a—g). Two clear large and small pulsation waveforms can be seen as in Figures (6.7 g,h) with a further pair of "ghost"peaks superimposed. The repetition frequency of the pulsations falls between 7 to 14 kHz.

Now, special attention is drawn to a full inspection and comparison between the results obtained under different conditions in one and two-cavity maser systems as follows: Figure (6.1) with (6.6), Figure (6.2) with (6.7) and (6.5), Figure (6.2) with (6.3) and (6.4).

Despite the fact that each experimental result has been obtained under quite different conditions, it is quite difficult to perceive any substantial difference between these results. It may therefore be concluded that there is one common origin responsible for the gross feature of these phenomena.

The operational conditions associated with such common feature are: Three similar types of pulsation wave patterns, frequency repetition between 7 to 14 kHz, and 100% amplitude modulation. In addition these pulsations altogether, behave in a very similar manner with respect to change of the operational parameters such as separator voltage, gas pressure, nozzle-to-skimmer distance, klystron power and even with weak external electric or magnetic fields.

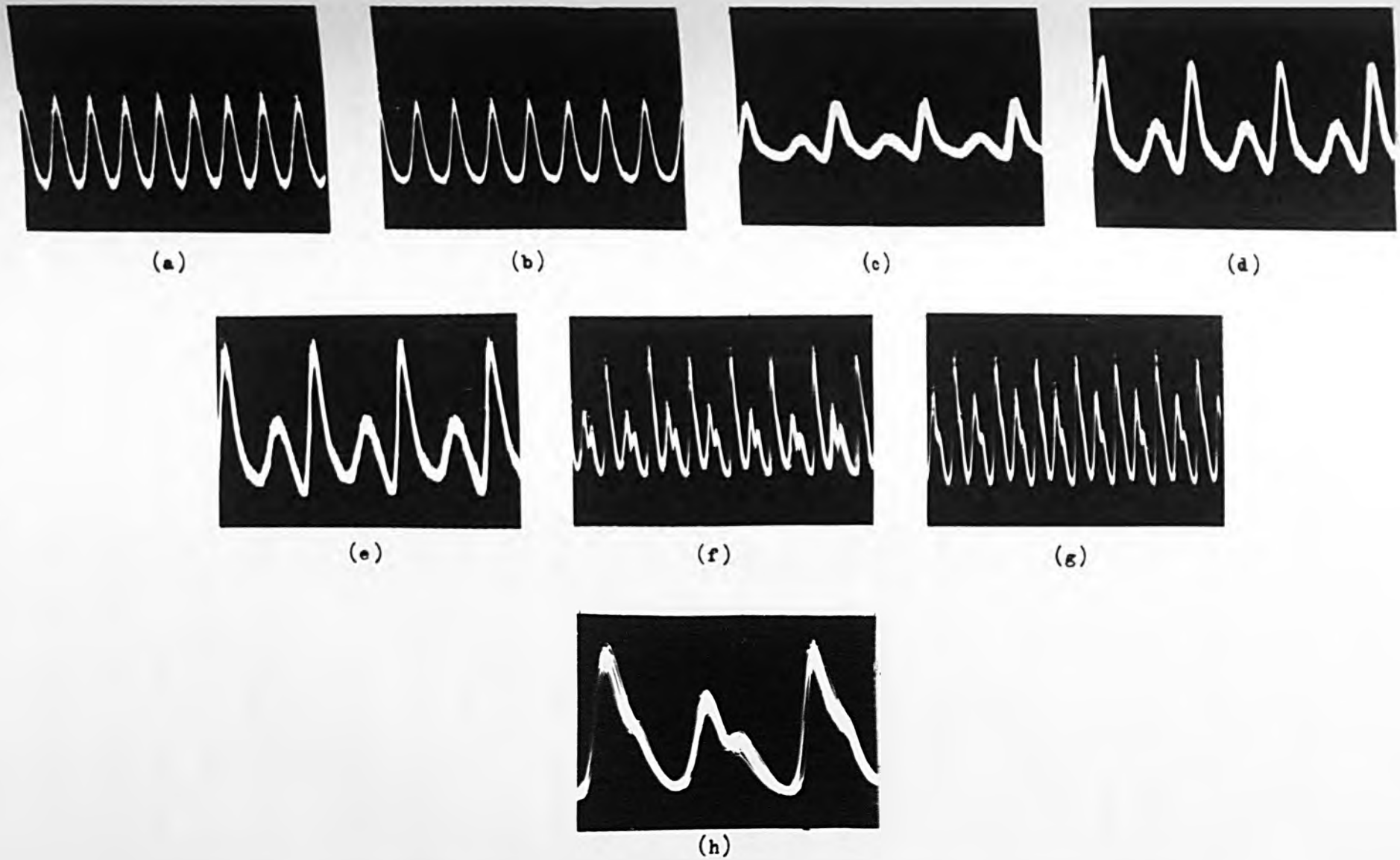

FIGURE(6.7) OSCILLATION AMPLITUDE PULSATIONS IN SINGLE-CAVITY MASER SYSTEM PICTURES (a)-(g) CORRESPONDING TO SUCCESSIVE CAVITY DETUNINGS (ZERO SWEEP MODE OF OPERATION) .

However, a possible basis for an interpretation of the results lies in the possibility of extending the notion of synchronous or parametric excitation to accomodate the present data. Such a mechanism exists if it is assumed that two or more quadrupole magnetic structure lines oscillate in addition to the oscillation at the frequency of the main line. Details of such mechanism will be given in the following sections.

6.6 Radiation damping phenomena in an ammonia maser

This section is mainly concerned with various radiation damping phenomena which have been observed recently in the ammonia maser operated under exceptionally high level of excitation. Transients, self-induced spiking and continuous pulsations which have been observed are analogous to similar phenomena in laser oscillators. Strong oscillation settling transients which are related to the process of periodic transfer of energy between the molecules and the radiation field have been observed to occur in ammonia beam masers. These provide a direct method of determining the degree by which the oscillation condition is overfulfilled. Therefore, a detailed study of the dynamic behaviour of the ammonia maser is of considerable interest since the experimental results obtained are relevant to the phenomena of transient processes in quantum oscillators in general.

According to Shimoda et al (1956), and Basov et al (1966) in the case of an ammonia beam maser operated on J=K=3 line transition with an E_{010} mode cavity of maximum possible Q factor of 10,000, a molecular flux greater by a factor of one hundred times than the oscillation threshold value is

required, before continuous pulsations can occur. Moreover, Lefrère (1974, Ph.D thesis) suggested for such self-induced pulsations to occur in a molecular beam maser, a cooled cavity, and a narrow beam with molecular flux of 20 to 30 times that of the normal oscillation threshold value are all required. However, it is evident that in the present maser oscillator, the above mentioned stringent requirements have been practically overfulfilled, since transients, self-induced spiking and continuous oscillation pulsations in one as well as in two-cavity maser systems have been realized experimentally.

There are several techniques for changing the oscillation level in a beam maser in such a way as to induce oscillation transients and related phenomena. These include;(a) the rapid passage of a high level injected signal into the maser resonator at, or near ω_o, which normally acts by saturation broadening to quench the maser oscillation (Lainé and Bardo 1971). (b) The technique of suddenly altering the molecular population rate in particular energy levels (Grasyuk and Oraevskii 1964). (c) The molecular Q-switching via Stark (Alsop et al 1957) or Zeeman line broadening.

Although it is a relatively easy matter to apply some form of step perturbation (method c) rather than to quench the oscillation in an ammonia maser (method a), it was found in the present case that the method (a) is more convenient to evoke settling transients, transitory or continuous amplitude pulsations. With method (a), if the driving signal is sufficiently strong, the oscillation can be completely

quenched, thus the maser oscillation can be switched on and off. Moreover, a similar technique has also been used successfully at the quadrupole line resonance frequencies.

The rapid passage of an external microwave signal through the magnetic satellites on the high frequency side of the main $J = K = 3$ inversion line of ammonia, yields strong amplitude settling transients following oscillation quenching, as shown in Figure (6.8 a). The damped oscillation amplitude transient associated with the oscillation build-up process only appears with a high beam flux. The period of the settling transient decreases as the amplitude of the maser oscillation is increased. This result simply shows that the maser is oscillating strongly and the condition $\tau_R < T_2 < T_1$ is satisfied, where τ_R, T_2, T_1 are respectively the times for radiation damping, transverse and longitudinal relaxation.

It will be seen that this method, which may be regarded as one form of molecular Q-switching since it relies on saturation broadening of the spectral line, provides qualitative confirmation of the existence of strong transient pulsations accompanying oscillation build-up. However, with such a method, transients as shown in Figure (6.8a) are nearly as clearly marked as those obtained with the most effective method of quenching-that of Stark broadening (Lefrère 1974 Ph.D thesis).

Consideration of the energy-level diagram of the $^{14}NH_3$ molecule Figure (6.9) shows that transients can be evoked, if switching is effected by changing the emission rate of molecules in the cavity resonator at the main line transition

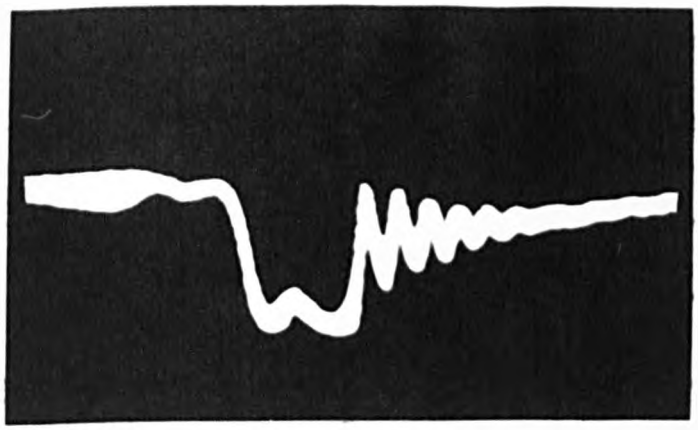

(a)

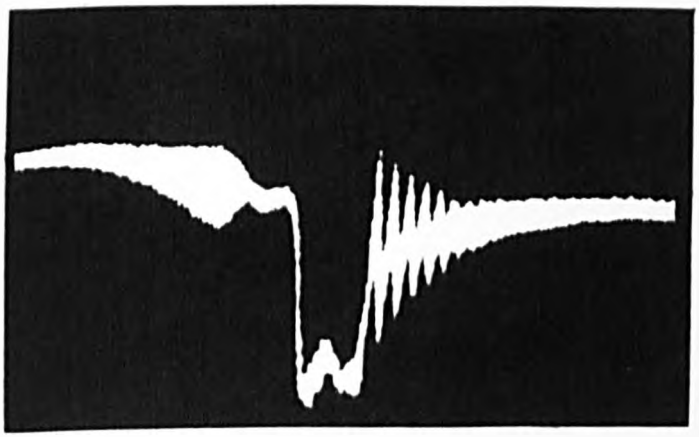

(b)

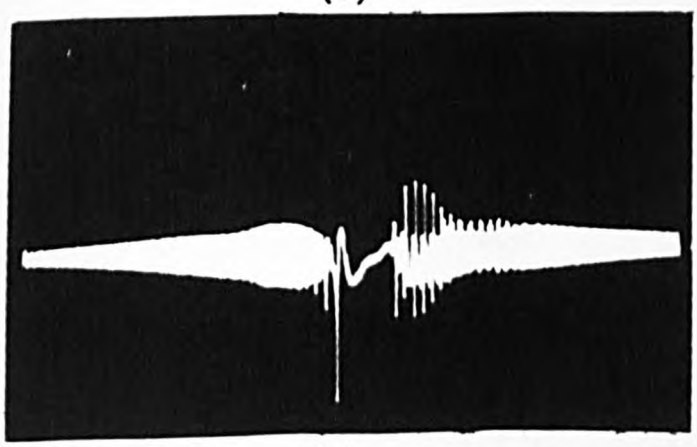

(c)

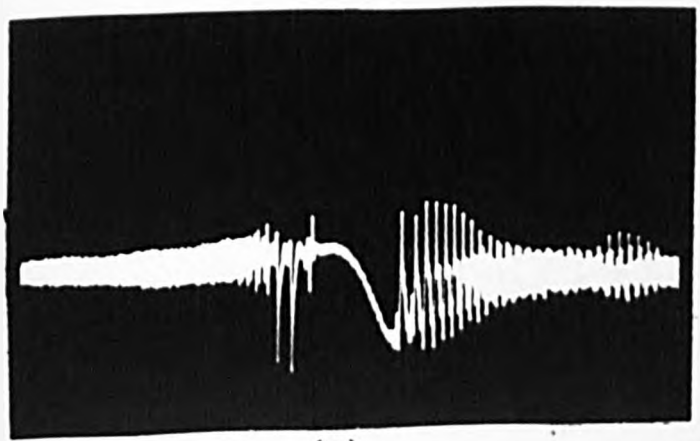

(d)

FIGURE(6.8) OSCILLATION SETTLING TRANSIENTS (a),(b) AND STRONG PULSATIONS (c),(d) FOLLOWED OSCILLATION QUENCHING OF THE MAIN LINE .

frequency. Since the magnetic and quadrupole satellite lines have energy levels in common with the main line, saturation of one of the satellites lines will change the transition probability at the frequency of the main line of the maser. Subsequently, the resulting population depletion may be sufficient to quench the maser oscillation completely and hence excitation and detection occur at two different frequencies. This quenching procedure can be visualized if it is assumed that the external oscillation quenching signal is used to excite the system at one of the upper quadrupole frequencies. This causes a considerable reduction in the number of molecules in the $F_1 = 3$ upper state. As a result, the $F_1 = 3$, $\Delta F = 0$ transition as well as $F_1 = 2$ $\Delta F = 0$ rate, will be reduced by the same amount. Consequently the intensity of the main line will be reduced while regeneration associated with the $F_1 = 2$, $\Delta F = 1$ transition is enhanced and regeneration of the $F_1 = 3$, $\Delta F = 1$ transition is reduced. In the following sections a detailed analysis of this quenching method will be given.

It has been shown that strong settling transients can be seen clearly with a strongly oscillating ammonia beam maser when a strong saturating signal is injected at, or near, the molecular resonance frequency. Now, if this saturation signal is swept rapidly through the maser emission line using the sideband technique, the beat between the injected signal and the free maser oscillation, is found to give way to a stimulated emission signal. With a further increase in the strength of the maser oscillation and by careful adjustment of the klystron power and microwave bridge components, pronounced spiky oscillation amplitude pulsations

can be obtained following rapid passage through the maser emission line. Typical examples of such induced spiking effects are shown in Figures (6.8 b,c,d). Figure (6.8d) shows a condition of strong induced spiking before and after the region of oscillation quenching.

As can be seen, these oscillation spikes are of relatively large amplitude, and therefore it can be concluded that their establishment is related to a repetitive perturbation in the maser system which follows the beat frequency between the injected microwave signal and the natural frequency of maser oscillation.

6.7 The experimental investigation of quadrupole superhyperfine structure

Shimoda and Wang (1955), used a molecular beam maser as a spectrometer with sufficient resolving power and large signal-to-noise ratio to investigate the hyperfine structure of the $J=K=3$ inversion line of $^{14}NH_3$. Microwave power at frequencies corresponding to quadrupole satellite transition frequencies was injected into the cavity resonator while the maser was oscillating at the frequency of the main line. When the external microwave signal was swept across the quadrupole satellites frequencies, a reduction in the amplitude of the main line oscillation was recorded. This reduction is due to induced quadrupole transitions which occur between energy levels shared with the main line transitions. The change in populations of these energy levels caused by the external signal are therefore accompanied by a reduction in the main line amplitude of oscillation.

With such a technique, Shimoda and Wang were able to observe about 20 components of the quadrupole satellites and to determine their frequency separation from the main line. Certain transitions of the quadrupole satellites on the low frequency side of the main line were not easily observed because of the weakness of their transitions, as a consequence of poor state separator efficiency for focusing molecules with low values of F_1.

Accordingly, a similar technique has been used in the present investigation on the four quadrupoles satellites which lie in pairs at either side of the main line; inner and outer quadrupoles on the lower frequency side of the main line (henceforth designated $Q_{I.L}$ and $Q_{O.L}$ respectively), inner and outer quadrupoles on the upper frequency side of the main line ($Q_{I.H}$ and $Q_{O.H}$ respectively). In fact, this probing technique, made the excitation of all the quadrupole satellites and their characteristic oscillation pulsations feasible and extremely interesting. Based on the evidence of several experimental results, these oscillation pulsations are strongly connected to the quadrupole line transitions and the oscillation strength of the main line. Since the energy levels between various transitions of both the main line and quadrupole lines are shared, an energy-level diagram for all the possible transitions may be constructed. A specific model based on this energy level scheme to account for the possible excitation of each quadrupole line and which leads to instantaneous perturbation on the magnetic satellites and the main line is given. This model is found to be in good agreement with the experimental results.

Figure (6.9) is a schematic diagram of all energy levels, hyperfine sublevels and associated transitions for the J=K=3 inversion line of $^{14}NH_3$. The top twelve horizontal lines represent the energy levels of the molecules in the upper inversion state (V=1), while the bottom twelve lines are the energy levels of the molecules in the lower inversion state (V=0). Each one of the main levels $F_1 = 3$, $F_1 = 4$ and $F_1=2$ has four sub-levels determined by the quantum number F, where $F = F_1 + I_H$, $I_H = I_1 + I_2 + I_3$ and $F_1 = J + I_N$ (see section 1.4).

As can be seen there are 56 possible transitions between the upper and lower energy states according to their selection rules (each arrow represents a transition). The main line is composed of 12 individual hyperfine transitions for which $\Delta F_1 = \Delta F = 0$. These lines are close flanked on either side by 9 magnetic satellites. Further out is the inner quadrupole satellite on the high-frequency side of the main line ($Q_{I.H}$) which is composed of 7 transitions for which $\Delta F_1 = -1$, $\Delta F = 0, +1$. The outer quadrupole satellite ($Q_{O.H}$) is also composed of 7 transitions but for $\Delta F_1 = -1$ $\Delta F = 0, -1$. On the lower-frequency side of the main line, each of the inner ($Q_{I.L}$) and outer ($Q_{O.L}$) quadrupoles is also composed of 7 transitions for which $\Delta F_1 = -1$, $\Delta F = 0, -1$ and $\Delta F_1 = +1$, $\Delta F = 0, +1$ respectively. Both inner and outer quadrupole satellites lie at a frequency interval of 1.6 and 2.2 MHz respectively on either side of the main line. (See figures 6.16 and 6.17).

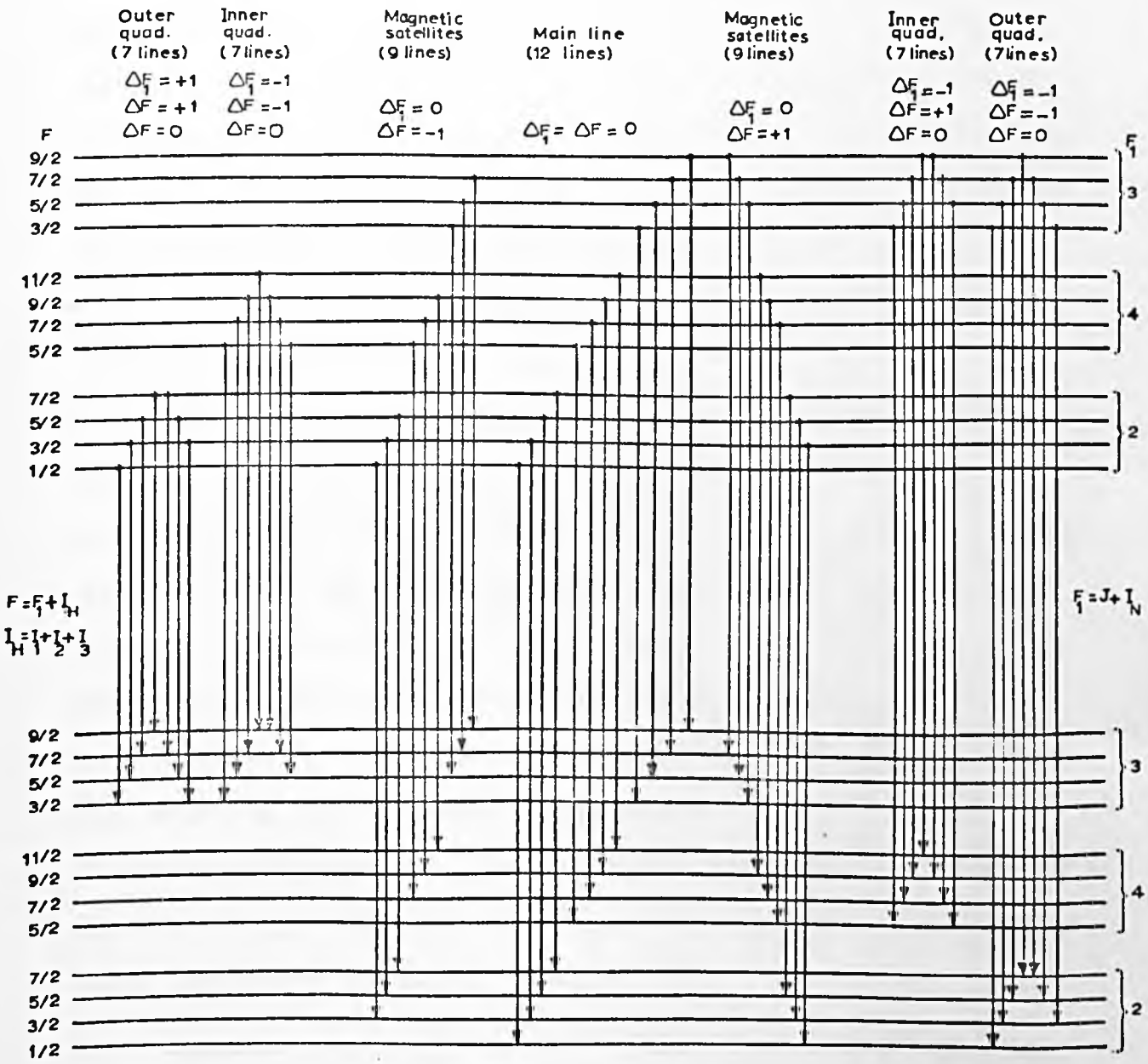

Fig. (6.9) SCHEMATIC DIAGRAM OF ENERGY LEVELS FOR (J=K=3) INVERSION LINE IN $N^{14}H_3$ MOLECULE

6.8 Simultaneous population robbing mechanism

With reference to the energy-levels diagram constructed for the $^{14}NH_3$, (3.3) line shown in Figure (6.9), the basic principle of possible excitation of quadrupole, magnetic satellite and the main lines leading to a population transfer via common energy levels may be understood. It can also be shown that regeneration of several superhyperfine components of both quadrupole and magnetic satellite lines can be enhanced at the expense of some components of the main line, with energy levels in common.

Under the strong interaction of the focusing electric field on the state separator, nearly all the molecules which enter the cavity resonator will be in the upper inversion state (V=1). If a probing signal is at a frequency which corresponds to one of the quadrupole satellite transitions, then the field inside the cavity consists of two components, one of which is the field produced by the probing signal, and the other by the molecular oscillation at the main line transition frequency. Therefore, the molecules are stimulated by both the probing signal (ω_p) and the field at the main line transition frequency (ω_o).

Consider that ω_p represents the transition frequency of one of the outer quadrupole lines on the higher frequency side of the main line ($Q_{o.H}$), for example, the transition $(F_1 = 3, F = \frac{3}{2})_{v=1} \longrightarrow (F_1 = 2, F = \frac{3}{2})_{v=0}$. As a result some of the molecules in the state $(F_1 = 3, F = \frac{3}{2})_{v=1}$ will make transitions to the state $(F_1 = 2, F = \frac{3}{2})_{v=0}$. Thus, the population of the state $(F_1=3, F = \frac{3}{2})_{v=1}$ will be decreased

by stimulated emission at the frequency ω_p, whereas the population of the state $(F_1 = 2, \quad F = \frac{3}{2})_{v=0}$ will increase. Since this energy level is shared by four other lines, all will be affected, particularly two of the main line components. Consequently, the emission rate due to the transitions

$$(F_1 = 3, \quad F = \tfrac{3}{2})_{v=1} \longrightarrow (F_1 = 3, \quad F = \tfrac{3}{2})_{v=0},$$

and the transition rate from $(F_1 = 2, \quad F = \frac{1}{2})_{v=1} \longrightarrow (F_1 = 2, F = \frac{1}{2})_{v=0}$ will also decrease. Thus the amplitude of oscillation at the molecular resonance frequency ω_o is reduced, and the amplitude of the induced emission of quadrupole satellites is increased by the same order of magnitude.

However, for a more detailed treatment, the transition probability of each satellite component and their intensities relative to the main line intensity, should be determined quantum mechanically. The energy diagram could then be simplified considerably by ignoring those transitions which are weak relative to the main line transition. The theoretical results could then be compared with experimental data. Details of such a theoretical basis are given in chapter 2.

6.9 Oscillation pulsations on the quadrupole satellites

It has been found experimentally, that the excitation of the two sets of quadrupole satellites on either side of the main line to cause amplitude pulsations is possible. If the excitation signal is sufficiently strong, the oscillation at the main line frequency can be completely quenched, thus the

oscillation level can be switched. It has already been seen that rapid passage of an external microwave signal through the quadrupole satellite frequencies gives rise to characteristic oscillation amplitude pulsations. It is also found that pulsations may be obtained under conditions of slow or even zero sweep.

The oscillation pulsation behaviour for each of the four quadrupole lines is obtained by excitation of each satellite in turn, under a condition of very strong main line oscillation with the cavity resonator tuned to the upper or lower sets of the quadrupole satellites. Examples of such oscillatiion pulsations for each quadrupole line at 25, 32, 37 kV on the state separator are shown in Figure(6.10),(6.11),(6.12),&(6.13) each of which corresponds to $Q_{I.L}$, $Q_{O.L}$, $Q_{I.H}$, and $Q_{O.H}$, respectively.

Strong pulsations on each quadrupole lines can be excited by setting the local oscillator and side band power at a high level, and adjusting the microwave bridge components accordingly. Figure (6.14) and (6.15) show the oscillation amplitude pulsations (corresponding to Figure 6.11 and 6.12 respectively) under a condition of narrow band frequency swept excitation across the $Q_{O.L}$ and $Q_{I.H}$ respectively. The pulsation repetition frequency is about 14 kHz.

Figures (6.16) and (6.17) show the excitation of the four quadrupole lines obtained by a wide band frequency sweep of the stimulated signal across their line structure. Strong amplitude oscillation pulsations for both lower (i.e $Q_{O.L}$ and $Q_{I.L}$) and higher (i.e. $Q_{O.H}$ and $Q_{I.H}$) quadrupole satellites can be seen in Figure (6.16) and (6.17) respectively. It should be noted that these pulsations are bounded at the

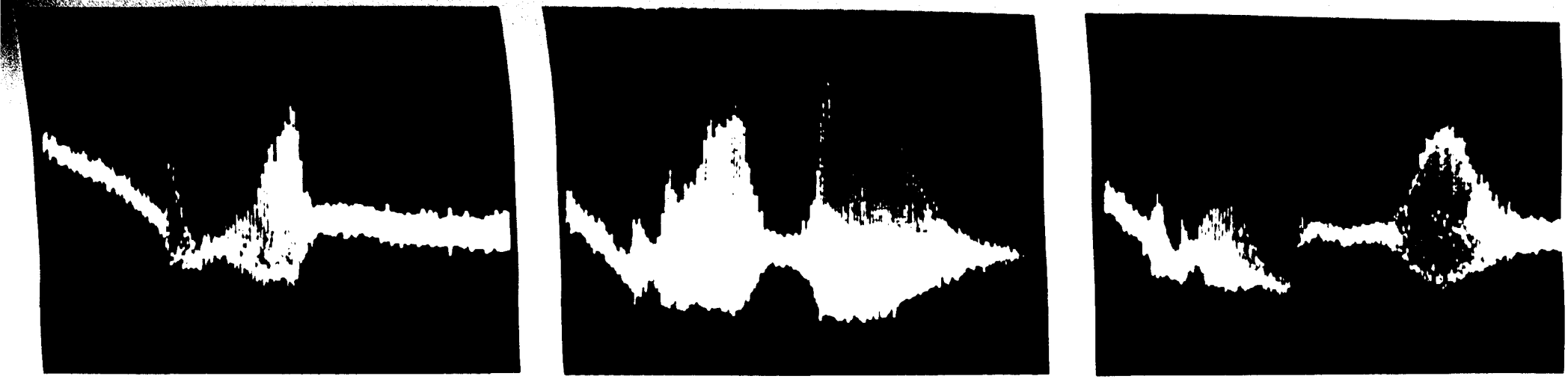

(a) 25 kV (b) 32 kV (c) 37 kV

FIGURE(6.10) OSCILLATION PULSATIONS WITH WIDE BAND FREQUENCY SWEPT EXCITATION OF $Q_{I.L}$ FOR VARIOUS SEPARATOR VOLTAGES.

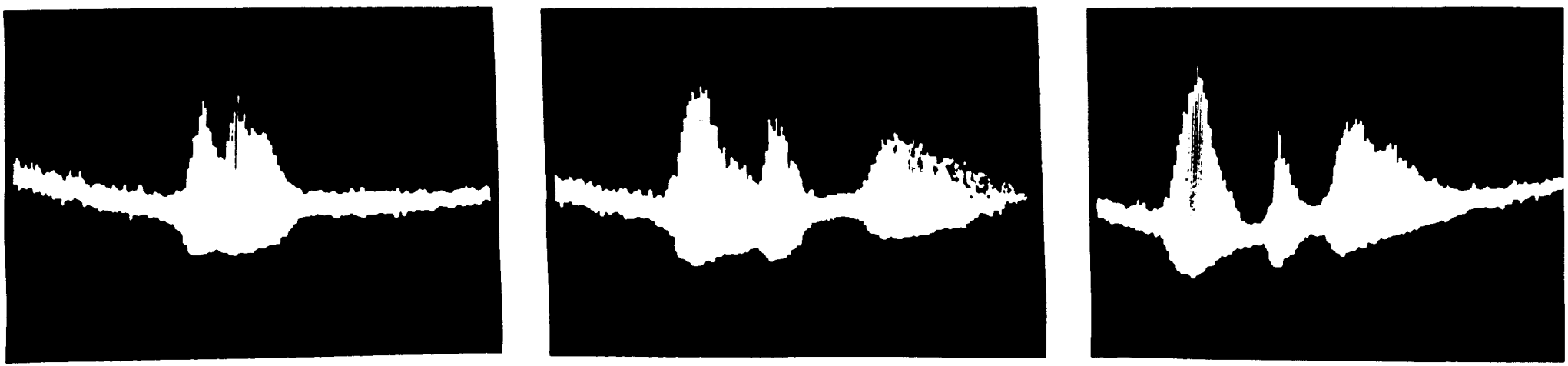

(a) 25 kV (b) 32 kV (c) 37 kV

FIGURE(6.11) OSCILLATION PULSATIONS WITH WIDE BAND FREQUENCY SWEPT EXCITATION OF $Q_{O.L}$ FOR VARIOUS SEPARATOR VOLTAGES.

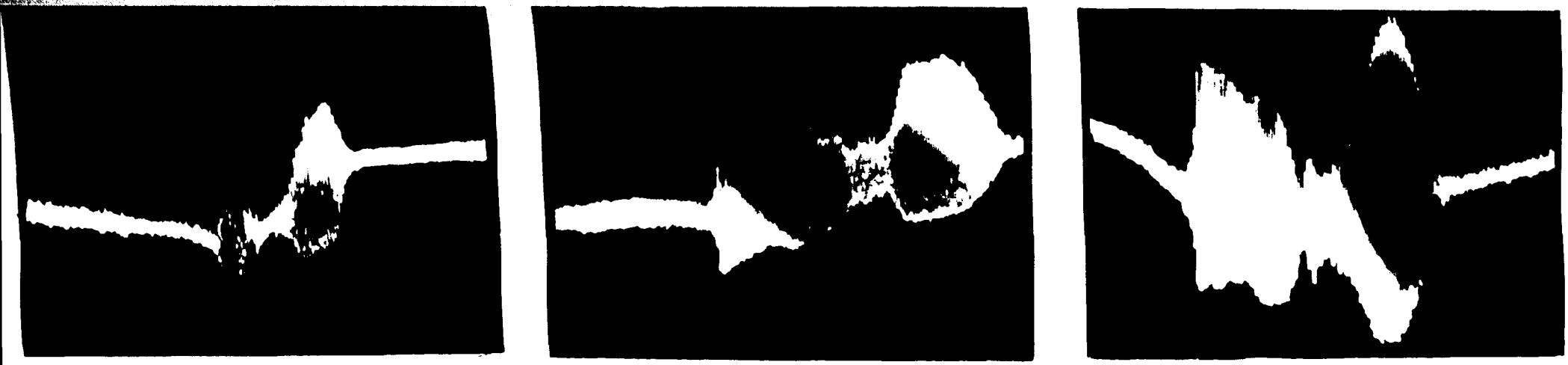

(a) 25 kV (b) 32 kV (c) 37 kV

FIGURE(6.12) OSCILLATION PULSATIONS WITH WIDE BAND FREQUENCY SWEPT EXCITATION OF $Q_{I.H}$ FOR VARIOUS SEPARATOR VOLTAGES.

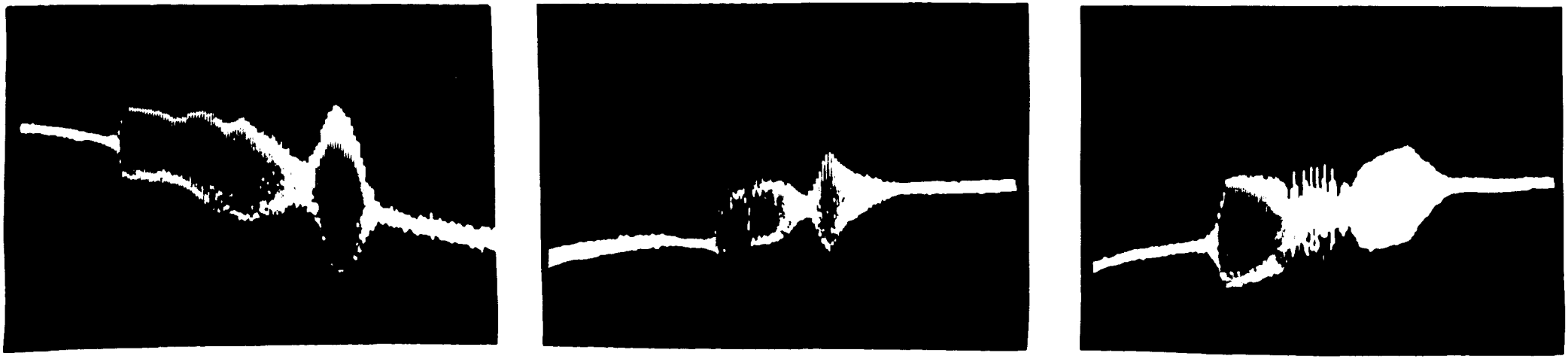

(a) 25 kV (b) 32 kV (c) 37 kV

FIGURE(6.13) OSCILLATION PULSATIONS WITH WIDE BAND FREQUENCY SWEPT EXCITATION OF $Q_{O.H}$ FOR VARIOUS SEPARATOR VOLTAGES.

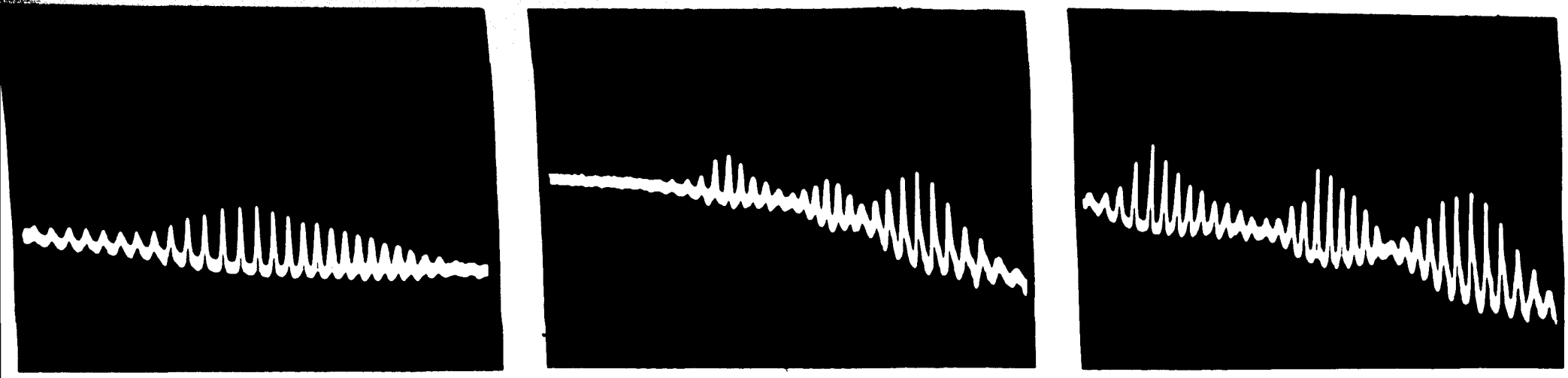

(a) 25 kV (b) 32 kV (c) 37 kV

FIGURE(6.14) OSCILLATION AMPLITUDE PULSATIONS WITH NARROW BAND FREQUENCY SWEPT EXCITATION OF $Q_{O.L}$ FOR VARIOUS SEPARATOR VOLTAGES

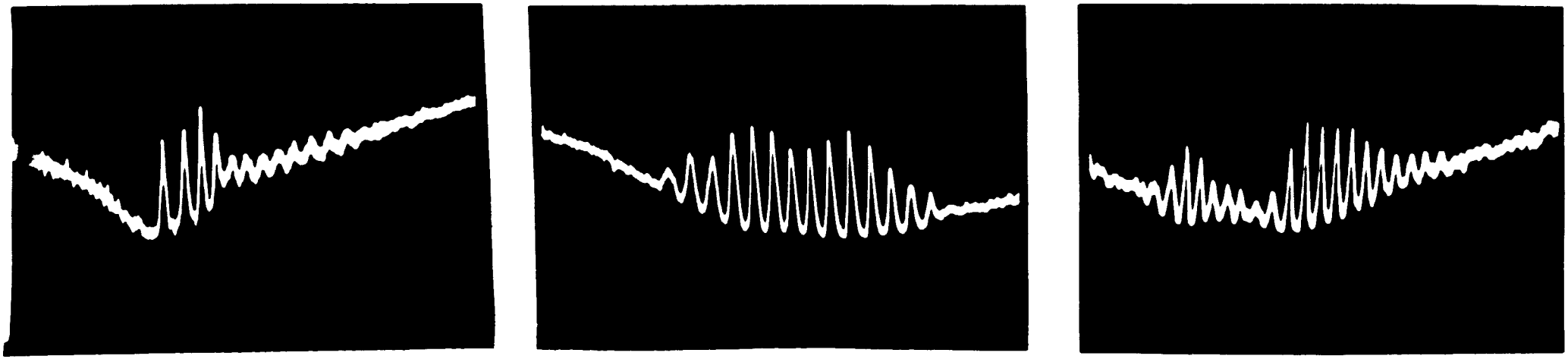

(a) 25 kV (b) 32 kV (c) 37 kV

FIGURE(6.15) OSCILLATION AMPLITUDE PULSATIONS WITH NARROW BAND FREQUENCY SWEPT EXCITATION OF $Q_{I.H}$ FOR VARIOUS SEPARATOR VOLTAGES

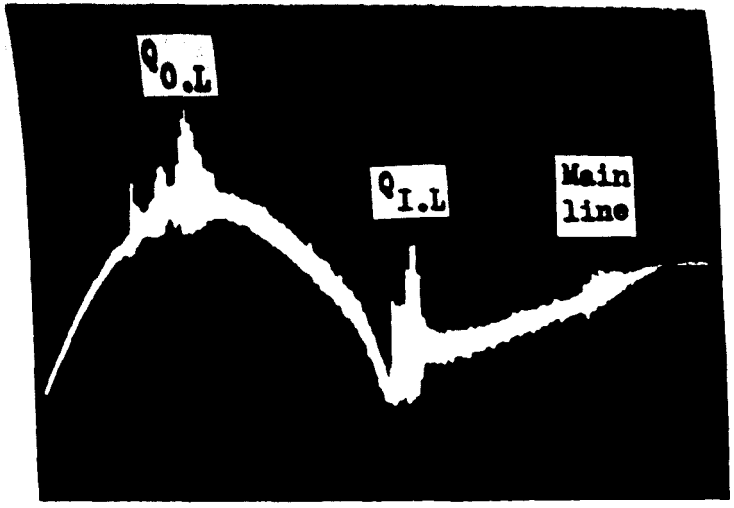

FIGURE(6.16) OSCILLATION PULSATIONS ON $Q_{O.L}$ AND $Q_{I.L}$ WITH NARROW BAND FREQUENCY SWEPT EXCITATION .

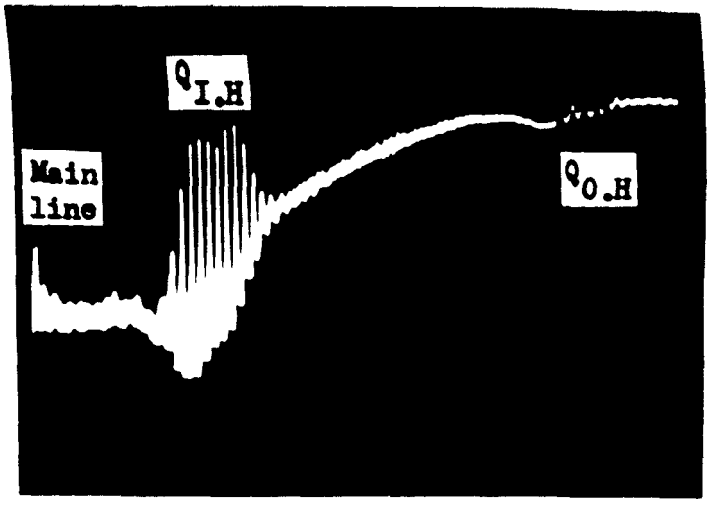

FIGURE(6.17) OSCILLATION PULSATIONS ON $Q_{I.H}$ AND $Q_{O.H}$ WITH NARROW BAND FREQUENCY SWEPT EXCITATION .

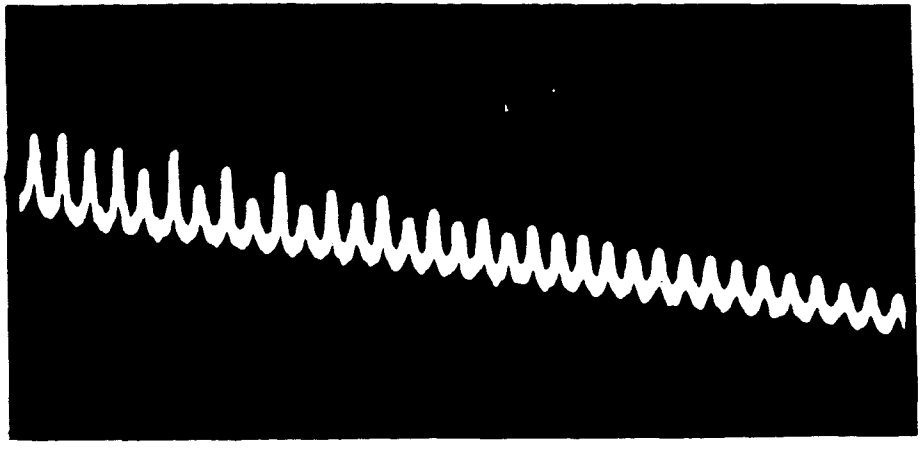

FIGURE(6.18) CONTINUOUS OSCILLATION PULSATIONS WHEN THE EXTERNAL SIGNAL FREQUENCY IS CLOSE TO THE REGION OF SUPPRESSION OF FREE MASER OSCILLATION .

location of each quadrupole line, 1.6 and 2.2 MHz on either side of the main line. The maximum frequency repetition of these pulsations is about 14 kHz. These two photographs reveal the important fact that the excitation at each set of quadrupole lines is accompanied by a considerable reduction in the oscillation amplitude of the main line. The reduction in the amplitude of oscillation to the point of near total suppression of the main line can be seen to the right of Figure (6.16) and to the left of Figure (6.17).

Moreover, continuous amplitude oscillation pulsations in the maser are produced under the condition of zero sweep when the excitation is sufficiently strong and close to the frequency region for suppression of free maser oscillation. Figure (6.18) is a typical result obtained under such conditions when the exciting signal is about 1 MHz below the main line frequency.

6.10 Discussion and phenomenological interpretation

In the previous sections it has been demonstrated experimentally that with a sufficiently strong exciting signal the main line oscillation can be completely quenched Figures (6.8a, b, c, d). Amplitude oscillation pulsations on the four quadrupole satellites have been obtained Figures (6.10 → 6.17). Continuous amplitude pulsations are produced when the external signal frequency is near to that for suppression of free maser oscillation Figure (6.18). Moreover, amplitude pulsations can also be obtained without auxiliary excitation, provided that the klystron power is set to a high level and the cavity (C_1) is tuned to one or other sets of the quadrupole lines. Figure (6.7). These results however, do not seem

to owe their origin to rapid passage effects since they may also be produced under conditions of slow or even zero frequency sweep.

The possibility of self-excitation of oscillation pulsations in a simple two-level quantum oscillator has been discussed by Grasyuk and Oraevskii (1964). In view of the present experimental evidence obtained with excitation of the quadrupole satellites, their analysis does not appear to be adequate to explain the present results. Whilst such a model cannot be totally ruled out for the main line, an alternative interpretation is sought which accommodates all results to date, including those involving excitation of the quadrupole satellites. Possible approaches are (i) relaxation oscillations, or (ii) excitation of a three-level quantum oscillator, or (iii) synchronous excitation of oscillation transients. Here, only the latter approach will be discussed.

In section (6.3) it has been shown experimentally that oscillation pulsations can be synchronously sustained in the strongly oscillating maser by the presence of a strong driving signal whose frequency offset is the same or a low value harmonic of the oscillation settling transient ν_t. In the present system ν_t has a typical maximum frequency of 12-14 kHz, whereas in other maser systems, settling transient frequencies in the region of 10kHz have been observed (Lainé and Bardo 1969, Bardo and Lainé 1971). Thus a possible basis for an interpretation of the present results arises if it is assumed that two or more quadrupole magnetic structure lines oscillate in addition to the oscillation at the frequency of the main line. The possibility of maser oscillation

arising on such weak lines has been verified by the observation of biharmonic oscillation in the quadrupole satellites of the J = K = 1 inversion transition of $^{14}NH_3$ (Krupnov and Shchuko 1969).

Consideration of the energy level scheme for the J = K = 3 inversion transition reveals that oscillation on the main line tends to suppress oscillation on the quadrupole satellite lines, since these transitions possess common energy states Figure (6.9). If the main line transition can be suppressed, even in part, oscillation on resolved components of the magnetic structure of the quadrupole satellites lines is highly probable. Thus, simultaneous oscillation on several magnetic components is expected to occur with frequency separations in the region of 12-20 kHz. A beat frequency between such oscillations could then synchronously sustain the pulsations as experimentally observed in Figures (6.10→ 6.17).

The fact that the maser cavity must be tuned to the particular transition excited for pulsation to arise, is evidence of competition between main and quadrupole satellite line transition frequencies, using the same pool of molecules. When strong excitation of a given quadrupole line occurs, consideration of the energy level diagram, Figure (6.9) illustrates that the excitation of the quadrupole transitions results in population transfer, which will favour increased regeneration, not only for some components of the main line, but also on one or more quadrupole lines other than the one being excited.

Since there are 28 possible pumping schemes corresponding to the various components of the quadrupole satellites, only two representative examples are given. These are shown in Figure (6.19). Strong excitation of a given quadrupole line to the point of saturation or even partial saturation, causes molecular population transfer between the levels involved. Figure (6.19a) shows enhanced regeneration on two close spaced quadrupole lines and, Figure (6.19b) reveals regeneration enhancement for three quadrupole lines. In both cases, two of the main line components are weakened and two components of the magnetic satellites are enhanced. The experimental results obtained as in Figures (6.16) and (6.17) support the above phenomenological approach.

It can be readily seen that the strength of each set of quadrupole lines can be enhanced by molecular robbing of the main line which in turn enhances regeneration, leading to a condition for oscillation fulfillment at the frequencies of the quadrupole lines involved. The fact that the maser cavity is tuned to the particular quadrupole transitions excited for pulsations to occur, could favour strong simultaneous oscillation on the main line and the magnetic or quadrupole lines as a consequence of population transfer. Oscillation on the satellite lines combined with the non-linearity of the maser system could excite settling transients to continuous amplitude pulsations as observed in a single cavity maser. The experimental observation of oscillation pulsations obtained with a one-cavity system may also be interpreted in terms of a synchronous excitation model. These pulsations, which are local-oscillator power dependent

Key: C = centre line, M = magnetic satellites, Q = quadrupole lines, W = weaker regeneration, e = enhanced regeneration .

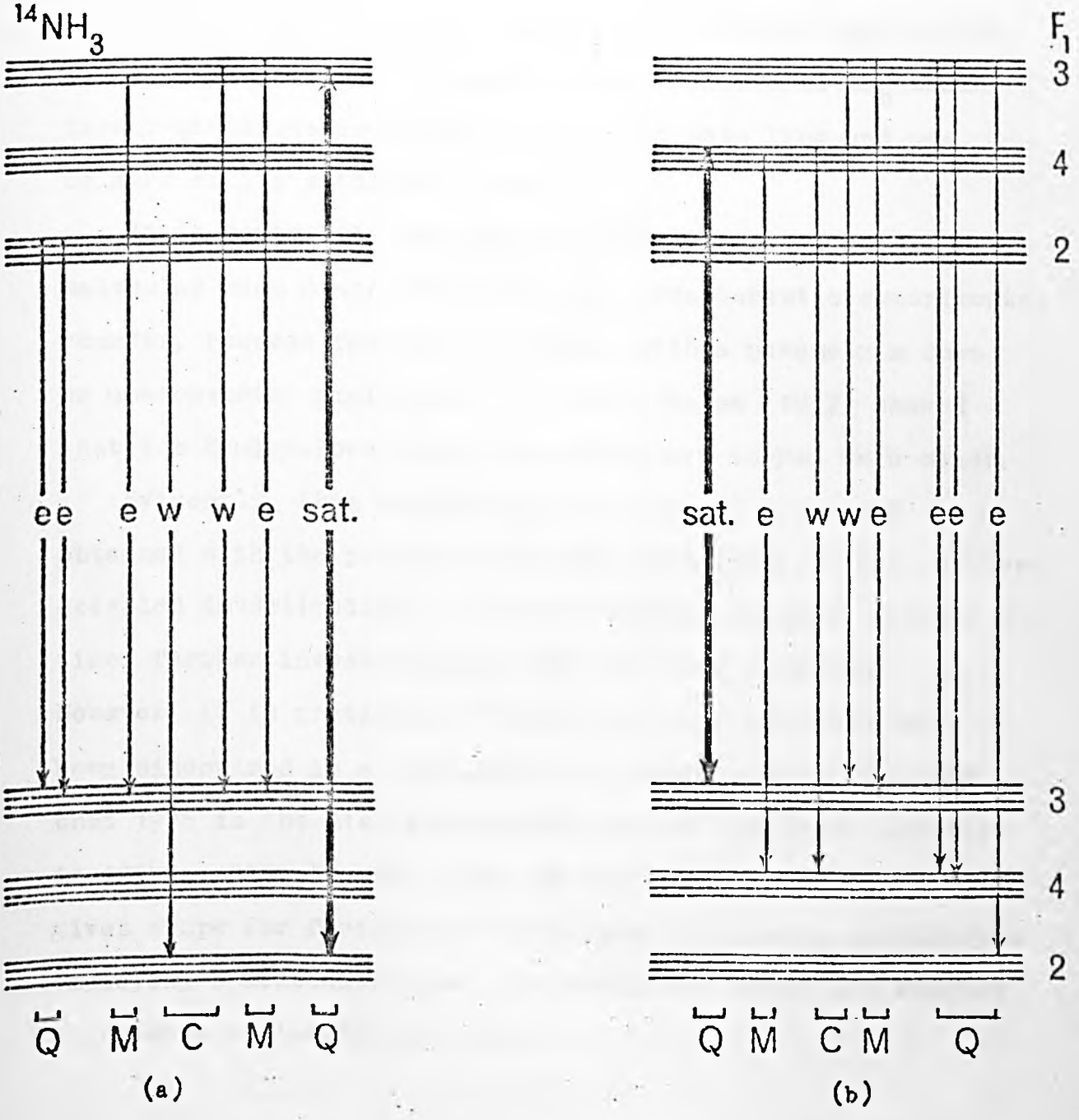

FIGURE(6.19) ENERGY LEVEL SCHEME FOR $^{14}NH_3$, J=K=3 INVERSION TRANSITION WITH TWO EXAMPLES OF PARTIAL SATURATION OF QUADRUPOLE SATELLITE TRANSITIONS.

can be attributed to frequency dispersion of the microwave bridge which presents a frequency dependent load to the maser cavity. Since the detector and modulator crystal impedances are dependent upon the local oscillator power, under favourable conditions of bridge balance, differential loading for one or other set of quadrupole lines relative to ω_o could favour simultaneous oscillation on the main line and one or more of its satellite lines.

It is worthwhile to emphasize here that the present molecular beam maser behaviour and characteristic experimental results, possess features in common with a parametric down or up-converter amplifier. In fact, Weiss (1957) showed that the Manley-Rowe (1956) relations are obeyed in a maser.

Evidently, this complex dynamic mode of operation obtained with the present molecular beam maser, needs further detailed investigation. Unfortunately, owing to limited time, further investigations have not been possible. However, it is gratifying that so many new phenomena have been discovered in a molecular beam maser, bearing in mind that 1975 is the 21st anniversary year of its first creation in 1954. Clearly, the study of molecular beam masers still gives scope for further investigations of quantum oscillators employing a molecular beam, the results of which are related to quantum oscillators in general.

6.11 Conclusions and suggestions for future work

In 21 years of molecular beam maser research, several types of masers have been constructed with the aim of producing an intense, highly collimated beam. Great attention has been given to the problem of producing high beam intensities and a narrow molecular velocity distribution in order to improve the signal-to-noise ratios in maser devices used as a spectrometer (Lainé 1975).

In the investigations reported in this thesis, however, emphasis has been placed on the operation of the maser as an oscillator from the point of view of investigations of non-linear effects and the technology of operation without recourse to cryogenic pumping. These considerations are directly related to details of construction of the molecular beam source, the state selector, and the fast pumping system which is necessary to maintain the low background pressure required. Accordingly, consideration of these important details led to the present form of the molecular beam maser actually constructed.

The present maser undoubtedly, owes its success to the use of a nozzle-skimmer combination similar to that employed in supersonic molecular beam work, which provides a molecular flux some two orders of magnitude greater than in a conventional beam maser. In fact, the nozzle-skimmer technique provides a powerful tool central to the beam formation problem, provided that the first stage pumping is sufficiently fast.

As a consequence, with the present experimental device, many new discoveries have been obtained using the J=K=3 line of ammonia in both single and two-cavity maser systems. In addition, successful operation without cryogenic pumping or time limit on the J=3, K=2 inversion line of $^{14}NH_3$ now makes the present device

highly attractive for secondary frequency work. Thus, there is no reason why such a maser system cannot now be operated on a continuous basis for years at a time without deterioration of its frequency resettability or stability.

Moreover, one of the most encouraging aspects of the system is that of its versatility for a wide variety of experiments. Examples are, spectroscopic investigations of both weak and strong ammonia inversion lines, studies of Stark and Zeeman perturbation effects including spatial reorientation of molecules in the maser oscillator, as well as general studies of strong oscillation in a relatively simple quantum oscillator.

Furthermore, it is found experimentally that the essential features of this apparatus are, high level of oscillation, thus good signal-to-noise ratio, low E.H.T values at the oscillation threshold, and continuous operation without cryogenic pumping. It is quite possible that an even lower oscillation threshold could be obtained by designing a focuser with an optimum length and tranparency.

Nevertheless, beam masers operated with nozzle gas sources provide an opportunity for further work in three directions: high resolution spectroscopy, molecular clocks, and studies of the non-liear behaviour of the maser oscillator.

It seems likely that the present apparatus will provide an opportunity, for the next few years at least, for more detailed investigations of the present results especially with the oscillation pulsation phenomenon on the four quadrupole satellite lines as well as for studies of the other properties of the maser system similar to those of lasers and n.m.r masers.

Accordingly, the author's suggestions fall into two groups:

(I)- Further detailed investigations based on each of the new results reported in this thesis. Since the new phenomena described here are interpreted phenomenologically in view of their preliminary nature, further quantitative results are required. The validity of the conclusions reached could then be checked, and in particular those concerned with the oscillation amplitude pulsation phenomena obtained in single and two-cavity maser systems, and on the quadrupole satellites.

(II)- It is also suggested that several other experiments should be carried out under strong oscillation conditions obtained in the present maser. These include, oscillation settling transients with an external Stark perturbation; phase locking of biharmonic oscillation in a weak field Zeeman maser to an external perturbation and Zeeman maser studies by observation of the state of the emergent beam from the first cavity. Also, several other possibilities include, Fabry-Perot maser operation; the study of the effect of molecular velocity distribution on the pulsating mode of operation; investigations of the focusing lower state molecules in "anti-maser" absorption.

Other possible investigations include oscillations on inversion transitions of $^{14}NH_3$ other than the J=K=3 line, especially the weak J=K=1 inversion transition; the possibility of establishing continuous maser oscillation with permanent state separation by the use of electrets, and the extension of beam maser techniques to the far infra-red region. The results observed elsewhere for n.m.r masers suggest that the two systems are closely related and hence, the two-cavity

ammonia maser can be studied by analogous experiments with a nuclear spin maser.

However, in spite of all the effort that has been expended in forming an intense molecular beam, it must be recognized that there is still much to be done before the nozzle-skimmer assembly can be regarded as optimised. It is possible that the performance of this molecular beam maser system could yet be improved by a second stage of beam skimming. However, the incorporation of this facility in the present apparatus is not envisaged in view of the host of interesting experiments which can be investigated without drastic modification of the experimental equipment in its present form.

PAGE/PAGES EXCLUDED UNDER INSTRUCTION FROM THE UNIVERSITY

APPENDIX 3

Oscillation pulsations in a single cavity molecular beam maser operated with a nozzle gas source

D.C. Lainé and A.K.H. Maroof*

Physics Department, University of Keele, Keele,

Staffordshire, ST5 5BG, U.K.

Abstract

Strong oscillation amplitude pulsations in the frequency region 5-14kHz have been observed to occur in a $^{14}NH_3$ molecular beam maser operated with a particularly intense beam produced by a nozzle type of gas source. Details of these results and a preliminary explanation of their possible origin are presented.

Introduction

Oscillation amplitude pulsations in a molecular beam maser (MBM) were first observed in a single cavity system, in which an external excitation signal was present with a frequency offset between 5-100kHz from that of the MBM oscillation (1). More recently (2) it has been shown that self-excited pulsations can be driven by biharmonic oscillations which can arise in the second cavity of a maser operated with two cavities in series. In this paper, results are presented for self-excited pulsations that are found to occur in a single cavity MBM operated under conditions of particularly strong oscillation. A possible phenomenological interpretation is suggested.

---

*on study leave from Physics Department, College of Science, Baghdad University, Iraq.

Experimental apparatus

In the present MBM, an unusually strong oscillation is obtained by the use of a nozzle-skimmer combination in conjunction with a differentially pumped vacuum chamber. Experimental details have been given previously (3). These are summarized as follows. Gas: $^{14}NH_3$ (J=3, K=3 inversion line at 23.87GHz); gas source: nozzle type, 0.1mm diameter, 0.2mm thick; skimmer: internal and external cone angles 35^o and 45^o respectively, hole size 1.6mm diameter, leading edge of skimmer spaced 10mm from nozzle; state selector: ring type, internal diameter of rings 3.4mm, total length 83mm, maximum EHT 37kV; cavity: TM_{010} mode, loaded Q of 8000, length 100mm. The optimum gas pressure behind the nozzle for maximum oscillation amplitude was 22 torr.

A single klystron superheterodyne microwave bridge system (4) permitted detection of the MBM oscillation with simultaneous excitation of quadrupole satellite transitions.

Experimental results and discussion

It was shown by Shimoda and Wang (5) that excitation of the quadrupole satellite transitions of the $^{14}NH_3$, J=K=3 inversion line in a MBM can reduce the amplitude of oscillation at the main line frequency ν_o via molecular population robbing by virtue of shared energy levels. It was demonstrated that with a sufficiently strong exciting signal, the main line oscillation can be completely quenched. However, it has now been discovered that an external microwave excitation which partially saturates the quadrupole lines of the present strongly oscillating maser, leads to an oscillation amplitude pulsation regime of operation, rather than simple quenching of the MBM oscillation at ν_o. These pulsations are obtained at the optimum nozzle pressure, EHT > 22kV, and the MBM cavity tuned to the mean frequency of the set of quadrupole lines being excited. Typical results obtained with quadrupole line excitation (method A) are shown in Figs. 1 and 2. These pulsations do not appear, however, to owe their origin to rapid passage effects since they may also

(a) 25kV

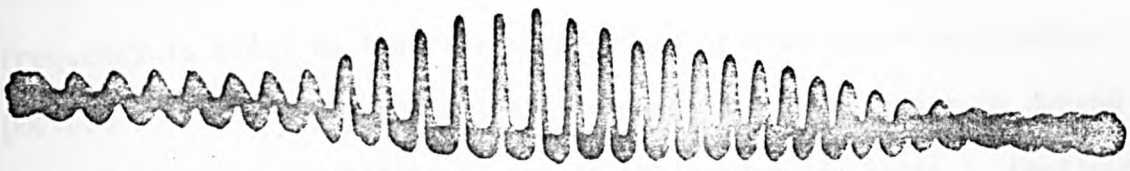

(b) 37kV

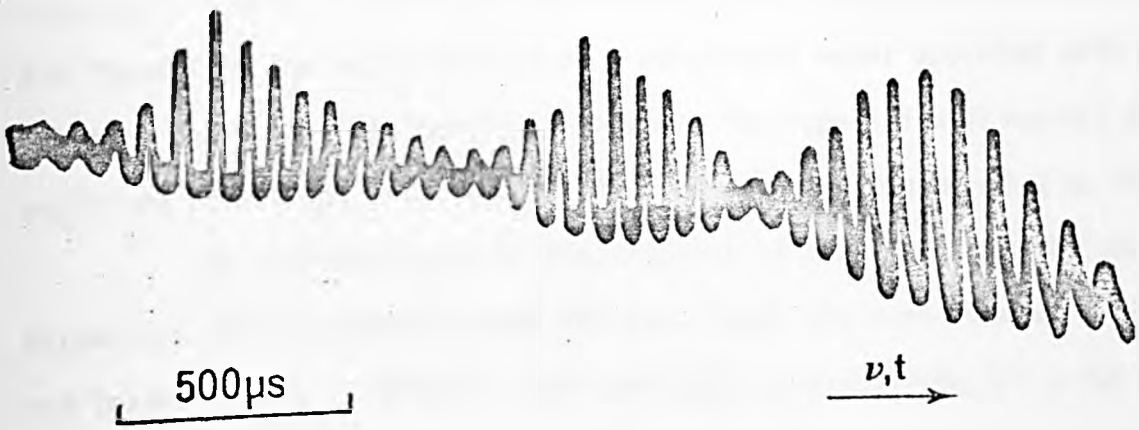

FIGURE (1)

35kV

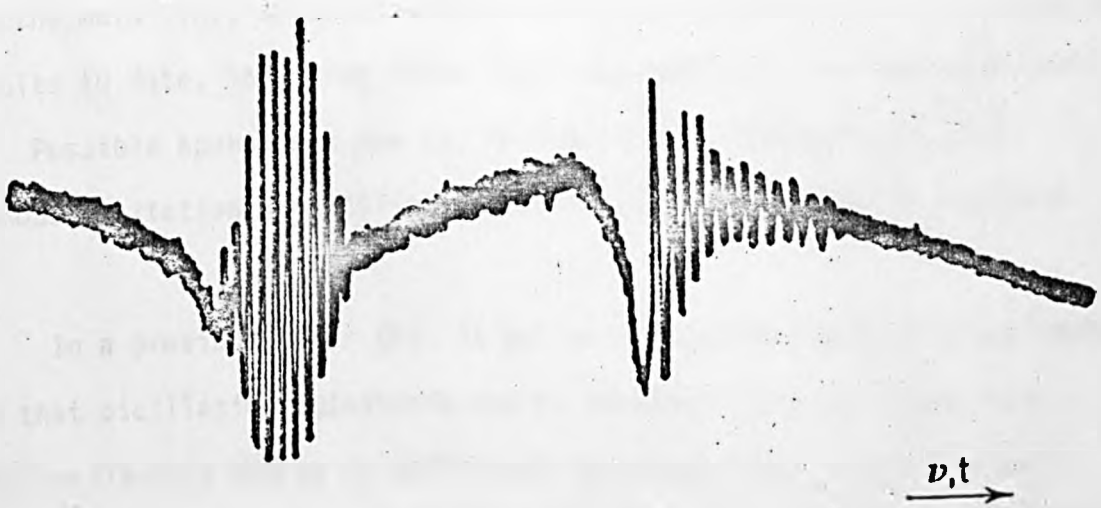

FIGURE (2)

be obtained under conditions of slow or even zero frequency sweep. Moreover, it is found that similar pulsations are obtained when the external signal frequency is close to that for suppression of free maser oscillation (6) (method B). Thus the pulsation phenomenon does not appear to depend exclusively upon excitation of one of the quadrupole lines. Continuous pulsations produced by this method are shown in Fig. 3.

Amplitude pulsations can also be obtained without external excitation (method C), provided that the local oscillator (L.O.) klystron power is set to a high level and the MBM cavity is tuned to one or other sets of quadrupole lines. The similarity between these pulsations, shown in Fig. 4, and those from the second cavity of a biharmonic maser operated with two cavities in series (2), should be noted. The repetition frequency of amplitude pulsations with methods (A-C) fall in the region of 5 to 14kHz.

The possibility of self-excitation of oscillation amplitude pulsations with a simple 2-level MBM oscillator has been studied by Grasyuk and Oraevskii (7). However, their analysis is inadequate for a full interpretation of the present results in view of experimental evidence obtained with excitation of the quadrupole satellites, which clearly invalidates a 2-level model. Whilst such a model cannot be totally ruled out for the main line, an alternative explanation is sought which accommodates all results to date, including those involving excitation of the quadrupole lines. Possible approaches are (i) relaxation oscillations, or (ii) synchronous excitation of oscillation transients. Only (ii) is explored here.

In a previous paper (2), it was argued on the basis of experimental results that oscillation pulsations can be synchronously sustained in a strongly oscillating MBM by an additional driving signal whose frequency offset is either the same or low value harmonic of the oscillation amplitude settling transient frequency, ν_t. The maximum frequency of ν_t is typically

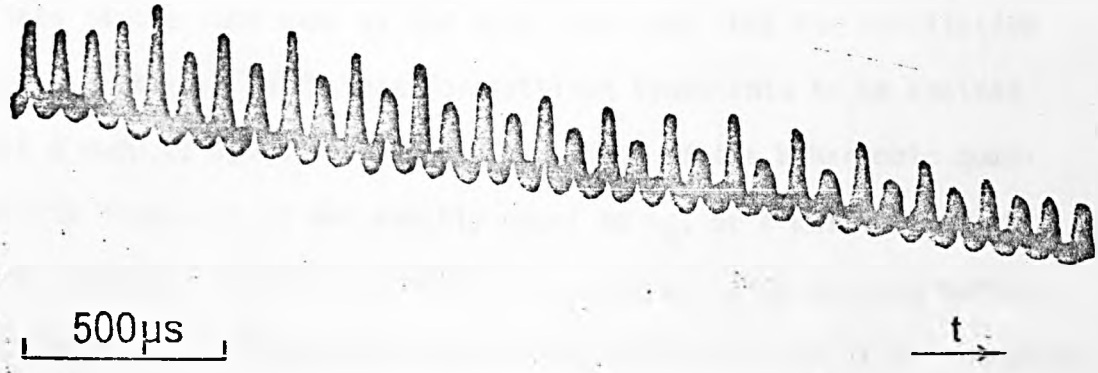

FIGURE (3)

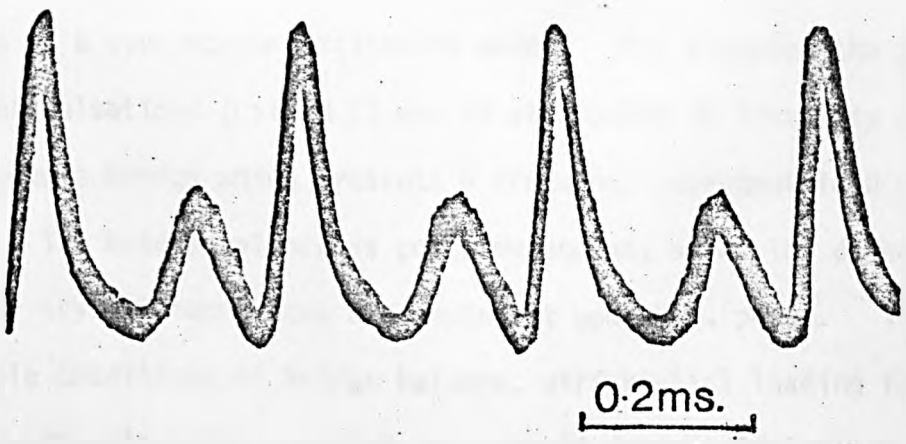

FIGURE (4)

10kHz (1,8) and 12-14kHz in the present system. The pulsation phenomena reported in this communication may also be understood on the basis of synchronous excitation of oscillation settling transients. Such a mechanism could exist if it is assumed that two or more close-spaced superhyperfine components of any one, or more, of the magnetic or quadrupole satellites lines oscillate at the same time as the main line, and that the oscillation strength of the latter is sufficient for settling transients to be excited at ν_t. Such a mode of operation is possible, even if the biharmonic quadrupole satellite frequency is not exactly equal to ν_t, or a multiple of it, in which case pulsations would be excited in a periodic time varying manner. This would produce a pulsation amplitude envelope whose period is the inverse of the frequency difference. Some evidence of this type of behaviour is shown in Fig. 1(b). The fact that MBM oscillation can occur on the relatively weak quadrupole satellites of an ammonia inversion transition has been demonstrated by the observation of biharmonic oscillation on a quadrupole satellite line of $^{14}NH_3$, J=K=1 line (9).

Certain of the experimental observations to date may be interpreted in terms of a synchronous excitation model. For example, the power dependent pulsations (method C) may be attributed to frequency dispersion of the microwave bridge which presents a frequency dependent load to the maser cavity. The bridge balance is power dependent, since the detector and modulator crystal impedances are dependent upon L.O. power. Thus, under favourable conditions of bridge balance, differential loading for one or other set of quadrupole lines relative to ν_o could favour simultaneous oscillation on the main line and one or more of its satellite lines.

When strong excitation of a given quadrupole line occurs (method A), consideration of the energy levels involved for the J=K=3 inversion transition of $^{14}NH_3$ shows that excitation to the point of partial saturation causes molecular population transfer between levels.

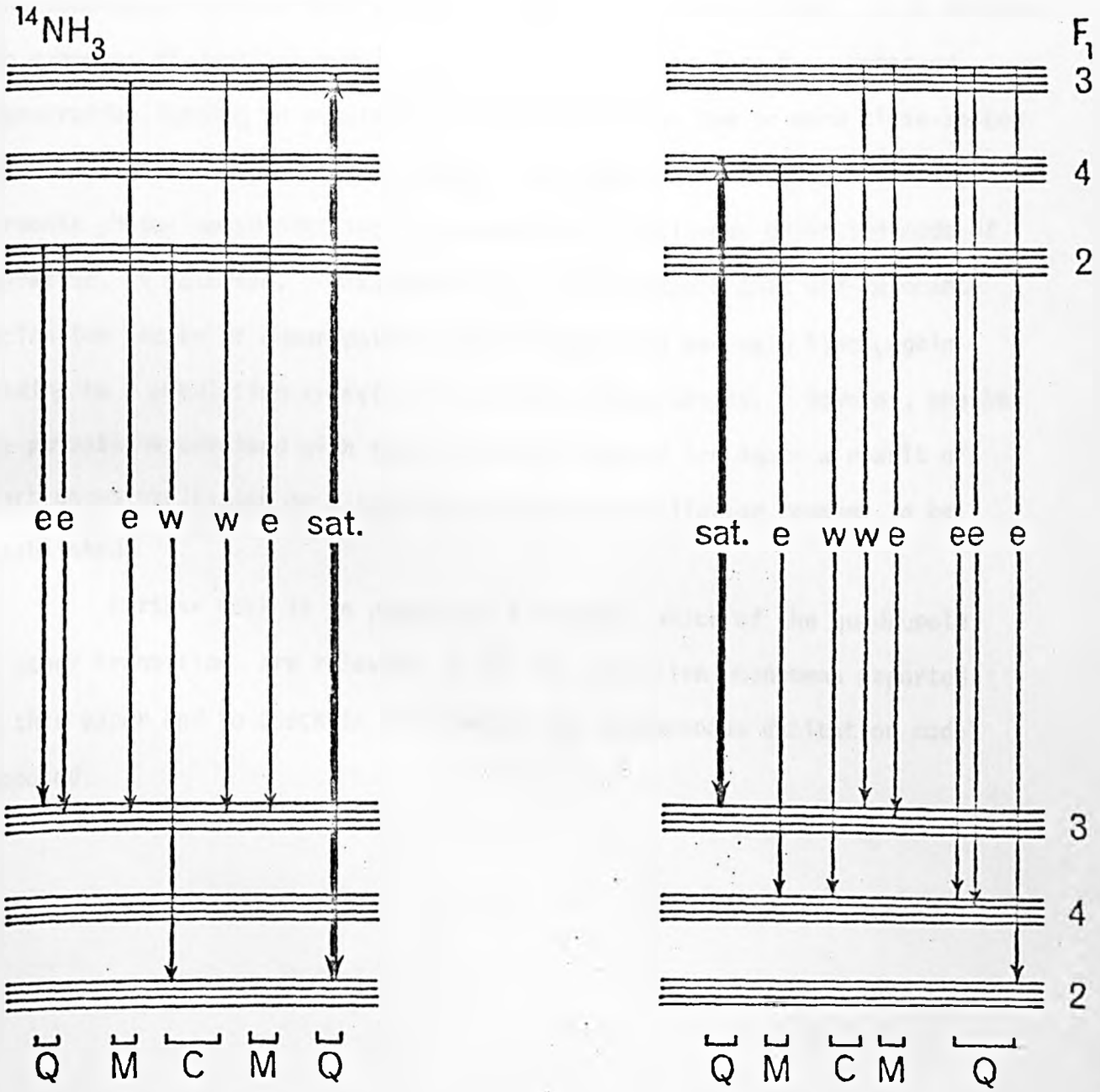

FIGURE (5)

This could favour an increase in oscillation strength of the main line under particular circumstances, possibly leading to pulsations of the Grasyuk-Oraevskii type. It can also be shown that regeneration of several superhyperfine components of both quadrupole and magnetic satellite lines can be enhanced. Two examples of possible pumping schemes are given in Fig. 5. Enhanced regeneration leading to simultaneous oscillations on two or more close-spaced but resolved superhyperfine components could then excite harmonic or sub-harmonic phase-locked settling transients to a continuous pulsation mode of operation, as observed. With method B, it is probable that off-resonance excitation occurs of quadrupole, magnetic satellite and main lines, again leading to a population transfer via common energy levels. However, whether the pulsations obtained with this particular method are again a result of synchronous excitation or a type of relaxation oscillation remains to be established.

Further work is in progress to identify which of the quadrupole or other transitions are relevant to all the pulsation phenomena reported in this paper and to check in more detail the synchronous excitation model proposed.

Figure Captions

Figure 1 $^{14}NH_3$ molecular beam maser oscillation amplitude pulsations with narrow band frequency swept excitation of the lowest frequency quadrupole satellite line, 2.2MHz below the frequency of the main oscillating line (J=K=3). Pulsation frequency (a) ∿13kHz, (b) 14kHz.

Figure 2 Maser oscillation amplitude pulsations with wide band frequency swept excitation over the two high frequency quadrupole satellite lines, respectively 1.6 and 2.2MHz above main oscillating line frequency.

Figure 3 Continuous oscillation amplitude pulsations in maser when external excitation signal frequency is close to the region of suppression of free maser oscillation, about 1.0MHz below main line frequency.

Figure 4 Continuous oscillation amplitude pulsations in maser produced when strong L.O. power only, offset 30MHz from main line maser transition, is applied to microwave bridge.

Figure 5 Energy level scheme for $^{14}NH_3$, J=K=3 inversion transition with two examples of partial saturation of quadrupole satellite transitions. Only two of the possible 12 main line transitions, of immediate relevance drawn.

Key: w = weaker regeneration, e = enhanced regeneration, Q = quadrupole lines, M = magnetic satellites, C = centre line (oscillating main line transition).

References

1. Lainé, D.C. and Bardo, W.S., Electron. Lett., 5, 323, (1969).

2. Lainé, D.C. and Maroof, A.K.H. In "18th Ampere Congress" (P.S. Allen, E.R. Andrew and C.A. Bates, eds.) in press. University of Nottingham, Nottingham, U.K. 1974.

3. Maroof, A.K.H. and Lainé, D.C., J. Phys. E: Sci. Instrum. 7, 409, (1974).

4. Bonanomi, J. and Herrmann, J., Helv. Phys. Acta, 29, 225, (1956).

5. Shimoda, K. and Wang, T.C., Rev. Sci. Instrum., 26, 1148 (1955).

6. Lainé, D.C., Phys. Lett., 23, 557, (1966).

7. Grasyuk, A.Z. and Oraevskii, A.N., In "Quantum Electronics and Coherent Light" (C.H. Townes Ed.) New York: Academic Press pp.192-7 (1964).

8. Bardo, W.S. and Lainé, D.C., Electron. Lett., 5, 688, (1969).

9. Krupnov, A.F. and Shchuko, O.B., Izv. Vyssh. Uch. Zav. Radiofiz. 12, 1780, (1969). Eng. transl. Radiophys. Quant. Electron. 12, 1385 (1972).

APPENDIX 4

Calculation of the transition probabilities for the three components of the central line ($F_1=2$, $F_1=3$ and $F_1=4$) for the ammonia inversion line J=3, K=3:

$$\sum_{-F_1}^{+F_1} M^2 = \tfrac{1}{3} F_1 (F_1 + 1)(2F_1 + 1) \qquad (2.41)$$

$$\sum_{-2}^{+2} M^2 = \tfrac{1}{3} \times 2 \times 3 \times 5 = 10$$

$$\sum_{-3}^{+3} M^2 = \tfrac{1}{3} \times 3 \times 4 \times 7 = 28$$

$$\sum_{-4}^{+4} M^2 = \tfrac{1}{3} \times 4 \times 5 \times 9 = 60$$

$$A = \left[K^2/J^2(J+1)\right] M^2 \left\{\left[J(J+1)-I(I+1)+F_1(F_1+1)\right]^2/4F_1^2(F_1+1)^2\right\} \qquad (2.37)$$

$$A_{F_1=2} = \left[9/9\times16\right]\ 10\ \left\{(12-2+6)^2/4\times4\times9\right\} = 640/576$$

$$A_{F_1=3} = \left[9/9\times16\right]\ 28\ \left\{(12-2+12)^2/4\times9\times16\right\} = 847/576$$

$$A_{F_1=4} = \left[9/9\times16\right]\ 60\ \left\{(12-2+20)^2/4\times16\times25\right\} = 1215/576$$

Calculation of the weighting factors for the three components:

$$\sum_M N(M)\, M^2/(2F_1 + 1) \qquad (2.11)$$

$F_1=2$ $\quad (3\times0 + 2\times1)/\ 5 = 2/5$

$F_1=3$ $\quad (4\times9 + 2\times4 + 1\times1)/\ 7 = 45/7$

$F_1=4$ $\quad (2\times9 + 4\times2 + 1\times1)/\ 9 = 37/9$

APPENDIX 5

Calculation of the relative intensities (R) of the satellites to the intensity of the central line for the ammonia inversion line J=3, K=3:

$$Q(J) = (J+1)^4 + J^4 + \left[J(J+1) - 1\right]^2 \qquad (2.43)$$

$$Q(1) = 2^4 + 1 + 1^2 = 18$$

$$Q(2) = 3^4 + 2^4 + 5^2 = 122$$

$$Q(3) = 4^4 + 3^4 + 11^2 = 458$$

$$Q(4) = 5^4 + 4^4 + 19^2 = 1242$$

$$Q(5) = 6^4 + 5^4 + 29^2 = 2762$$

$$Q(6) = 7^4 + 6^4 + 41^2 = 5378$$

$$R_{J-1,J} = (A_{J-1,J}/A_{J,J}) = (J+1)^2(2J-1)/(2J+1)\,Q(J) \qquad (2.45)$$

$$R_{J,J+1} = (A_{J,J+1}/A_{J,J}) = J^2(2J+3)/(2J+1)\,Q(J) \qquad (2.46)$$

J	$R_{J-1,J}$	$R_{J,J+1}$
1	$4x1/3x18 = 7.407x10^{-2}$	$1x5/3x18 = 9.259x10^{-2}$
2	$9x3/5x122 = 4.426x10^{-2}$	$4x7/5x122 = 4.590x10^{-2}$
3	$16x5/7x458 = 2.495x10^{-2}$	$9x9/7x458 = 2.526x10^{-2}$
4	$25x7/9x1242 = 1.565x10^{-2}$	$16x11/9x1242 = 1.574x10^{-2}$
5	$36x9/11x2762 = 1.066x10^{-2}$	$25x13/11x2762 = 1.069x10^{-2}$
6	$49x11/13x5378 = 0.770x10^{-2}$	$36x15/13x5378 = 0.772x10^{-2}$

REFERENCES

ANDERSON,J.B., ANDRES,R.P., FENN,J.B., MAISE,G., Rarefied Gas Dynamics, Ed.DE LEEUW,J.H., Vol.2, 1966, 106-126.

BARDO,W.S., LAINÉ,D.C., J.Phys.E: Sci.Instrum., 1971, 595-597.

BARDO,W.S., LAINÉ,D.C., 1971, J.Phys.B: Atom.Molec.Phys., 4, 1523-1535.

BARNES,F.S., Stanford University Micowave Report No.486 (1958), Quantum Electronics Symposium, Ed. C.H.TOWNES, 1960.

BASOV,N.G., ORAEVSKII,A.N., 1959, Zh.Eksper.Teor.Fiz., 37, 1068-1071 (Eng.transl. 1960, Sov.Physics-JETP, 10, 761-763).

BASOV,N,G., ORAEVSKII,A.N., 1962, Zh.Eksper.Teor.Fiz., 42, 1529-1535 (Eng.transl. 1962, Sov.Physics-JETP, 15, 1062-1066).

BASOV,N.G., ORAEVSKII,A.N., STRAKHOVSKII,A.N., TATARENKOV,V.M., 1963, Zh.Eksper.Teor.Fiz., 45, 1768-1777(1964, Sov.Physics-JETP, 18, 1211-7) and 1964, Quantum Electronics III, Eds. P.GRIVET, N.BLOEMBERGEN, (New York: Columbia University Press), 377-392.

BASOV,N.G., STRAKHOVSKII,G.M., CHEREMISKIN,I.V., 1961, Radioteckh. i.Electron., 6, 1020-1028 (Eng.transl. 1961, Radio Engng. Electron. Physics, 6, 232-244.

BASOV,N.G., ORAEVSKII,A.N., USPENSKII,A.V., 1967, Optics and spectroscopy, 23, 504.

BECKER,E.W., BIER,K., 1954, Z.Naturforsch., 9a., 975.

BECKER,E.W., KLINGELHOFER,R., LOHSE,P., Z.Naturforsch., 1962, 17a, 432.

BECKER,G., 1963, Zeit.angew Phys., 15, 281.

BIER,K., HAGENA,O., Rarefied Gas Dynamics, Ed. DE LEEUW, Vol.2, 1966, 260-78.

BIER,K., SCHMIDT,B., 1961, Zeit.angew.Phys., 13, 493.

BLEANEY,B., PENROSE,R.P., 1946, Nature, 157, 339.

BONANOMI,J., de PRINS,J., HERRMANN,J., KARTASCHOFF,P., 1958, Helv.Phys.Acta, 30, 492-494.

CAMPARGUE,R., 1964, Rev.Sci.Instrum., 35, 111.

CLEETON,C.E., WILLIAMS,N.H., 1934, Phys.Rev., 45, 235.

COLES,D.K., GOOD,W.E., 1946, Phys.Rev., 70, 979.

DECKERS,J., FENN,J.B., 1963, Rev.Sci.Instrum., 34, 96.

DICKE,R.H., 1954, Phys.Rev., 93,99.

FEYNMAN,R.P., VERNON,F.L., HELLWARTH,R.W., 1957, J.Appl.Phys., 28, 49-52.

GOOD,W.E., 1946, Phys.Rev., 69, 539.

GOOD,W.E., COLES,D.K., GUNTHER-MOHR,G.R., SHAWLOW,A.L., TOWNES,C.H., 1951, Phys.Rev., 83, 880.

GORDON,J.P., 1955, Phys.Rev. 99, 1253.

GORDON,J.P., 1960, Quantum Electronics, Ed. TOWNES,C.H. (Columbia University Press. New York), 3-16.

GORDON,J.P., ZEIGER,H.J., TOWNES,C.H., 1954, Phys.Rev., 95, 282.

GORDON,J.P., ZEIGER,H.J., TOWNES,C.H., 1955, Phys.Rev. 99, 1264-1274.

GRASYUK,A.Z., ORAEVSKII,A.N., Quantum Electronics and Coherent Light, (C.H.TOWNES, Ed.), New York: Academic Press, 1964, 192-197.

GRIGOR'YANTS,V.V., ZHABOTINSKII,M.E., Radiotekh.i.Electron. 6, 175-177, Radio Engng.Electron.Phys., 1961, 6, 290-263.

GUNTHER-MOHR,G.R., WHITE,R.L., SCHAWLOW,A.L., GOOD,W.E., COLES,D.K., and TOWNES,C.H., VAN VLECK,J.H., 1954, 94, 1184, and 1191.

HARVEY,A.F., Microwave Engineering, 1963, Academic Press: London, New York.

HELMER,J.C., 1957, J.Appl.Phys., 28, 212-215.

HIGA,W.H., 1957, Rev.Sci.Instrum., 28, 726.

HUNDERSON,R.S., VAN VLECK,J.H., 1948, Phys.Rev., 74, 106.

JANES,E.T., CUMMINGS,F.W., 1963, Proc.IEEE, 51, 89-109.

JAUCH,J.M., 1947, Phys.Rev., 72, 715.

KANTROWITZ,A., GREY,J., 1951, 22, 328.

KAZACHOK,V.S., 1965, Zh.Tekh.Fiz., 35, 1145-1149 (Eng.transl. 1965, Soviet Phys.Tech.Phys., 10, 882-885).

KISTIAKOWSKY,G.B., SLICHTER,W.P., 1951, Rev.Sci.Instrum., 22, 333.

KRAUSE,W.H.U., 1968, Phys.Lett., 28A, 380-381.

KRAUSE,W.H.U., LAINÉ,D.C., 1973, J.Phys.B: Atom.Molec.Phys., 6, 1510.

KRUPNOV,A.F, 1959, Izv.Vyssh.Zav.Radiofiz., 2, 658-659.

KRUPNOV,A.F., SHCHUKO,O.B., Izv.Vyssh.Uch.Zav.Radiofiz., 1969, 12, 1780, (Eng.transl.Radiophys.Quant.Electron. 1972, 12, 1385).

KRUPNOV,A.F., SKVORTSOV,V.A., 1964, Zh.Eksper.Teor.Fiz., 47, 1605-1611, (Eng.transl. 1965, Sov.Physics-JETP, 20, 1079-1083).

KUKOLICH,S.G., 1967, Phys.Rev., 156, 83.

LAINÉ,D.C., 1970, Rep.Prog.Phys., 33, 1001-1067.

LAINÉ,D.C., BARDO,W.S., 1969, Electron.Lett., 5, 323.

LAINÉ,D.C., BARDO,W.S., 1970, J.Phys.B., 3, L23-4.

LAINÉ,D.C., MAROOF,A.K.H., 1974, "18th Ampere Congress" (Eds. P.S.ALLEN, E.R.ANDREW, C.A.BATES), in Press. University of Nottingham, U.K.).

LAINÉ,D.C., MAROOF,A.K.H., 1975, "5th International Symposium on Molecular Beams", in Press.

LAINÉ,D.C., SMITH,A.L.S., 1966, Proc.IEEE.J., Quant.Electron., QE-2, 399-408.

LAINÉ,D.C., SRIVASTAVA,R.C., J.Brit.I.R.E., 1963, 26, 173.

LI TIE-CHENG, FANG LI-ZHI, 1964, Acta Physica Sinica, 20, 753.

MANLEY, J.M., ROWE,H.E., 1956, Some General Properties of Non-linear Elements Part 1. General Energy Relations., Proc.IRE.44, 904.

MAROOF,A.K.H., LAINÉ,D.C., 1974, J.Phys.E: Sci.Instrum. 7, 409.

MEDINKOV,O.I., PARYGIN,V.N., 1963, Radiotekhn.i.Electronika, t.8,No.4, Str.653.

MONTGOMERY,C.G., 1947, Radiation Lab.Series, Vol.2, McGraw-Hill, New York.

MUKHAMEDGALIEVA,A.F., ORAEVSKII,A.N., STRAKHOVSKII,G.M., 1965, Sov.Phys.-JETP Letters, 1, 13-15.

ORAEVSKII,A.N., 1964, Molecular Generators (Moscow: Nauka Press).

ORAEVSKII,A.N., 1967, Usp.Fiz.Nauk., 91, 181-191 (Eng.transl.1967, Sov.Phys. Usp., 10, 45-51.

ORAEVSKII,A.N., 1967, Foreign Technology Division Wright-Patterson Air Force Base, Ohio (AD 677 023), Produced by the "Clearinghouse" for Federal Scientific and Technical Information, Springfield Va.22151.

PARKER, H.M., KUHLTHAU,A.R., ZAPATA,R.N., SCOTT, J.E.JR., IN DEVIENNE, F.M., Ed.,Rarefied Gas Dynamics, Pergamon Press, New York, 1960, 69-79.

SENITZKY.I.R., 1958, Phys.Rev., 111, 3.

SHENG,H., BAKER,E.F., DENNISON,D.M., 1941, Phys.Rev., 60, 786.

SHCHEGLOV,V.A., 1961, Izv.Vyssh.Uch.Zav.Radiofiz., 4, 648-655.

SHIMODA,K., 1961, J.Phys.Soc.Japan, 16, 1728-1739.

SHIMODA,K., WANG,T.C., 1955, Rev.Sci.Instrum., 26, 1148.

SHIMODA,K., WANG,T.C., TOWNES,C.H., 1956, Phys.Rev., 102, 1308-1321.

SIMONS,J.W., GORDY,W., 1948, Phys.Rev., 73, 713.

SKVORTSOV,V.A., KRUPNOV,A.F., NAUMOV,A.I., Izv.Vyssh.Uch.Zav.Radiofiz., 1960, 3, 1128-1129.

SMITH, A.L.S., LAINÉ,D.C., 1968, J.Phys.D: Appl.Phys.Ser.2, 1, 727-732.

STRAKHOVSKII,G.M., CHEREMISKIN,I.V., Trudy Fiz.Ins.P.N.Lebedev, 21, 68-106, (Eng.Transl.1964, Soveit Maser Research,Ed. D.V.SKOBEL'TYSN, 56-87, Consultants Bereau, New York).

STRAKHOVSKII,G.M., TATARENKOV,V.M., 1962, Sov.Physics-JETP., 15, 625.

STRAKHOVSKII,G.M., TATARENKOV,V.M., 1964, Izv.Vyssh.Uch.Zav.Radiofiz., 7,994.

VAN VLECK,J.H., 1947, Phys.Rev., 71, 468.

VONBUN,F.O., 1960, Rev.Sci.Instrum., 31, 900-902.

VUYLSTEKE,A.A., 1960,""Elements of Maser Theory", Van Nostrand, Princeton.

WEISS, M.T., " Quantum Derivation of Energy Relations Analogous to Those for Non-linear Reactance", 1957, Proc.IRE., 45, 1012.

WELLS,W.H., 1958, J.Appl.Phys., 29, 714.

WITTKE,J.P., 1957, Proc.IRE., 47, 291-316.

WHITE,L.D., 1959, Proc. 13th Ann.Symp.Freq.Control (Fort Monmouth: U.S.Army Signal Research and Development Lab.), 596-602.

ZAPATA,R.N., PARKER,H.M., BODINE,J.H., 1961, Advances in Applied Mechanics, Suppl.1: Rarefied Gas Dynamics, Ed. L.TALBOT, (Academic Press: London, New York), 67-81.